Usefulness of Nuclear Magnetic Resonance in the Study of a Variety of Battery Systems and Materials

by:

Nicole D. R. Leifer

A dissertation submitted to the Graduate Faculty in Physics in partial fulfillment of the requirements for the degree of Doctor of Philosophy

The City University of New York

2009

This manuscript has been read and accepted by the Graduate Faculty in Physics in satisfaction of the dissertation requirement for the degree of Doctor of Philosophy

Nicole Dvora Rifka Leifer

December 16th 2008
Date

Prof. Steve Greenbaum
Chair of Examining Committee

December 16th 2008
Date

Prof. Steve Greenbaum
Executive Officer

Prof. Clare Grey

Prof. Gregory Boutis

Prof. Ying Chih Chen

Dr. Thomas Reddy
Supervisory Committee

THE CITY UNIVERSITY OF NEW YORK

Abstract

Usefulness of Nuclear Magnetic Resonance in the Study of a Variety of Battery Systems and Materials

by

Nicole Dvora Rifka Leifer

Advisor: Professor Steve G. Greenbaum

The usefulness of solid state Nuclear Magnetic Resonance (NMR) spectroscopy in the analysis of lithium ion batteries is presented. Some background information on lithium batteries is given, in addition to a summary of current research areas. A comprehensive review of the use of NMR and Electron Paramagnetic Resonance (EPR) in lithium batteries research thus far is also presented. The electrodes studied were the standard $LiCoO_2$ cathode cycled against mesocarbon microbead (MCMB) anodes, as well as $Li_2Ag_2V_4O_{11}$ and CF_x cathodes cycled against metallic lithium anodes in primary batteries. The focus of half of the work concerns the elucidation of the Solid Electrolyte Interphase (SEI), an irreversibly formed side-product found on the electrode surfaces, composed mainly from the electrolyte components; one study provides a deeper insight into the inorganic components of the SEI, while the other SEI study focuses on the organic components via ^{13}C MAS NMR studies of cycled electrodes. The other half is comprised of two additional studies in which atomic and electronic rearrangement are monitored in the electrodes at different stages of the battery cycling process.

Who knows what women can be when they are finally free to become themselves?

Who knows what women's intelligence will contribute when it can be nourished without denying love?

Who knows of the possibilities of love when men and women share not only their children, home and garden, not only their fulfillment of their biological roles, but the responsibilities and passions of the work that creates the human future and the full human knowledge of who they are?

-Betty Friedan, 1963

Acknowledgements

I would like to honor and thank some rockstars I know: Dr. Phil Stallworth for always being willing (and able!) to explain everything I asked him; Patricia Harris for reminding me of my sanity when I would often lose track of it; Nicolas Dupre for being, beneath the death metal, a sweet, kind, big-hearted smart dude, who gave generously; Dr. Ben Meyer for being such an excellent, patient mentor; Dr. Martine Ziliox for running such a tight ship! Faisal Alamgir for always giving us the low down; Ameesh Khalfan for all the gossip! Dale McLachlan for all of his wise words on life; Christoph Weise for always and readily giving me DFT help, NMR exlanations, and of course, a hard time; Boris Itin ...because NMR is so much more fun when you have a crush on your spectroscopist! Dr. Valencia Johnson for the little lessons of surviving as a woman in a man's world: speaking one's mind and demanding total respect! Lina Gonzalez -- she called me her inspiration! What more could I want in an intern? Gabriel Goenaga for reminding me how beautiful I am, every morning! Arun Ramjan for getting us through the quals! My extraordinary mother, Dr. Jacqueline Maier, for teaching us compassion, above all; and in whom doubt in my intellect and power have never existed; my bigger-than-life father, Rabbi Meyer Leifer, for praising my intelligence above everything, bringing me special salads on the late nights and shepping nachas like no other; my sibs: Lori Leifer for being my dependable best friend and biggest cheerleader; Danny Leifer for nerding out with me, in life, in general… Mark Leifer who really is always there for me 'in a heartbeat'; David Leifer for always respecting my thinking and for whose quiet wisdom about life I have a deep respect in exchange; my dear aunt Mara Popper, who invokes a beautiful heritage of pragmatism and classiness; in another time and place, you

would have been in my shoes right now; my uncle Dr. Walter Maier for being so interested in my work, and consistently supportive of my pursuits; my aunt Susie Maier for being the man behind the machine; Prof. Raina Maier for being a powerhouse of a truth-seeking scientist with morals of high temperature treated steel; my wonderful aunt Ruth Shonfeld, for continually reminding us all what *really* matters; Dr. Marilyn Vogel for going for it first! And reminding me to keep enough copies of the thesis around that it should survive a nuclear holocaust; Johnathan Yevin for always introducing me in the superlative; Isaac Shonfeld for continuously challenging me to live up to myself; the chulent crew for being the best science class *ever*; Gregory Warner for being *so* psyched for me; Emily Lopez-Cercone for being my smartest friend since 4th grade; Abby Kerlin for being my teaching role model; Whitney Pine-Hoermann for never forgetting our critical connection, and for adopting me into the family; Sasha Alcott for her unabashed excitement about science; Wendy Maier for her kind and understanding ways with us nerds; Olga Livanis who said "go to Hunter, talk to someone named Steve Greenbaum…"; Emmy Rainwalker for being my rock, my Teacher, and for ultimately convincing me to do this! Odelia Shargian for always, always being there, loving and solid; Maisha Innis for being as dependable as the sunrise; Prof. Marc Scott for listening to, believing in, and trusting my thinking so fully; Prof. Clare Grey for being so confident in my intelligence, and for providing a most respectable role model as the purist of scientists; and of course, Prof. Steve Greenbaum, who said 'when', when I said 'if', never gave me a hard time about anything, yet never ceased to keep me challenged, and in general made this an incredibly enjoyable 5+ years of my life!

Table of Contents

List of Tables

List of Figures

I. Introduction

Today's battery industry is burgeoning with new performance breakthroughs, announced in both science journals and popular media on an almost weekly basis. Industry experts predict major increases still to come in the capabilities of conventional battery technologies, advancing ever-closer toward the theoretical and practical limitations of those materials.[i] What is more, the limits themselves are being challenged with the development of entirely new materials and systems.

The pertinent parameters used to indicate battery performance necessarily depend on the properties and arrangements of the battery materials. Many techniques have been employed in the investigation of these materials and their successful application in electrochemical cells. Nuclear Magnetic Resonance (NMR) stands out in this regard because of its sensitivity to local atomic environments. Both electronic environments (e.g. changes in oxidation states) and structural surroundings (e.g. octahedral versus tetrahedral coordination) can be distinguished with this technique. NMR is also not limited to ordered materials. Due to its function as a probe on a very small local order, it is equally useful in the analysis of amorphous materials. NMR is also nuclear-specific which means that nuclei relevant to lithium ion batteries can be specifically probed. Lastly, the NMR signal is quantitative; that is, the integrations of separate peaks in a spectrum are proportional to the number of active nuclei giving rise to those individual environments in the sample.[ii]

The projects discussed here offer examples of using these techniques to examine several of the most fundamental factors dictating battery performance. These include Li-

ion insertion/de-insertion mechanisms, ionic and electronic motion/conductivities in the electrolyte and the electrode, changes in the electronic structure of the electrodes, and irreversible side reactions.

---

[i] Sadoway, M. "Portable Power: Advanced Rechargeable Lithium Batteries." *MRS Bulletin* 27.8 (2002): 590-596.

[ii] Grey, C. P. and S. G. Greenbaum. "Nuclear Magnetic Resonance Studies of Lithium-Ion Battery Materials." *MRS Bulletin* 27.8 (2002): 613-618.

II. Batteries

A. Fundamentals

The standard electrode potential, abbreviated E^o, is the measure of the individual reduction potential of any electrode at standard ambient conditions (see table 1 for a partial list). It is the voltage associated with the removal or addition of an electron from/to a species. These values are defined relative to the standard hydrogen potential (arbitrarily considered 0.00V) and depend on the ionization energies of the elements involved. The basis for all electrochemical cells, such as a galvanic cell (one that produces electrical energy) or an electrolytic cell (one which requires electrical energy) is the *RedOx* reaction. This reaction consists of a coupling of two individual half-reactions: *red*uction, which occurs at the cathode and involves the gain of electrons(s); and *ox*idation, which occurs at the anode and involves the loss of electron(s). Electricity is

Half-Reaction Standard Potential: E° (volts)	
$Li^+(aq) + e^- \rightarrow Li(s)$	-3.04
$K^+(aq) + e^- \rightarrow K(s)$	-2.92
$Na^+(aq) + e^- \rightarrow Na(s)$	-2.71
$Zn^{2+}(aq) + 2e^- \rightarrow Zn(s)$	-0.76
$Cu^{2+}(aq) + 2e^- \rightarrow Cu(s)$	0.34
$O_3(g) + 2H^+(aq) + 2e^- \rightarrow O_2(g) + H_2O(l)$	2.07
$F_2(g) + 2e^- \rightarrow 2F^-(aq)$	2.87

Table 1: *A partial list of E^0 values for the reduction of certain elements; for oxidation values, reverse the sign of E^0*

generated due to differences in electric potential between these two electrodes. The difference between the individual half-cell potentials of the two electrodes is referred to as the electromotive force, E, the sign of which determines the direction of the reaction.

A battery is an example of a galvanic electrochemical cell. The spontaneous exchange of electrons between two species is exploited upon battery discharge. The electrons are forced through an external circuit, powering a load. In a rechargeable, or secondary battery, the (re)charge process is the reverse: an external source of electricity is used to drive the electrons back towards the original electrode. The conservation of charge forces the lithium ions in the same direction. Such a configuration is illustrated in figure 1.

In all lithium ion batteries, it is the lithium atom, with an E^0 value of -3.04V, which is oxidized upon discharge. In transition metal lithium-ion batteries $Li_xM_yO_z$ (M = Ni, Mn, Co, V etc.) serves as the positive electrode and it is the transition metal that is reduced against the lithium. The E^0 value of Li^+ against graphite, which is typically used as the negative electrode in these systems, is -2.8V.

There are numerous other configurations of different metals which have been and are currently exploited for electrical energy storage and delivery, from the first prototype by Alessandro Volta, (using Zn/Cu), to the latest in nano-scale lithium iron phosphates.

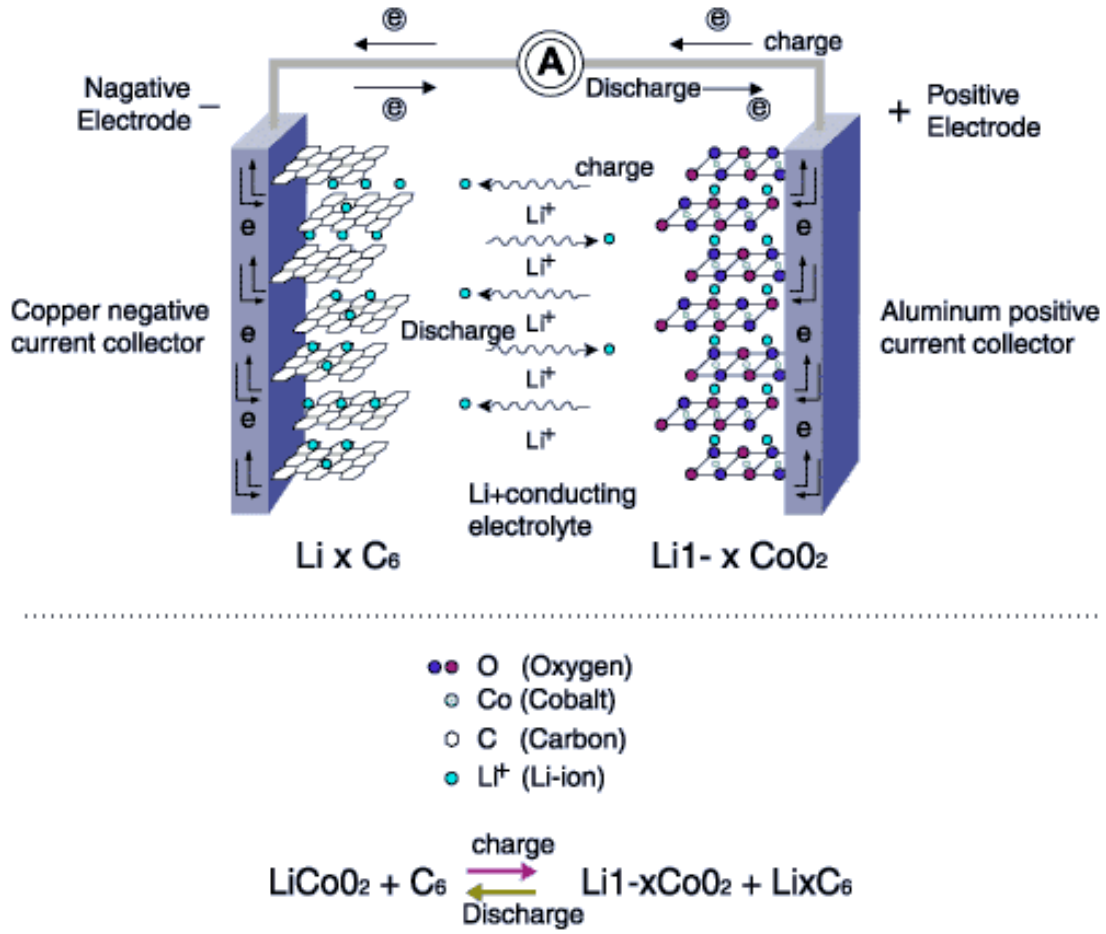

Figure 1: *A secondary lithium ion battery: Electrodes are separated by a semi-permeable membrane in a lithium salt-containing electrolyte that allows the passage of Li+ ions, while preventing the flow of electrons, forcing them instead through an external circuit.*
Electrons and ions flow toward the anode upon charge (motivated by an external voltage), and back to the cathode upon discharge (motivated by an overall positive E^{0}*; i.e. a chemically spontaneous reaction) producing electricity used to power a load, (A). (image taken from Gaston Nerada Lithium Battery Products, ref. i)*

In each case the ΔE^{0} of the reduction and oxidation reactions determines the maximum voltage; the amount of active material determines the capacity; the weight or size of the material determines the energy density; the rate of ion/electron motion throughout the

battery components and the voltages determine the current; the stability and amount of the materials in different circumstances determines the battery lifetime; the reactivity of the materials themselves determine the safety; and all factors combined will determine the batteries' applications.

B. Key Areas of Battery Research & Development

The current maximum specific energy capacity of standard lithium batteries remains below 500Wh/kg. In addition, lithium ion insertion/removal rates limit the maximum power (rate of energy delivery) to less than 700W/kg. Improvements sought in battery materials include: chemical stability of electrolyte salt/solvents to avoid side reactions; sufficient rate of electrode reaction so activation polarization is not too high (achievable through high surface area/porous electrode structure); adequate electrolyte transport to reduce IR polarization (porosity of electrode, structure of separator, etc.); optimized cell design to minimize electrode polarization; and mechanical as well as chemical stability of reaction products (esp. in secondary batteries). All of these requirements have to be met and of course still meet the requirements of a successful commercial product (availability of materials, cost, safety, low environmental impact). Future research will focus on reducing the ratio of inactive to active components to improve energy density, increasing conversion efficiency and re-chargeability, and maximizing performance under extreme conditions.[ii,iii]

Some key definitions relevant to battery research include the following: ***C-rate*** is the charge or discharge rate of a cell, expressed in terms of the capacity of a battery

divided by one hour (e.g. C for a 1600 mAh battery would be 1.6 A, C/5 for the same battery would be 320 mA and C/10 would be 160 mA); ***specific energy*** is the ratio of stored energy to weight of the cell; ***faradaic current*** is the current flow causing (or caused) chemical reactions (charge transfer) to occur at the electrode surfaces, versus ***capacitive current***, which does not involve any chemical reactions (or charge transfer), but is rather a result of accumulation (or removal) of electrical charges on the electrode/electrolyte solution interface near the electrode, and is therefore flowing when the potential of the electrode is changing and is generally zero when the potential is constant; ***faradaic efficiency*** is the efficacy with which charge is transferred in an electrochemical reaction (also called ***coulombic efficiency*** or ***current efficiency***); ***thermal runaway*** refers to a negative feedback cycle where an initial increase in temperature changes the conditions in a way that causes a further increase in temperature leading to a destructive result; ***depth of discharge (DoD)*** is an indication of the amount of capacity that has been removed from a battery and is expressed as a percentage of the total capacity of the battery; ***open-circuit voltage (OCV)*** refers to the no-load condition; a ***primary battery*** refers to a system which cannot be efficiently recharged by an electric current; a ***secondary battery*** refers to a rechargeable system; ***battery capacity*** is the electrical energy output of a cell before it reaches a specified final electrical condition (expressed in watt-hours, $W \cdot h$, where $W \cdot h = (A \cdot h)(V)$; ***rated capacity*** is the optimized capacity, under specific conditions; ***shelf-life*** is the period of time from the date of manufacture, at a storage temperature of $21^{o}C$, after which the cell retains a specific amount (e.g. 90%) of its original energy content; ***self-discharge*** is the effect of internal chemical reactions in the battery system causing a decrease in the availability of the

stored energy; ***end-point voltage*** is the limit below which the battery will not operate or operation is not recommended; ***nominal voltage*** is that of a fully charged cell when delivering rated current; ***deep/shallow charge/discharge*** is gauged with respect to the end-point voltage of the system; ***energy density*** is the ratio of stored energy to the total volume of the cell; ***cycle life*** is the average number of charge/discharge cycles that a battery can undergo before it loses its ability to hold a useful charge; ***polarization curve*** is a plot of the current against the electrode potential or cell voltage; ***overpotential*** is the difference between the electromotive force on open circuit and the voltage when a current is flowing, indicating the extra energy needed (i.e. energy loss, usually in the form of heat) to force the electrode reaction to proceed at a determined rate (also called ***polarization***).[ii,iv,v,vi]

C. Solid Electrolyte Interphase, or SEI

An important focus of research of conventional battery systems is the passivating layer of breakdown products that forms on the surfaces of the electrode particles from irreversible side reactions involving the electrolyte and electrode materials. Since the discovery of the concept and initial first use of the term Solid Electrolyte Interphase, or SEI, in the oft-referenced article by Emanuel Peled in 1979,[vii] there has been a flurry of activity in the battery world aimed at understanding this phenomenon which has, in recent years, been found to be of even more critical importance than was initially recognized. Initially the SEI was thought to only occur on the anode side, but it was later recognized that such passivation layers, though different in chemical make-up,

accumulate on the cathode electrodes as well.[viii,ix,x,xi] Similar analyses have been conducted on the SEI formation on various forms of graphite, as well as lithium metal anodes, and on most of the key lithium metal oxide cathode materials. The role of the SEI has been shown to affect the safety, self-discharge (shelf-life), power capability (charge/discharge rate), high/low temperature performance, cycle life, faradaic efficiencies, and irreversible capacity losses.

Thus far, most of the relevant research has focused on: the effects on the SEI of various electrolyte mixtures, performance-enhancing electrolyte additives, salt compositions and/or electrode components; the thermal stability/dependence of the SEI (and therefore the complete battery system); and the performance of the batteries with respect to SEI growth and composition.

Peled initially asserted that "the electrochemical behavior of the electrodes will be governed by the properties of the SEI, including: its morphology (compact or porous, size of the crystallites); its thickness; the type and the concentration of the lattice defects; the transference numbers of electrons (t_e), cationic defect (t_+), anionic defect (t_-); [and] the mobility of these defects."[vi] The thickness of the anodic SEI was believed to be in the range of 15-25Å, and thought to depend on the electron tunneling range across the grain boundaries within the electrode. In the overall picture of ion kinetics through the battery, there are generally three steps: (i) the lithium ion crosses the solution/SEI interface, (ii) it migrates through the SEI via Shottky vacancies, and finally (iii) crosses the SEI/electrode interface, entering the bulk of the electrode, accepting an electron therein. In the case of a highly conductive, thinly deposited SEI, the charge transfer reaction at one of the SEI interfaces may be the rate-determining step. When the SEI, which has solid ionic lattice

components, grows to a certain thickness, however, the rate determining step becomes the migration of the ions through that lattice, further illuminating the importance of the role that the SEI plays.

Since the initial studies on the topic, the SEI has been thought to be composed of a multi-layer of different conglomerations of breakdown components. These multi-layers are depicted in terms of an equivalent circuit with an overall resistance in the range of 10 to 1000 Ω/cm^2.[xii,xiii,xiv] Each homogeneous layer/region is represented as a component in the circuitry with an assigned dielectric constant, measure of ionic conductivity, energy of activation, etc. The component in the circuitry presumed to be the most significant in term of its contribution to the overall resistance is the grain-boundary resistance, associated with the crossover of ions from particle to particle through grain boundaries perpendicular to the current flow (or parallel to the field lines).[xi]

Across the spectrum of investigations, there remain several generally accepted characteristics of what makes a desirable SEI, including: a thin, completely protective film which causes minimal voltage delay at the beginning of discharge but which will reform rapidly following a high current discharge pulse,[xv] one that protects the electrode from (further) exfoliation, prevents co-intercalation of solvent and/or salt compounds; one that remains stable at elevated operating or storage temperatures, high voltages (up to 4.5V); has low values for t_- and t_e, values close to unity for t_+, and a reduced resistivity value through the SEI;[vi] and finally, meets the flexibility requirements demanded of an expanding/contracting electrode (which occurs in some materials due to repeated intercalation/deintercalation).

[i] "Gaston Nerada Lithium Battery Products FAQ." *Gaston Nerada Lithium Battery Products*. Gaston Nerada Int'l Ltd. Dec 2009 <http://www.gaston-narada.com/tech-certificates.html>.

[ii] Sadoway, M. "Portable Power: Advanced Rechargeable Lithium Batteries." *MRS Bulletin* 27.8 (2002): 590-596.

[iii] Linden, D. and T. B. Reddy. *Handbook of Battery Materials*, 3rd ed. New York: McGraw-Hill, 2001.

[iv] Nagy, Zoltan. *Electrochemistry Dictionary*. 2008. Case Western Reserve University. Dec 2008 <http://electrochem.cwru.edu/ed/dict.htm>.

[v] Randolph, Curtis. "Glossary of Technical Battery Terminology." *Green Batteries*. 2008. Responsible Energy Corporation. Dec 2008 <http://www.greenbatteries.com/batteryterms.html>.

[vi] "Lithium Battery." *Wikipedia*. 2008. Wikimedia Foundation, Inc.. 28 Jan 2009 <http://en.wikipedia.org/wiki/Lithium_battery>.

[vii] Peled, E. "The Electrochemical-Behavior of Alkali and Alkaline-Earth Metals in Non-Aqueous Battery Systems - the Solid Electrolyte Interphase Model." *Journal of the Electrochemical Society* 126.12 (1979): 2047-2051.

[viii] Balasubramanian, M., H. S. Lee, X. Sun, X. Q. Yang, A. R. Moodenbaugh, J. McBreen, D. A. Fischer and Z. Fu. "Formation of SEI on Cycled Lithium-Ion Battery Cathodes: Soft X-Ray Absorption Study." *Electrochemical and Solid-State Letters* 5.1 (2002): A22-A25.

[ix] Aurbach, D., B. Markovsky, A. Rodkin, E. Levi, Y. S. Cohen, H. J. Kim and M. Schmidt. "On the Capacity Fading of $LiCoO_2$ Intercalation Electrodes: The Effect of Cycling, Storage, Temperature and Surface Film Forming Additives." *Electrochimica Acta* 47.27 (2002): 4291-4306.

[x] Aurbach, D., K. Gamolsky, B., Y. Gofer, M. Schmidt and U. Heider. "On the Use of Vinylene Carbonate (VC) as an Additive to Electrolyte Solutions for Li-Ion Batteries." *Electrochimica Acta* 47.9 (2002): 1423-1439.

[xi] Aurbach, D., B. Markovsky, M. D. Levi, E. Levi, A. Schechter, M. Moshkovich and Y. Cohen. "New Insights into the Interactions Between Electrode Materials and Electrolyte Solutions for Advanced Nonaqueous Batteries." *Journal of Power Sources* 81-82 (1999): 95-111.

[xii] Peled, E., D. Golodnitsky and G. Ardel. "Advanced Model for Solid Electrolyte Interphase Electrodes in Liquid and Polymer Electrolytes." *Journal of the Electrochemical Society* 144.8 (1997): L208-L210.

[xiii] Thevenin, J. G. and R. H. Muller. "Impedance of Lithium Electrodes in a Propylene Carbonate Electrolyte." *Journal of the Electrochemical Society* 134.2 (1987): 273-280.

[xiv] Aurbach, D. and A. Zaban. "Impedance Spectroscopy of Lithium Electrodes: Part 1. General Behavior in Propylene Carbonate Solutions and the Correlation to Surface Chemistry and Cycling Efficiency." *Journal of Electroanalytical Chemistry* 348 (1993): 155-179.

[xv] Vincent, C. A. "Lithium Batteries: A 50-year Perspective, 1959-2009." *Solid State Ionics* 134.1-2 (2000): 159-167.

III. Nuclear Magnetic Resonance

A. Fundamentals

The entire field of nuclear magnetic resonance (NMR) spectroscopy is based on the very existence of non-zero nuclear spin angular momenta, and by corollary, inherent nuclear magnetic moments. The foundation of the NMR experiment is based on the fact that it is possible to non-destructively perturb these magnetic moments as they precess along a uniaxial magnetic field and glean information about the system from the energy re-radiated during relaxation back to their equilibrium states. The ratio of the nuclear spin angular momentum, $\boldsymbol{I}$, to the magnetic moment, $\boldsymbol{\mu}$, is called the gyromagnetic ratio, γ: $\boldsymbol{\mu} = \gamma \boldsymbol{I}$. The value of γ is proportional to the nuclear magneton, μ_p and to the charge/mass ratio of the nucleus: $\gamma = \frac{\mu_p}{\hbar} g = \frac{e}{2m_p} g$, where g is the nuclear g-factor. The relevance of NMR to chemical materials is alone due to the fact that the values of γ are distinct for every atomic isotope with a non-zero nuclear spin (see table 1 for a partial list). This means that in the presence of an external magnetic field, each nucleus will precess about the axis of that field at a unique frequency. This is called the Larmor frequency, ω_o, and is simply: $\omega_o = \gamma B_o$, where B_o is the strength of the field in Tesla (T). The elementary properties of angular momentum dictate that nuclear spin is specified by a quantum number (I) with integer or half-integer values, while the z-component, (I_z) along the $\boldsymbol{B_o}$-field direction is represented by m, and quantized: $m = -I, -I+1, \ldots I-1, I$. In that the spin magnitude has a constant value of $\hbar [I(I+1)]^{1/2}$, the quantization of I_z implies

a total of $2I+1$ possible orientations of spin angular momentum in the presence of a magnetic field. The orientations correspond to the z-component of the spin via Planck's constant: $\boldsymbol{I}_z = m\hbar$.

The *z*-component of the magnetic moment is in turn quantized as: $\mu_z = m\gamma\hbar$ and the energy of the dipole, when placed in a field, is the quantized Zeeman energy: $E = \mu_z B_0 = -m\gamma\hbar B_0$. Different spin orientations correspond to different energy levels and the difference between the adjacent energy levels is given as: $\Delta E = \gamma\hbar B_0$. NMR is the process of inducing this excitation, using a radiofrequency (rf) pulse chosen to match the inherent precession frequency of the nucleus, and then detecting the signal that is produced as the system relaxes back to its thermal equilibrium.

The usefulness of NMR lies in the fact that this resonant frequency is highly sensitive to the magnetic and electronic environment about the nucleus of interest. For example the external magnetic field can induce additional magnetic fields through the induction of electron currents in the surroundings of the nucleus. These additional fields

Nuclei	Spin (***I***)	γ ($s \cdot T^{-1}$)	$\nu_o = \omega_o/2\pi$, at B_0 = 7.04T
^{1}H	½	26.75	300.00
^{6}Li	1	3.93	44.14
^{7}Li	⅗	10.39	116.56
^{11}B	⅗	8.58	96.27
^{13}C	½	6.72	150.90
^{19}F	½	25.18	282.39
^{51}V	⅞	7.04	84.41

Table 1: *Partial list of nuclei, their spin, gyromagnetic ratios, and frequencies in a 7.04T field.*

act by reducing (shielding) or augmenting (deshielding) the external magnetic field. This slight change in the field correspondingly modifies the resonant frequencies (ΔE). So the same nuclei located in different environments can resonate at slightly different frequencies. This phenomenon is called the chemical shift, as it manifests as a frequency shift due to changes in the chemical structure. It is explained in more detail in the following section.

According to Boltzmann statistics the above-mentioned thermal equilibrium is given (for a spin-½ nucleus) as:

$$\frac{N_\beta}{N_\alpha} = e^{-\frac{\Delta E}{k_B T}} \approx 1 - \frac{\Delta E}{k_B T} = 1 - \frac{\gamma \hbar B_0}{k_B T} \qquad \textit{Equation 1}$$

where N_β is the number of nuclei in the excited state; N_α is the number of nuclei in the ground state; and k_B is the Boltzmann constant.

At room temperature N_β - N_α is only on the order of 10^{-6}. When the sample is irradiated during an NMR experiment, the populations of the states are equalized. Therefore the overall amount of energy re-radiated is quite small, given the small number of nuclei being excited. Therefore it is often necessary in an NMR experiment to repeat this process tens, and sometimes thousands of times in order to get decent signal resolution. The mechanism by which individual nuclei relax back to thermal equilibrium (re-alignment along the external magnetic axis) after saturation is mediated by longitudinal, or T_1 relaxation and follows an exponential relation with respect to time:

$$M_z = M_0\left(1 - e^{-\frac{t}{T_1}}\right), \qquad \textit{Equation 2}$$

where M_0 and M_z are measurements of the equilibrium magnetization and the magnetization at subsequent times, t, respectively. Another type of relaxation is that relating to the coherence of the spin precessions. When a sample containing an ensemble of identical nuclear spins is initially perturbed by an rf pulse, each spin will precess according to the nature of its surrounding environment. Slight physical/chemical differences in these surroundings cause the precession rates to differ slightly, and the spins fall out of synchronization with each other. This phenomenon is mitigated by transverse relaxation, as characterized by a time constant, T_2, and is inversely related to the frequency spectrum width. The equations that describe these dynamics are:

$$M_y = -M_0 \cos(\omega_0 t) e^{-\frac{t}{T_2}} \qquad \textit{Equation 3}$$

and

$$M_x = -M_0 \sin(\omega_0 t) e^{-\frac{t}{T_2}}, \qquad \textit{Equation 4}$$

where M_y and M_x are the magnetizations in the y- and x-direction, respectively.

The signal re-radiated from the sample in the NMR experiment as a result of the initial excitation pulse is in the form of an oscillating magnetization vector. This magnetization induces a current in a nearby pick-up coil, creating an oscillating electrical signal. This signal, called the free induction decay, or FID, is essentially a sum of all of the spin signals. In order to 'see' this on a frequency scale, the signal must be Fourier transformed (see figure 1).

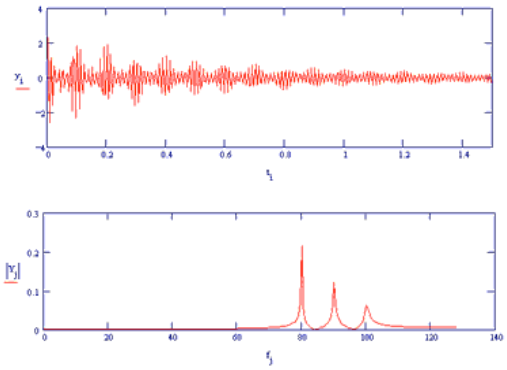

Figure 1. *An example of a free induction decay (fid) signal, and its associated Fourier transform; the length of the fid corresponds to the narrowness of the signal; the magnitude of the fid corresponds to the integrated intensity of the signal.*

B. NMR Spin Hamiltonians

The full nuclear spin Hamiltonian (in diamagnetic, nonconducting substances) is composed of seven terms: H_Z, the external static field, or Zeeman interaction; H_{RF}, the externally applied orthogonal field; H_{CS}, the chemical shift term; H_D, the dipole-dipole interaction; H_Q, the quadrupolar interaction; H_J, the J-coupling, or indirect dipole-dipole interaction; and H_{SR}, the spin rotation interaction. All but the last two, which are relatively insignificant in most solid-state systems, are described below:

$$\boldsymbol{H}_{\boldsymbol{Z}} = -B_z \sum_i \gamma_n^i I_z^i = -\sum_i \omega_o^i I_z^i \qquad \textit{Equation 5}$$

$$\boldsymbol{H}_{\boldsymbol{RF}} = -B_1(t)\cos(\omega_{RF} t)\sum_i \gamma_n^i I_x^i \qquad \textit{Equation 6}$$

$$\boldsymbol{H}_{CS} = \sum_i \gamma_n^i \vec{I}^i \otimes \vec{\sigma}^i \otimes \vec{B} \qquad \textit{Equation 7}$$

$$\mathbf{H}_{D} = \sum_{i<k} -2\gamma_n^i \gamma_n^k \hbar \sum_{\alpha,\beta=1}^{3} \left[\vec{I}_\alpha^i \bullet D_{\alpha\beta}^{ik} \bullet I_\beta^k \right] \qquad \textit{Equation 8}$$

$$\boldsymbol{H}_{Q} = \sum_i \frac{eQ^i}{6\hbar I^i (2I^i - 1)} \left[\vec{I}^i \otimes \vec{V}^i \otimes \vec{I}^i \right] \qquad \textit{Equation 9}$$

The **Zeeman interaction** is described in the previous section; it represents the basic interaction of the spins with the external magnetic field, B_o, and has energies of $\Delta E = \gamma \hbar B_0$.

The **radiofrequency Hamiltonian** represents the interaction of the spin system with the externally applied transverse field introduced in a pulsed NMR experiment. The maximum amplitude, $B_1(t)$, is determined by the limitations of the probe circuitry, and the frequency, ω_{RF}, is chosen to match the Larmor frequency, ω_L. This perturbation introduces a time-dependence into the spin system *in the stationary frame*. A coordinate transform to a *rotating coordinate frame* may be made, thereby removing the time-dependence:

$\boldsymbol{H}_{lab} = -\gamma B_o I_z - 2\gamma B_1 cos(\omega t I_x) \quad \rightarrow \quad \boldsymbol{H}_{rot} = -\gamma B_o I_z + \omega I_z - \gamma B_1 t$

re-establishing the applicability of the time evolution operator, which will be relevant in the NMR pulse sequence section below.

The **chemical shift Hamiltonian** represents the interaction of the nuclear spin with the local magnetic field, $\boldsymbol{B}_o'$. $\boldsymbol{B}_o'$ is the local field felt by the nucleus that is induced by the motion of the surrounding electron(s) that are circulating in response to the primary magnetic field, $\boldsymbol{B}_o$. $\boldsymbol{B}_o'$ is calculated as the product between a quantity called the

chemical shielding tensor, $\boldsymbol{\sigma}$, and the primary magnetic field, $\boldsymbol{B_o}$, as indicated in Equation 7. As the electronic distribution about the nucleus is rarely spherically symmetric, the resulting interaction depends on the relative orientation of the molecule with respect to the axis of the external magnetic field. This anisotropic interaction is contained in $\boldsymbol{\sigma}$, is a tensor of rank two, which can be written in spherical polar coordinates. In the solid state only the secular terms affect the energy levels and the equation is reduced to:

$$\mathbf{H}_{\mathbf{CS}} = -\sigma_i \omega_o I_z - \frac{1}{2}(3\cos^2\beta - 1)(\sigma_{zz} - \sigma_i)\omega_o I_z$$

where β is the polar angle between the principle magnetic field direction and the principal axis system of the tensor $\boldsymbol{\sigma}$. These two terms of the equation represents the isotropic and anisotropic chemical shift interaction, respectively.

The **dipolar interaction** describes the effect of neighboring (homo- and heteronuclear) dipoles on a nuclear spin system. Equation 8 can be written in expanded (linear) form:

$$\mathbf{H}_{\mathbf{D}} = \frac{\mu_o}{4\pi}\sum_{i<k}\left(-\frac{\gamma_n^i \gamma_n^k \hbar}{r_{ik}^3}\right)\left[\frac{3(\vec{I}^{\,i}\cdot\vec{r}_{ik})(\vec{I}^{\,k}\cdot\vec{r}_{ik})}{r_{ik}^2} - \vec{I}^{\,i}\cdot\vec{I}^{\,k}\right].$$

The components of the rank-two tensor matrix **D** are simply the coefficients of the $I_\alpha^i I_\beta^k$ terms in this expression.

In order to apply rotational transformations it is useful to transform this expression from Cartesian coordinates into spherical tensor representation. This is done by first writing I_x^1 and I_y^1 in terms of the raising and lowering operators, $I^+ = I_x + iI_y$ and $I^- = I_x - iI_y$, then expressing *x, y* and *z* in terms of r, θ, ϕ spherical harmonics, Y_{lm}, where l=2, therefore m=±2, ±1, 0. The full expression is given as:

$$\mathbf{H}_{\mathbf{D}} = \left(\frac{\mu_o}{4\pi}\right)\hbar^2\gamma_1\gamma_2\frac{1}{r^3}(A+B+C+D+E+F),$$

where

$$A = (1-3\cos^2\theta)I_{1z}I_{2z}$$

$$B = -\frac{1}{4}(1-3\cos^2\theta)(I_1^+I_2^- + I_1^-I_2^+)$$

$$C = -\frac{3}{2}\sin\theta\cos\theta e^{-i\phi}(I_1^+I_{2z} + I_{1z}I_2^+)$$

$$D = C^* = -\frac{3}{2}\sin\theta\cos\theta e^{i\phi}(I_1^-I_{2z} + I_{1z}I_2^-)$$

$$E = -\frac{3}{4}\sin^2\theta e^{-i2\phi}I_1^+I_2^+$$

$$F = E^* = -\frac{3}{4}\sin^2\theta e^{i2\phi}I_1^-I_2^-$$

The strength of the dipolar interaction is significant; for r_{ij} = 1.5A between two protons for example, the strength of the interaction is on the order of 100kHz. The normal tumbling motion of a liquid averages out this interaction. In solid systems the nuclear distances are fixed therefore these interactions are not averaged out and can dominate the spectra. However it is only the secular (diagonal) terms which commute with the Zeeman Hamiltonian and therefore A, (and when the spins are the same, B) affect the energy to first order (the effect of the remaining terms is on the order of 10^3 times weaker). This simplifies the interaction to:

$$\mathbf{H}_{\mathbf{D}} = \frac{1}{2}\left(\frac{\mu_o}{4\pi}\right)\hbar\gamma^2\sum_{i<j}\frac{1}{r_{ij}^3}(1-3\cos^2\theta_{ij})\left[3I_{iz}I_{jz} - \vec{I}_i\cdot\vec{I}_j\right]$$

over all spins.

The **quadrupolar term** represents the interaction between any spin > ½ nuclei with the local electric field gradient. Equation 9 can be written in expanded form as:

$$\boldsymbol{H}_{\boldsymbol{Q}} = \frac{eQ}{6\hbar I(2I-1)}\sum_{\alpha,\beta=1}^{3}V_{\alpha\beta}\left[\tfrac{3}{2}(I_\alpha I_\beta + I_\beta I_\alpha) - \delta_{\alpha\beta}(I)^2\right],$$

where the term eQ represents the nuclear quadrupole moment and $V_{\alpha\beta}$ is the second

derivative of the electric potential, $\frac{\partial^2 V}{\partial\alpha\partial\beta}$, at the location of the *i*th nucleus.

It is useful to define

eq,

e being the magnitude of the electric charge, and q the electric field gradient, EFG; and

$$\eta = \frac{V_{xx} - V_{yy}}{V_{zz}},$$

the EFG asymmetry parameter, with respect to the principal axis of the nucleus.

The equation (for a single spin system only) is now re-written as:

$$\mathbf{H}_{\mathbf{Q}} = \frac{e^2 qQ}{4\hbar I(2I-1)}\left[3I_{z,PAF}^2 - I^2 + \frac{1}{2}\eta(I_{x,PAF}^2 - I_{y,PAF}^2)\right].$$

However this equation is now defined with respect to the principal axis system of the nucleus; therefore a rotation into the laboratory frame (that is, with respect to the main B_o field) is necessary as well, in order to be in the same frame of reference as all of the other interactions. The product of this rotation is the final expression:

$$\begin{aligned}\mathbf{H}_{\mathbf{Q}} = \frac{e^2 qQ}{4\hbar I(2I-1)}\Big\{&\tfrac{1}{2}(3\cos^2\theta - 1)(3I_z^2 - I^2) \\ &+ \tfrac{3}{2}\sin\theta\cos\theta\left[\vec{I}_z,(\vec{I}^{+} + \vec{I}^{-})\right] \\ &+ \tfrac{3}{4}\sin^2\theta[(I^{+})^2 + (I^{-})^2]\Big\},\end{aligned}$$

where the terms are listed in order of strength, with respect to their effect on the Zeeman energy splittings. Clearly this entire expression, and therefore the effect of the quadrupolar interaction on the Zeeman energy, is zero when there is no electric field gradient, i.e. in cases of high symmetry in the electron distribution about the nucleus.

C. Magic angle spinning (MAS) NMR

In a liquid sample many of the interactions described above average out through normal rapid tumbling motion. In a solid sample the inter-nuclear distances are fixed, as is (in a static experiment), the orientation of each nucleus with the magnetic field. This leads to a large distribution of chemical shifts, along with the broadening due to dipolar effects, and in the case of a spin > ½ nucleus and a locally asymmetric electric field, quadrupolar effects. This fine distribution is usually broad and featureless. However in the case where the dominant broadening effect is from the chemical shift distributions, these spectra are referred to as chemical shift anisotropy (CSA) powder patterns and can sometimes display clear distributions of chemical shifts that correspond to chemical shift tensors, which relate to the symmetry of the molecules in the sample. Most of the time however, particularly in samples in which there exist more than one unique nuclear environment, these features are not easily analyzable. Therefore techniques have been developed to suppress these interactions, averaging out some of the interactions. The best results in terms of improved, and sometimes liquid-like resolution are from spinning the sample at high speeds, to simulate motional averaging. As can be seen in the equations above for each of the interactions, the anisotropic term of the chemical shift interaction, the dipolar interaction, and the first order quadrupolar interaction all contain the factor $(3\cos^2\theta - 1)$, where θ is the angle that the principal axis system of the nucleus makes with the main axis of the B_o field. Therefore if the spinning of the sample (rotor) is executed at the particular angle of $\theta = 54.44^{o}$, this term is zero and those three interactions are suppressed, leaving only the isotropic chemical shift term, $\sigma_i \omega_o I_z$, and any higher order

quadrupolar interactions, provided that the spinning speed exceeds the strength of the couplings, in Hz (see figure 3).

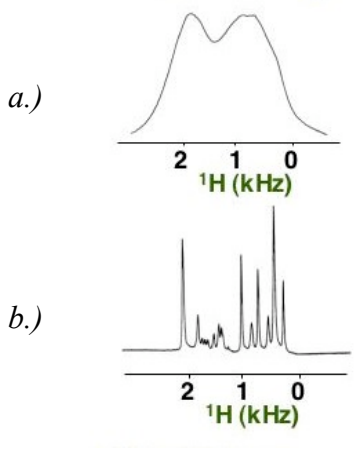

Figure 2. *a.) static spectrum b.) MAS spectrum, spinning at 5000Hz, at the magic angle 54.44°*

D. NMR Pulse Sequences

A simple mathematical description of the effects of radiofrequency pulses applied to spin states in a magnetic field is possible through the use of exponential operators, in particular, rotational exponential operators, such as the type used in classical systems for angular momentum. In this case, the angular momentum operator, L_α in the exponential is simply replaced with the *spin* angular momentum operator, acting on spin vectors instead of spatial vectors. The following is a generic form for a rotation about axis α by angle ϕ:

$$\hat{R}_\alpha(\phi) = e^{-i\phi\bar{I}_\alpha} \ .$$

A rotational transformation of a vector is written as:

$$\hat{\Psi}' = \hat{R}_\alpha(\phi)\hat{\Psi}\hat{R}_\alpha(\phi)^{-1},$$

where $\hat{\Psi}$ is the operator being rotated, and $\hat{\Psi}'$ is the rotated operator. An example of this

is the rotation about the *x*-axis by an angle ϕ of a spin vector initially oriented along the *z*-axis:

$$\hat{R}_\alpha(\phi)\hat{I}_z\hat{R}_\alpha(\phi)^{-1} = e^{-i\phi\hat{I}_x}\hat{I}_z e^{+i\phi\hat{I}_x}$$

using the exponential expansion: $e^{\hat{A}} = 1 + \hat{A} + \frac{\hat{A}^2}{2!} + \frac{\hat{A}^3}{3!} + \ldots$

the right hand side of this equation becomes:

$$= \left(1 - i\phi\hat{I}_x - \frac{\phi^2}{2}\hat{I}_x^2 - \frac{\hat{\phi}^3}{6}\hat{I}_x^2 + \ldots\right)\hat{I}_z\left(1 + i\phi\hat{I}_x - \frac{\phi^2}{2}\hat{I}_x^2 + \frac{\hat{\phi}^3}{6}\hat{I}_x^2 + \ldots\right)$$

$$= \hat{I}_z - i\phi\left[\hat{I}_x,\hat{I}_z\right] - \frac{\phi^2}{2}\left[\hat{I}_x,\left[\hat{I}_x,\hat{I}_z\right]\right] + \frac{i\phi^3}{6}\left[\hat{I}_x,\left[\hat{I}_x,\left[\hat{I}_x,\hat{I}_z\right]\right]\right] + \ldots$$

and using the commutation relations of the spin operators: $\left[\hat{I}_y,\hat{I}_z\right] = i\hat{I}_x\varepsilon_{xyz}$

$$= \hat{I}_z + \phi\hat{I}_y - \frac{\phi^2}{2}\hat{I}_z - \frac{\phi^3}{6}\hat{I}_y + \ldots$$

$$= \hat{I}_z\left(1 - \frac{\phi^2}{2} + \ldots\right) + \hat{I}_y\left(\phi - \frac{\phi^3}{6} + \ldots\right)$$

$$= \hat{I}_z\cos\phi + \hat{I}_y\sin\phi.$$

which is just $\hat{I}_y$ if $\phi = \frac{\pi}{2}$.

Besides the single (90°) pulse, two other simple sequences were used for these experiments. The first was a 90_x-τ-180_x-τ echo sequence used to minimize the probe background signal (used in the CF_x project, section V.C.). Using this same procedure, this sequence can be illustrated by the application of four successive operations: the 90° rotation about *x*, the chemical shift evolution during time τ, a 180° rotation about *y*, and then the chemical shift evolution once again before signal acquisition:

$$\hat{I}_z \xrightarrow{\frac{\pi}{2}\hat{I}_x} -\hat{I}_y \xrightarrow{\omega t\hat{I}_z} -\hat{I}_y\cos(\omega t) + \hat{I}_x\sin(\omega t) \xrightarrow{\pi\hat{I}_y}$$

$$-\hat{I}_y\cos(\omega t) - \hat{I}_x\sin(\omega t) \xrightarrow{\omega t\hat{I}_z} -\hat{I}_y$$

The usefulness of this transformation is not obvious. We had the fortuitous situation of the background signal exhibiting a much smaller T_2^* than our samples. Therefore the echo sequence basically acted as a filter for the species with shorter T_2^* times (i.e. the background) by providing a delay in acquisition without compromising the rest of the signal.

The quadrupole echo, 90_x-τ-90_y-τ, is the second sequence, used in the SVO project, section V.B). The dephasing of the signal in a quadrupolar system caused by the precession under the tensor interactions causes a rapid loss of signal that is often undetectable. The particular rotations in the solid echo, or quadrupole echo, are well suited to effectively reverse this precession and produce a clear echo signal. It is illustrated thus, where ω_Q is the 'quadrupolar precession frequency:

$$\hat{I}_{1z} \xrightarrow{-\frac{\pi}{2}(I_{1x}+I_{2x})} \hat{I}_{1y} \xrightarrow{\omega_Q\tau\hat{I}_{1z}\hat{I}_{2z}} \hat{I}_{1y}\cos(\Delta\omega_Q t) + 2\hat{I}_{1x}\hat{I}_{2x}\sin(\Delta\omega_Q t) \xrightarrow{-\frac{\pi}{2}(I_{1y}+I_{2y})}$$

$$\hat{I}_y\cos(\Delta\omega_Q\tau) + 2\hat{I}_{1x}\hat{I}_{2x}\sin(\Delta\omega_Q\tau) \xrightarrow{\omega_Q\tau I_{1z}I_{2z}} \hat{I}_y$$

The recovered signal is re-phased in +*y*.

References used for the previous three sections on NMR theory include:

Slichter, C. P. *Principles of Magnetic Resonance*, 2nd Ed. Berlin: Springer-Verlag, 1980.

Haeberlen, Ulrich. *High Resolution NMR in Solids Selective Averaging* New York:

Academic Press, 1976.

Duer, Melinda. *Introduction to Solid State NMR Spectroscopy* Boston: Wiley-Blackwell Publishers, 2005.

Callaghan, Paul. *Principles of NMR Spectroscopy*. Oxford: Clarendon Press, 1991.

E. NMR as applied to battery research

Solid-state nuclear magnetic resonance (NMR) spectroscopy has been employed to characterize a variety of phenomena that are central to the functioning of lithium and lithium-ion batteries, including the nature of the SEI and its formation. As detailed above, NMR is sensitive to many physical parameters that are relevant to battery systems. These include Li-ion mobility, electronic conductivity, and the changes of valence or electronic structure of the cations involved in the electrochemical processes. The following list is by no means comprehensive, but just offered as a sampling of the usefulness of this technique in different aspects of battery research, with a particular focus on the SEI.

NMR can be conducted on both solid and liquid samples, however there are limitations on spectral resolution of the former due mainly to chemical shift anisotropy, nuclear dipole-dipole and quadrupolar interactions. The presence of unpaired electrons associated with transition metal ions that are found in most positive electrode materials can also be a source of spectral broadening.[i] Hence in the case of a solid sample, MAS is employed to obtain better resolutions by averaging these interactions. NMR is nuclei-specific, however not all nuclei are NMR-active (e.g. ^{16}O), and among those that are, not all occur at sufficiently high natural abundances (e.g. ^{13}C). However among those that do

are ^{7}Li, ^{19}F, ^{29}P and upon isotopic enrichment, ^{13}C, all of which are highly relevant to lithium batteries and SEI formation. In addition, each local environment in a solid gives rise to its own distinct resonance, and as long as the environments are sufficiently different, these local environments can be resolved and quantified.[ii]

There are two main disadvantages of NMR. The first is that it is not easily amenable to in-situ measurements, that is, the cell must be disassembled and the powdered electrode material removed from the current collector prior to running the NMR experiment. The second is that because the energy transitions are in the radiofrequency range, the NMR signal intensities are generally low compared to optical or x-ray spectroscopies, thus often requiring tens of milligrams of sample. This latter attribute can present a significant challenge to SEI investigation due to the relatively low number of nuclei residing in the SEI. Nevertheless, the advent of higher magnetic fields and thus NMR frequencies has made these studies possible.

Since each local environment in a sample gives rise to a distinct resonance, and as long as the environments are sufficiently different, these local environments can be resolved and quantified. For instance, the chemical shift of lithium ions intercalated into a graphite anode exhibits Knight shift interactions, implying a metallic environment associated with lithium-intercalated graphite. Non-intercalated SEI lithium ions, however, do not display this shift, and are therefore easily distinguishable. Exploiting this, Smart et al. were able to quantify the non-intercalated Li ions in cycled batteries, and calculate the reversible and irreversible capacities of graphite as a function of various electrolyte solutions.[iii] On the same basis, Wang et al. quantitatively compared the SEI shift in samples held at different storage temperatures, noting an approximate 10%

increase in SEI formation on cathodes subjected to accelerated aging at 70°C versus 50°C, and almost no difference in the two anode samples under similar aging conditions. (The SEI signal was also shown to decrease by almost one-half in the same samples, pre- and post-rinsing in dry DMC solution.)[iv] Using this information, further work was conducted comparing the irreversible lithium losses at low temperatures using a variety of solvent mixtures and alkyl esters as co-solvents. Improved performance was noted in the ternary (EC, DMC and DEC) versus the binary solvent mixtures.[v] Menetrier *et al.* investigated a series of electrochemically intercalated $LiCoO_2$ cathodes and was able to track the biphasic domain in the cathode by the extent of the Knight shift of the lithium resonance.[vi] The same group investigated a series of mixtures of Li_2CO_3 and active material to shed light on the effect of proximity of Li_2CO_3 in the SEI layer to the active material.[vii] Grey and Lee compiled a review of the utility of lithium NMR in the study of lithium battery cathode materials, detailing the rigorous interpretations of the NMR data which are possible, and from which structural and electronic configurations in these materials can be very accurately determined.[viii] Several examples follow: ^{7}Li NMR measurements were used by Levasseur et al. to show that Ni^{3+} ions are the only paramagnetic species in the $LiCo_{1-y}Ni_yO_2$ phases while in the overlithiated complex, Ni^{3+} and intermediate spin Co^{3+} are indicated.[ix] This suggested the existence of structural defects associated with O vacancies, responsible for the suppression of the electronic delocalization and of the lithium/vacancy ordering upon lithium deintercalation in those systems. In other studies by the same group, ^{7}Li MAS NMR was performed on a variety of mixed-valence lithium cathode materials to monitor the oxidation states of the metallic species. For example, in a spectrum of Li_xCoO_2 materials, the data indicated the presence

of paramagnetic low-spin Co^{2+} and simultaneous cobalt and oxygen deficiencies.[x] In a similar study, the NMR data was used to suggest that the intermediate spin Co^{3+} ions were trapped in a square-based pyramidal environment because of an oxygen vacancy.[xi] In a study by Tucker et al. NMR was used to show that the local atomic and electronic structures of $Li_{0.5}CoO_2$ approach that of spinel phase, in addition to providing evidence of the coexistence of a diamagnetic Co^{3+} environment and a paramagnetic mixed-valence $Co^{3+/4+}$ environment, via NMR peaks arising from the vicinal lithium ions.[xii] Furthering these ideas, another group used both ^6Li and ^7Li NMR to suggest that only a small fraction (< 20%) of the excess Li in $Li_{y=0.35}CoO_2$ enters the structure ionically, reducing the formal cobalt valence.[xiii] The local and long-range structures of $LiZn_xMn_{2-x}O_4$ were also studied using ^6Li MAS NMR, indicating the presence of Li in the octahedral sites of the spinel structure, suggesting that Zn substitutes for lithium in the tetrahedral sites.[xiv] Another application of ^6Li MAS NMR was as a probe of lithium local environments in a series of layered metal-doped $LiCoO_2$ compounds in which a series of resonances are seen which indicated Cr^{3+} occupancy of the first and second cation coordination sphere surrounding Li.[xv] The size and sign of the shifts, caused by a transferred hyperfine interaction, were found to be dependent, and therefore provide information on, the Li-O-Cr bond angle. Carlier et al. monitored the Ni^{3+} to Ni^{4+} oxidation which occurs at the onset of deintercalation, leading to Ni^{3+}/Ni^{4+} hopping as an exchange of the ^7Li NMR signal was observed which was characteristic of a contact shift due to paramagnetic low spin Ni^{3+}.[xvi] The data collected allowed for discrimination between an electronic and an ionic exchange phenomenon, in addition to elucidating the Ni/Co hopping mechanism. The non-localization of the low spin Co^{4+} ions was also evidenced by the spectral data.

The results in a study by Kerlau et al. confirmed that NMR spectroscopy can also be used to probe particle isolation in these electrodes, a phenomenon responsible for the capacity and power fades since some of the active material particles are disconnected from the matrix.[xvii] This study also clearly showed the loss of electrochemically active lithium as the power fade increased. In a study of CF_x electrode materials, the evolution of some physico-chemical parameters such as the nature of the C-F bond and the structure of the fluorocarbon matrix was illuminated using ^{19}F NMR and EPR as a function of the depth of discharge.[xviii] A study of negative electrodes for lithium-ion batteries containing hard carbon were characterised by ^{7}Li NMR experiments in which covalently bonded, intercalated and pseudo-metallic lithium species were identifiable and quantifiable.[xix] An exchange between these sites/signals was also noted. In another study of the anodes, Imanishi et al. investigated lithium intercalation in a highly crystallized carbon fiber using ^{7}Li NMR spectroscopy, indicating resonance signals belonging to $LiC_{x>12}$, LiC_{12} and LiC_6 phases, thereby allowing for the monitoring of the transition between these phases as well.[xx] In some cases the quadrupolar interaction parameters are measurable, and these parameters can provide additional insight of the system. In one example the structural states of lithium and aluminum in Al-doped and Al_2O_3-coated $LiCoO_2$ samples were successfully identified by calculation of the quadrupole coupling constant and the asymmetry parameter from the ^{7}Li and the ^{27}Al NMR spectra of those materials.[xxi] In another study Stallworth et al. characterized the lithium and vanadium sites in $Li_xV_2O_5$ materials through the analysis of the ^{7}Li and ^{51}V NMR line shapes, as these are affected by motional narrowing, first-order quadrupolar and magnetic dipolar interactions.[xxii] Additionally, at and above room temperature, the relaxation mechanisms were

determined as being governed by a quadrupolar mechanism. Activation energies and diffusion coefficients were obtained from the NMR data as well. Nakamura et al. also used T_1 relaxation times at various temperatures, specifically to determine the activation energy for the diffusion of the Li^+ in $LiCoO_2$ and $LiNiO_2$.[xxiii] An experimentally novel approach by Letellier et al. allowed for the performance of in-situ NMR concomitant with electrochemical cycling.[xxiv] A detailed chronology of the events due to a monitoring of the Knight shift, the line width and the relaxation time (T_1) was elucidated, including the existence of a less-diffusive, quasi-metallic lithium, a factor identified as being responsible for the very good reversible capacities observed at low voltages.

Liquid state NMR has also been employed in the investigation of batteries. A somewhat comprehensive review of these investigations is given as well, but restricted to studies relating to the formation and characterization of the SEI. While having the benefit of greater resolution inherent to liquid state NMR due rapid averaging of the broadening interactions, the drawback lies in the required manipulation of the sample through either dissolution of the SEI or ex-situ electrolyte simulations. Moshkovich et. al used ^1H, ^{13}C, ^{31}P and ^{19}F NMR, in parallel with other techniques to confirm the onset potential for the electro-oxidation of certain electrolytes.[xxv] Ravdel et al. investigated the thermal stability of $LiPF_6$ salt in various ratios of EC, DEC and DMC by preparing the solutions and subjecting them to elevated temperatures.[xxvi] Subsequent investigations using ^{19}F, ^{31}P and ^1H NMR confirmed the presence of salt/electrolyte decomposition products which likely form under normal battery systems, contributing to the SEI. Later experiments by the same group used the same procedures to test the efficacy of Lewis basic electrolyte additives in stabilizing these same systems against thermal decomposition.[xxvii] NMR

measurements indicated a reversible sequestration of the PF_5^- ion by the basic additive, which was the proposed explanation for the significant improvement in electrolyte stability noted in these systems. The same group used NMR combined with GC-MS to examine the breakdown products formed in typical electrolyte solutions under high temperature conditions.[xxviii] Products identified included alkylfluorophosphates (OPF_2OR and $OPF(OR)_2$ where R = CH_3 and C_2H_5), in addition to the previously reported alkylfluorides (RF where R = CH_3 and C_2H_5), phosphorus oxyfluoride (OPF_3), LiF and polymers. This decomposition was inhibited in the presence of Lewis basic additives and/or lithium metal oxides typical of cathode materials. Ota et al. used the method of dissolving the surface components in DMSO, then conducting ^{13}C and ^{1}H NMR in one and two dimensions.[xxix] Proposed breakdown components all derive from the breakdown of the vinylene carbonate (VC), which was introduced into the EC/DMC electrolyte solution to undergo chemical breakdown at more positive (>1V) potentials than EC. The identification of the breakdown components confirmed this hypothesis, as all of them appeared to derive from the VC molecules.

---

[i] Grey, C. P. and S. G. Greenbaum. "Nuclear Magnetic Resonance Studies of Lithium-Ion Battery Materials." *MRS Bulletin* 27.8 (2002): 613-618.

[ii] Wang, Y. F., X. D. Guo, S. G. Greenbaum, J. Liu and K. Amine. "Solid Electrolyte Interphase Formation on Lithium-Ion Electrodes - A ^{7}Li Nuclear Magnetic Resonance Study." *Electrochemical and Solid State Lett*ers 4.6 (2001): A68-A70.

[iii] Smart, M. C., B. V. Ratnakumar, S. Surampudi, Y. Wang, X. Zhang, S. G. Greenbaum, A. Hightower, C. C. Ahn and B. Fultz. "Irreversible Capacities of Graphite in Low-Temperature Electrolytes for Lithium-Ion Batteries." *Journal of the Electrochemical Society* 146.11 (1999): 3963-3969.

[iv] Li, W., C. Campion, B. Lucht, B. Ravdel, J. DiCarlo and K. M. Abraham. "Additives for Stabilizing $LiPF_6$-Based Electrolytes Against Thermal Decomposition." *Journal of the Electrochemical Society* 152.7 (2005): A1361-A1365.

[v] Ratnakumar, B. V., M. C. Smart and S. Surampudi. "Effects of SEI on the Kinetics of Lithium Intercalation." *Journal of Power Sources* 97-98 (2001): 137-139.

[vi] Menetrier, M., I. Saadoune, S. Levasseur and C. Delmas. "The Insulator-Metal Transition upon Lithium Deintercalation from $LiCoO_2$: Electronic Properties and ^{7}Li NMR Study." *Journal of Materials Chemistry* 9.5 (1999): 1135-1140.

[vii] Menetrier, M., C. Vaysse, L. Croguennec, C. Delmas, C. Jordy, F. Bonhomme and P. Biensan. "^{7}Li and ^{1}H MAS NMR Observation of Interphase Layers on Lithium Nickel Oxide Based Positive Electrodes of Lithium-Ion Batteries." *Electrochemical and Solid State Letters* 7.6 (2004): A140-A143.

[viii] Grey, C. P. and Y. J. Lee. "Lithium MAS NMR Studies of Cathode Materials for Lithium-Ion Batteries." *Solid State Sciences* 5.6 (2003): 883-894.

[ix] Levasseur, S., M. Menetrier and C. Delmas. "Combined Effects of Ni and Li doping on the Phase Transitions in Li_xCoO_2 - Electrochemical and ^{7}Li Nuclear Magnetic Resonance Studies." *Journal of the Electrochemical Society* 149.12 (2002): A1533-A1540.

[x] Levasseur, S., M. Menetrier, E. Suard and C. Delmas. "Evidence for Structural Defects in Non-Stoichiometric HT-$LiCoO_2$: Electrochemical, Electronic Properties and ^{7}Li NMR Studies." *Solid State Ionics* 128.1-4 (2000): 11-24.

[xi] Levasseur, S., M. Menetrier and C. Delmas. "On the Dual Effect of Mg Doping in $LiCoO_2$ and Li^{1+}[delta]-CoO_2: Structural, Electronic Properties and ^{7}Li MAS NMR Studies." *Chemistry of Materials* 14.8 (2002): 3584-3590.

[xii] Tucker, M. C., J. A. Reimer, E. J. Cairns, S. Choi and A. Manthiram. "^{7}Li NMR Studies of Chemically-Delithiated $Li_{1-x}CoO_2$." *Journal of Physical Chemistry B* 106.15 (2002): 3842-3847.

[xiii] Carewska, M., S. Scaccia, F. Croce, S. Arumugam, Y. Wang and S. G. Greenbaum. "Electrical Conductivity and ^{6}Li, ^{7}Li NMR Studies of $Li_{1+y}CoO_2$." *Solid State Ionics* 93.3-4 (1997): 227-237.

[xiv] Lee, Y. J., S. H. Park, C. Eng, J. B. Parise and C. P. Grey. "Cation Ordering and Electrochemical Properties of the Cathode Materials $LiZn_xMn_{2-x}O_4$, $0 < x < 0.5$: A ^{6}Li Magic-Angle Spinning NMR Spectroscopy and Diffraction Study." *Chemistry of Materials* 14.1 (2002): 194-205.

[xv] Pan, C., Y. J. Lee, B. Ammundsen and C. P. Grey. "^{6}Li MAS NMR Studies of the Local Structure and Electrochemical Properties of Cr-doped Lithium Manganese and Lithium Cobalt Oxide Cathode Materials for Lithium-Ion Batteries." *Chemistry of Materials* 14.5 (2002): 2289-2299.

[xvi] Carlier, D., M. Menetrier and C. Delmas. "^{7}Li MAS NMR Study of Electrochemically Deintercalated $Li_xNi_{0.30}Co_{0.70}O_2$ Phases: Evidence of Electronic and Ionic Mobility and Redox Processes." *Journal of Materials Chemistry* 11.2 (2001): 594-603.

[xvii] Kerlau, M., J. A. Reimer and E. J. Cairns. "Investigation of Particle Isolation in Li-Ion Battery Electrodes Using ^{7}Li NMR Spectroscopy." *Electrochemistry Communications* 7.12 (2005): 1249-1251.

[xviii] Guerin, K., M. Dubois and A. Hamwi. "Electrochemical Discharge Mechanism of Fluorinated Graphite Used as Electrode in Primary Lithium Batteries." *Journal of Physics and Chemistry of Solids: Proceedings of the 13th International Symposium on Intercalation Compounds* 67.5-6 (2006): 1173-1177.

[xix] Guerin, K., M. Menetrier, A. Fevrier-Bouvier, S. Flandrois, B. Simon and P. Biensan. "A ^{7}Li NMR Study of a Hard Carbon for Lithium-Ion Rechargeable Batteries." *Solid State Ionics* 127.3-4 (2000): 187-198.

[xx] Imanishi, N., K. Kumai, H. Kokugan, Y. Takeda and O. Yamamoto. "^{7}Li NMR Study of Carbon Fiber and Graphite Anodes for Lithium Ion Batteries." *Solid State Ionics* 107.1-2 (1998): 135-144.

[xxi] Lee, Y. J., F. Wang, S. Mukerjee, J. McBreen and C. P. Grey. "^{6}Li and ^{7}Li Magic Angle Spinning Nuclear Magnetic Resonance and In-Situ X-Ray Diffraction Studies of the Charging and Discharging of $Li_xMn_2O_4$ at 4V." *Journal of the Electrochemical Society* 147.3 (2000): 803-812.

[xxii] Stallworth, P. E., F. S. Johnson, S. G. Greenbaum, S. Passerini, J. Flowers and W. Smyrl. "Magnetic Resonance Studies of Chemically Intercalated $Li_xV_2O_5$ Aerogels." *Journal of Applied Physics* 92.7 (2002): 3839-3852.

[xxiii] Nakamura, K., M. Yamamoto, K. Okamura, Y. Michihiro, I. Nakabayashi and T. Kanashiro. "NMR Investigation on the Motion of Li^+ Defects in $LiCoO_2$ and $LiNiO_2$." *Solid State Ionics* 121.1-4 (1999): 301-306.

[xxiv] Letellier, M., F. Chevallier, F. Beguin, E. Frackowiak and J.-N. Rouzaud. "The First In-Situ ^{7}Li NMR Study of the Reversible Lithium Insertion Mechanism in Disorganised Carbons." *Journal of Physics and Chemistry of Solids* 65.2-3 (2004): 245-251.

[xxv] Moshkovich, M., M. Cojocaru, H. E. Gottlieb and D. Aurbach. "The Study of the Anodic Stability of Alkyl Carbonate Solutions by In-Situ FTIR Spectroscopy, EQCM, NMR and MS." *Journal of Electroanalytical Chemistry* 497.1-2 (2001): 84-96.

[xxvi] Ravdel, B., K. M. Abraham, R. Gitzendanner, J. DiCarlo, B. Lucht and C. Campion. "Thermal Stability of Lithium-Ion Battery Electrolytes." *Journal of Power Sources* 119-121 (2003): 805-810.

[xxvii] Campion, C. L., W. Li, W. B. Euler, B. L. Lucht, B. Ravdel, J. F. DiCarlo, R. Gitzendanner and K. M. Abraham. "Suppression of Toxic Compounds Produced in the Decomposition of Lithium-Ion Battery Electrolytes." *Electrochemical and Solid-State Letters* 7.7 (2004): A194-A197.

[xxviii] Matsuta, S., Y. Kato, T. Ota, H. Kurokawa, S. Yoshimura and S. Fujitani. "Electron Spin Resonance Study of the Reaction of Electrolytic Solutions on the Positive Electrode for Lithium-Ion Secondary Batteries." *Journal of the Electrochemical Society* 148.1 (2001): A7-A10.

[xxix] Ota, H. Y. S., A. Inoue and S. Yamaguchi. "Analysis of Vinylene Carbonate Derived SEI Layers on Graphite Anode." *Journal of the Electrochemical Society* 151 (2004): A1659-A1669.

IV. Electron Paramagnetic Resonance (EPR)

A. Fundamentals of EPR

Electron Spin Resonance (ESR), or Electron Paramagnetic Resonance (EPR) Spectroscopy is often used as a supplement in chemical analyses. EPR is a spectroscopic technique in which electromagnetic energy in the microwave region (gigahertz, or GHz range) is used to excite species containing unpaired electron spins, i.e. in which the spin angular momentum, $s \neq 0$. Free electrons of spin-½ have two possible spin states, $m_s = \pm ½$. When placed in a magnetic field, energy splittings are produced corresponding to $\Delta E = (m_{s=½} - m_{s=-½}) g_e m_B B_0$, where m_B is the Bohr magneton, B_0 is the magnetic field, and g_e is the electron g-factor (in most cases $g \approx 2$). Nearby non-zero spin nuclei ($I \neq 0$) may also contribute to (or detract from) the Zeeman energy, resulting in a more complicated energy level distribution. This is referred to as the hyperfine interaction and is simply: $E = g_N m_I m_N \vec{B}_0$, where g_N is the nuclear Bohr magneton, g_N is the nuclear g-factor, and m_I are the $2I+1$ projections of the nuclear spin in the field. (see figure 1)

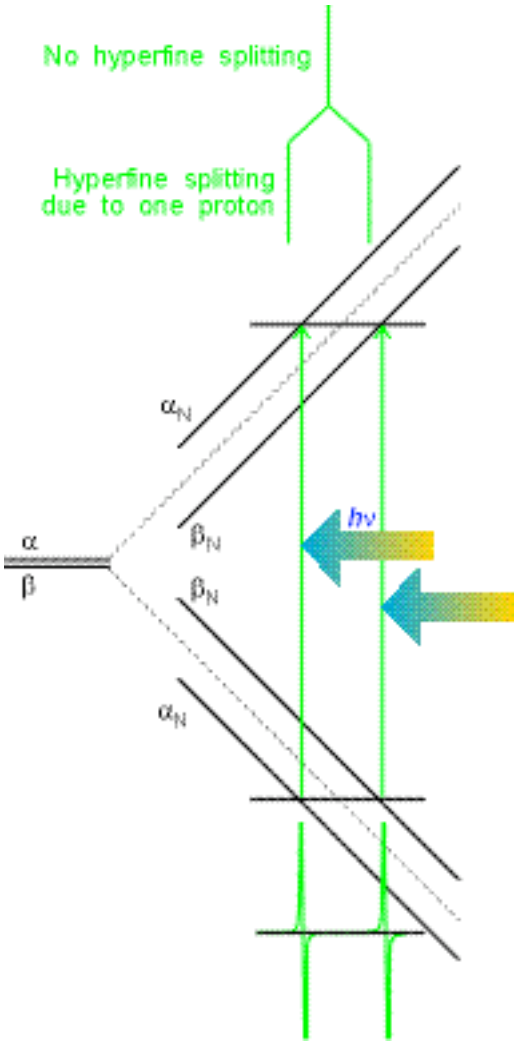

Figure 1: *The splitting pattern of two spin states, α and β in the presence of an external magnetic field. The dotted line indicates the simple Zeeman effect; the solid lines indicate the result of hyperfine interactions with a neighboring nuclei of spin I=½. The arrows indicate allowed transitions, corresponding to $\Delta E = h\nu$. The resulting spectral splitting pattern is indicated at the bottom, in green. Image taken from Smirnov, ref. i*

B. EPR as applied to Battery Research

Besides its high sensitivity compared to NMR, EPR has the benefit of using very low power microwave radiation, thereby reducing the likelihood of activating additional chemical reactions through the experimentation method itself. For example in one experimental setup where electrolytic solutions were held in contact with a charged, positive $LiCoO_2$ electrode, the quantity of radical solvent species were measured as they

were being generated; the number of radical species almost doubled, from $3x10^{17}$ at room temperature, to $5x10^{17}$ at $80^{o}C$. Experimental g-values suggested that the radical species was delocalized on the -OCO- bond and these in turn were coordinated to neighboring solvent molecules.[ii] Endo et al. used EPR analysis, aided by molecular orbital calculations, to pinpoint an initiation mechanism in electrolyte decomposition.[iii] Electron transfer is calculated to occur from the cathode to the solvent molecule, which is coordinated with the solvent anion. This in turn would produce a radical anion of the solvent molecule that would reach electron-transfer equilibrium with the neighboring solvent molecules (coordinated with the same lithium cation); it is this stable intermediate that is detected in the EPR spectra, thereby confirming this electrolyte decomposition initiation process. The same group also investigated electrolyte decomposition using a particular EPR method known as spin-trapping, in which a short-lived free radical reacts with another species, the spin trap, to produce a longer lived (and therefore detectable) radical.[iv] Continuous production of active alkyl radicals in the electrolyte solution was confirmed by this procedure, suggesting the phenomenon of a chain decomposition reaction of the electrolyte alone, initiated by the polarization of the electrode, as noted above. Liquid chromatography experiments confirmed the existence of the produced polymer in the electrolyte solutions after 4 weeks of electrolysis. This is suggestive of a polymerization process that has been proposed by others as well.[v,vi] EPR has also been used to measure the density of states (DoS) at the Fermi level in a metallic system.[iii] It is evident that graphitic, as well as disordered carbon compounds display metallic electronic behavior when doped with an element or compound which will transfer its charge to the carbon host, e.g. in the case of intercalated lithium). As the DoS changes with the

percentages of lithium intercalated, this data can be used to measure the amounts of lithium remaining in the carbon matrix (as intercalate) upon full discharge. The remaining loss of capacity is attributed to lithium in the SEI layer, or lithium atoms bound to edge carbons. Another application was illustrated by Guerin et al. in which the number of spin carriers in a fluorinated graphite anode was shown to change, both in quantity and line shape, with electrochemical discharge. Dangling bonds, as well as more delocalized charges were seen to decrease with lithium intercalation, providing insight into the reduction and intercalation process.[vii] Kosova et al. used EPR to trace the reduction of vanadium ions in correspondence with structural transformations. The additional narrowing of the signal at low temperatures was evidence of free electron behavior, as opposed to short range delocalization suggested by the temperature independent lines, hinting at phase separated particles.[viii] In a study of $LiMg_yNi_{0.5-y}Mn_{1.5}O_4$ electrode materials, the order of the reduction of the transition metals was easily traced by the loss of signal from Ni^{2+} by the simple disappearance of the EPR signal.[ix] In a similar study the Co^{2+} oxidation state of the starting material was verified as being maintained upon precipitation, but altered to Co^{3+} during calcination.[x] In another instance EPR was used to monitor the creation of broken carbon-carbon bonds during the graphite fluorination process, a detail that has significant effects on the electrochemical performance of the material.[xi] In another study of graphite intercalation compounds as active electrodes, EPR revealed that small band gaps and/or semi-metallic features are evident in the graphite particles on the mesocarbon microbead surfaces. In two separate studies on vanadium cathode materials, Stallworth et al. were able to identify and monitor the VO_2 impurity which is known to be particularly deleterious towards cycling over

normal voltages,[xii] and monitor structural disorder within the host.[xiii] In another study EPR was shown to be useful for directly observing the reaction of electrolytic solution on the charged positive electrode by monitoring the formation of solvent breakdown intermediates indicated by delocalized radical species as a function of temperature.[xiv]

---

[i] Smirnov, S. N. "Experiment 7. ESR Spectroscopy. Introduction." *New Mexico State University - Department of Chemisty and Biochemistry*. 2007. New Mexico State University. Dec 2008 <http://www.chemistry.nmsu.edu/studntres/chem435/Lab7/intro.html>.

[ii] Endo, E., M. Ata, K. Tanaka and V. Sekai. "Electron Spin Resonance Study of the Electrochemical Reduction of Electrolyte Solutions for Lithium Secondary Batteries." *Journal of the Electrochemical Society* 145.11 (1998): 3757-3764.

[iii] Endo, E., M. Ata, K. Sekai and K. Tanaka. "Spin Trapping Study of Gradual Decomposition of Electrolyte Solutions for Lithium Secondary Batteries." *Journal of the Electrochemical Society* 146.1 (1999): 49-53.

[iv] Chevallier, F., S. Gautier, J. P. Salvetat, C. Clinard, E. Frackowiak, J. N. Rouzaud and F. Béguin. "Effects of Post-Treatments on the Performance of Hard Carbons in Lithium Cells." *Journal of Power Sources* 97-98 (2001): 143-145.

[v] Thevenin, J. G. and R. H. Muller. "Impedance of Lithium Electrodes in a Propylene Carbonate Electrolyte." *Journal of the Electrochemical Society* 134.2 (1987): 273-280.

[vi] Peled, E., D. Golodnitsky, G. Ardel and V. Eshkenazy. "The SEI Model -- Application to Lithium-Polymer Electrolyte Batteries." *Electrochimica Acta* 40.13-14 (1995): 2197-2204.

[vii] Guerin, K., M. Dubois and A. Hamwi. "Electrochemical Discharge Mechanism of Fluorinated Graphite Used as Electrode in Primary Lithium Batteries." *Journal of Physics and Chemistry of Solids: Proceedings of the 13th International Symposium on Intercalation Compounds* 67.5-6 (2006): 1173-1177.

[viii] Kosova, N. and E. Devyatkina. “Soft Mechanochemical Synthesis: Preparation of Cathode Materials for Rechargeable Lithium Batteries.” *Les Annales de Chimie – Science des Matériaux* 27.6(2002): 77-90.

[ix] Alcantara, M. Jaraba, P. Lavela, J. L. Tirado, E. Zhecheva and R. Stoyanova. "Changes in the Local Structure of $LiMg_yNi_{0.5-y}Mn_{1.5}O_4$ Electrode Materials During Lithium Extraction." *Chemistry of Materials* 16 (2004): 1573-1579.

[x] Boyle, T. J., D. Ingersoll, T. M. Alam, C. J. Tafoya, M. A. Rodriguez, K. Vanheusden and D. H. Doughty. "Rechargeable Lithium Battery Cathodes. Nonaqueous Synthesis, Characterization and Electrochemical Properties of $LiCoO_2$." *Chemistry of Materials* 10.8 (1998): 2270-2276.

[xi] Li, J., K. Naga, Y. Ohzawa, T. Nakajima, A. I. Shames and A. M. Panich. "Effect of Surface Fuorination on the Electrochemical Behavior of Petroleum Cokes for Lithium Ion Battery." *Journal of Fluorine Chemistry* 126 (2005): 265-273.

[xii] Stallworth, P. E., F. S. Johnson, S. G. Greenbaum, S. Passerini, J. Flowers and W. Smyrl. "Magnetic Resonance Studies of Chemically Intercalated $Li_xV_2O_5$ Aerogels." *Journal of Applied Physics* 92.7 (2002): 3839-3852.

[xiii] Stallworth, P. E., F. S. Johnson, S. G. Greenbaum, S. Passerini, J. Flowers, W. Smyrl and J. J. Fontanella. "Magnetic Resonance Studies of Chemically Intercalated $Li_xV_2O_5$ (x=1.16 and 1.48)." *Solid State Ionics* 146.1-2 (2002): 43-54.

[xiv] Matsuta, S., Y. Kato, T. Ota, H. Kurokawa, S. Yoshimura and S. Fujitani. "Electron Spin Resonance Study of the Reaction of Electrolytic Solutions on the Positive Electrode for Lithium-Ion Secondary Batteries." *Journal of the Electrochemical Society* 148.1 (2001): A7-A10.

V. Studies

Three different types of lithium ion battery systems were studied: $LiCoO_2$||graphite; $Li_2Ag_2V_4O_{11}$||$Li^0_{(s)}$, and CF_x||$Li^0_{(s)}$.

$LiCoO_2$/graphite: Originally discovered by Prof. Goodenough, and later developed by SONY Corporation in 1991 as the first commercially available lithium-ion battery, the $LiCoO_2$ system is widely used today in most portable electronic devices. This system has been favored primarily for its high energy densities (110-190Wh/kg). It has a nominal voltage of 3.6V but its drawbacks include a relatively low power output, with an optimized c-rate of ~1C.[i]

$Ag_2V_4O_{11}$/$Li^0_{(s)}$: Often termed 'Li-SVO' batteries, this technology is often used in medical applications, e.g. implantable defibrillators, neurostimulators, and drug infusion systems. These cells have high energy densities (>600Wh/kg), long shelf lives (0.5%/yr), and are capable of continuous operation at nominal body temperature (~37 °C). Their output voltage decreases proportionally to the degree of discharge, and are known to be relatively resistant to abuse.[i]

CF_x/$Li^0_{(s)}$: Developed in the 1970s by Matsushita, CF_x cathode materials are usually formed by high-temperature intercalation of fluorine gas into graphite powder. These systems have a high energy density (~680 Wh/L), and a low self-discharge rate (<0.5%/year at 60 °C), which allows for a long (7+ years) shelf life. They are generally used for low to moderate current applications, eg. memory and clock backup batteries and have a very good safety record. They are also used in aerospace and military applications, both terrestrial and marine, and in missiles, in addition to use in cardiac

pacemakers and other medical applications.[i]

Chapters V. A and V. D include research conducted on the inorganic and organic SEI formation in $LiCoO_2$ batteries, respectively. Chapter V. B covers an investigation on the insights of the discharging mechanism in the Li-SVO system in terms of structural, chemical, and electrochemical changes that occur upon lithiation. Chapter V. C is a summary of an investigation into the CF_x system and the chemical and microstructural effects of chemical lithiation.

[i] Linden, D. and T. B. Reddy. *Handbook of Battery Materials*, 3rd ed. New York: McGraw-Hill, 2001.

A. High Field Multinuclear NMR Investigation of the SEI Layer in Lithium Rechargeable Batteries

(In collaboration with the DCI Postdoctoral Program; Prof. Clare Grey, Dr. Ben Meyer, Sarah Sakamoto at Stony Brook)

Introduction

In this study the goal was to attempt an elucidation of the SEI in terms of its chemical and physical make-up, formation pathways and temperature dependence. The cells were cycled several thousand times before cell death. Direct, post-mortem investigations (^{7}Li and ^{19}F NMR) were conducted on $LiCoO_2$||graphite pouch cell batteries. It was then possible to compare percentages of lithium *not* re-intercalated into the $LiCoO_2$ cathode by direct comparison to a previously conducted study in which the shift of the lithium was shown to depend on the cell voltage/percentage discharge.

Because the range of ^{7}Li chemical shifts in diamagnetic and non-metallic compounds is limited, ^{19}F NMR was used to complement the ^{7}Li data. The presence of an internal reference (PVdF, used as a binder material) in the electrodes allowed for the absolute quantification of LiF. Finally this data was used to demonstrate correlations between the amount of LiF formed on both electrode surfaces, the number of cycles, and the (ir)reversible electrode capacities.

Lastly, with respect to hypothesized LiF formation, Song et al. recently used ex situ Fourier transform IR spectroscopy with the attenuated total reflection technique to investigate the surface film formation on a $LiNi_{0.8}Co_{0.15}Al_{0.05}O_2$ cathode; however, they

were not able to detect LiF as one of the decomposition products of $LiPF_6$ due to the invisibility of LiF in the mid-IR (700 to 1400cm^{-1}) range.[i] Therefore ^{19}F NMR, which is a very reliable probe of fluorine-containing species, was used in this study in order to attempt the determination of LiF content in the cells.

Experimental

For all cells in this study, the cathode was commercial $LiCoO_2$ mixed with PVDF and graphite, and the anode was graphitic meso-carbon micro-beads (MCMB) mixed with the Super P and PVDF. The electrolyte used in this study was 1M LiPF6 dissolved into a mixture of EC, PC, EMC, and DEC. Cell A was cycled at 60ºC from 3.0 to 3.9V. Cells B-F were cycled from 3.0 to 4.2V at room temperature with a C/2 charge rate and a 2/3C discharge rate. All cells were removed from cycling at failure. The criterion for failure in this study was defined as the point when 40% of their intrinsic capacity (x=0.5 to x=1.0) had been irreversibly lost as determined electrochemically. The cells were then fully discharged to 3.0V at the 2/3C rate prior to disassembly. For NMR, the cathode and anode material were scraped from the foil backing inside an argon dry box and packed into 2.5mm rotors. Lithium loss in the cathode was determined by chemical shift comparison instead of ^{7}Li spin counting. The extra unknown amounts of the different lithium environments formed in the SEI in cycled cells makes spin counting problematic and leads to larger errors in estimation. It is important to note that the Li loss determined electrochemically and by NMR may differ. Electrochemically, any particles that have been isolated will result in capacity loss even though intercalated lithium is still present.

Alternatively, NMR will be sensitive to all particles isolated or not in the active material.

The ^{7}Li MAS spectra was acquired at 272.1MHz using a Bruker 700MHz system. Data was collected using a single π/2 pulse, 10 second delays between scans, and a 25kHz spinning speed. ^{19}F MAS spectra were acquired at 564.6MHz using a Bruker 600MHz system. Data was collected using a single π/2 pulse, 10 second delays between scans, and spinning speeds of 25 to 35kHz. ^{7}Li and ^{19}F chemical shifts are quoted relative to the external references 1M LiCl (in H_2O) and CCl_3F, respectively, both set to 0ppm.

^{19}F integrated intensities were determined by using spectral simulation and the presence of PVDF binder as a fluorine reference. The LiF content was then calculated and normalized to allow comparisons between cathodes and corresponding anodes using equation 1. In this study, only calculations using equation 1 for unrinsed cells are reported.

$$\frac{LiF\ Integrated\ Intensity}{(LiF + PVDF)\ Integrated\ Intensity} \times PVDF\ content = Normalized\ LiF\ content \qquad [Eq.1]$$

Results and Discussion

The first focus of this study was to build a chemical shift library for ^{7}Li inorganic compounds using the high field NMR 700MHz spectrometer. Several spectra are displayed in figure 1. Since diamagnetic lithium has a very small chemical shift range (~10 ppm), the high field was necessary to gain enough resolution to separate the different compounds that may be present in the SEI.

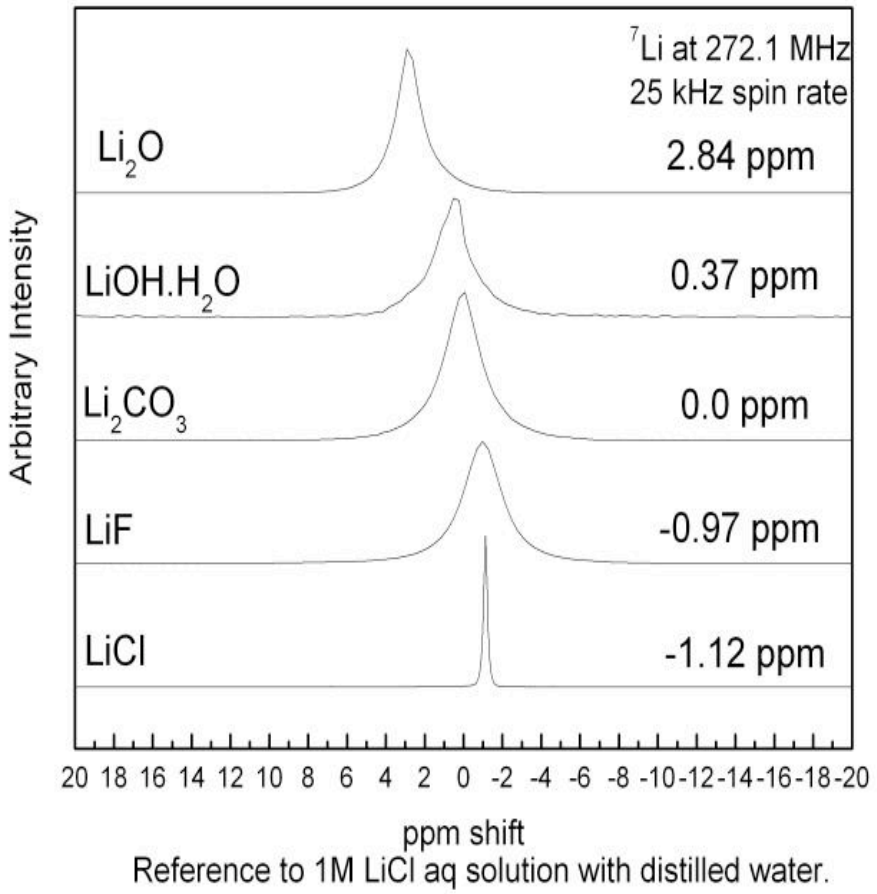

***Figure 1**: [7]Li chemical shift spectra of various inorganic compounds that may be present in the SEI layer*

The second technique used in this study was a careful comparison of data published by Menetrier et al., in which the ^{7}Li NMR spectra for $LiCoO_2$ at different states of charge were collected and reported (see figure 2).[ii] Li_xCoO_2, where $1 < x < 0.94$, has a chemical shift of –0.45ppm. During the initial stage of charging, a new resonance appears near 60ppm, which coexists with the resonance due to Li_xCoO_2 until 25 to 30% of the lithium has been removed. The new resonance was ascribed to the presence of a second

phase, $Li_{0.75}CoO_2$, caused by the insulator to metal transition that occurs in $LiCoO_2$ upon Li deintercalation. Upon further charging, the resonance at around 60ppm shifts toward more positive frequencies until it reaches approximately 100ppm when x=0.5 in Li_xCoO_2. This information was used to follow the state of charge of Li_xCoO_2 in $LiCoO_2$||graphite full cells as a function of cycle number, and the fraction of Li lost to side reactions (which include the formation of the SEI on the cathode and anode and any Li that remains stuck in the anode).

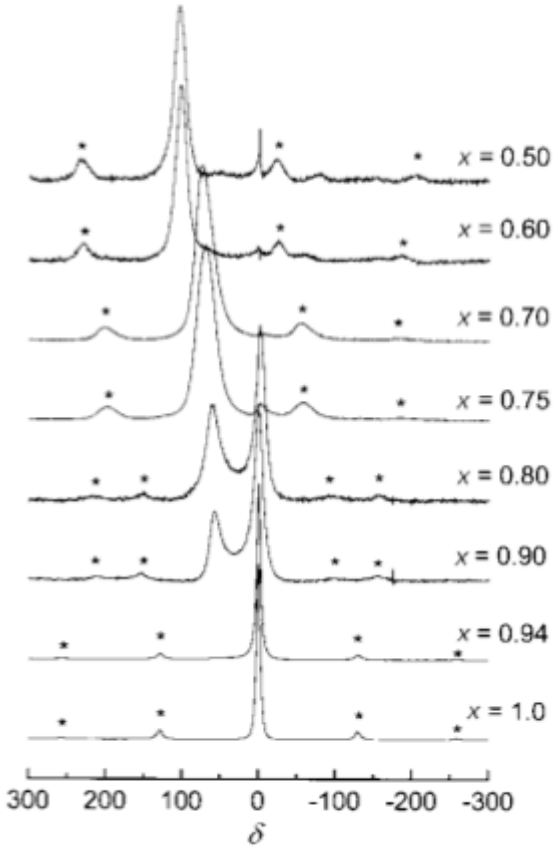

Figure 2: *^{7}Li MAS NMR spectra for various Li_xCoO_2 deintercalated phases (spinning sidebands indicated by *). The lithium shifts downfield (more positive) as its phase becomes more metallic. This is called a Knight shift. (from Menetrier 1999, ref. ii)*

Figure 3 shows the ^{7}Li MAS NMR spectrum (at 272.1 MHz) of a cell cycled at 60ºC for 3000 cycles from 3.0 to 3.9 V (cell A). Two resonances are seen at 60ppm (strong) and 0.3ppm (weak), which are assigned to Li_xCoO_2 and to the SEI, $LiPF_6$, and residual $Li_{1.0}CoO_2$, respectively. Unfortunately, the 0.3ppm resonance lacks sufficient resolution to allow the individual components in the SEI layer to be distinguished. The broadening is ascribed to the anisotropic magnetic susceptibility of the carbon used to fabricate the electrodes and the presence of Co^{4+}/metallic $Li_{0.75}CoO_2$. The overall shift of the resonance suggests that Li_2O or Li_2CO_3 may be present but no further analysis is possible. Based on the frequency of the more intense resonance at 60ppm, and the earlier work by Menetrier et al.,[ii] an estimate for the Li loss from the cathode of approximately 25% can be determined. As a result, the cathode composition at the time of disassembly is approximately $Li_{0.75}CoO_2$.

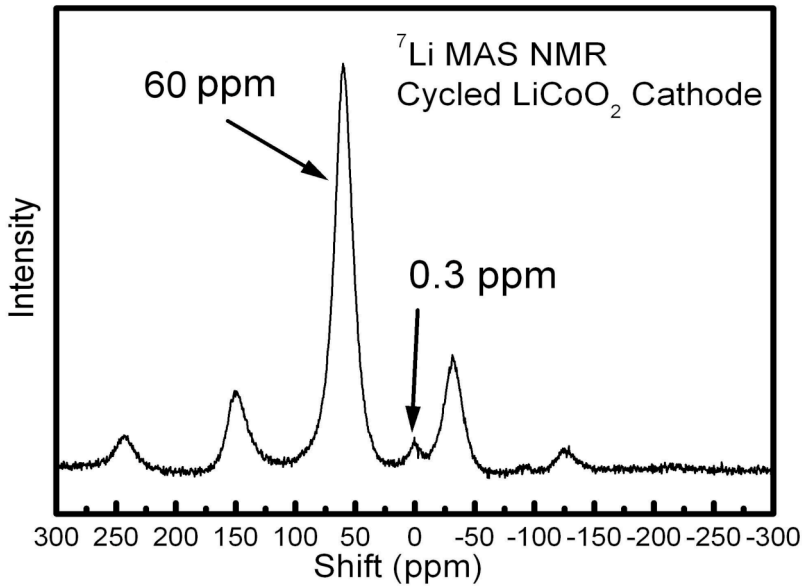

Figure 3: *^{7}Li MAS NMR spectra for a cycled $LiCoO_2$ cathode (cell A). Isotropic resonances are seen at 60ppm and 0.3ppm; all other peaks are spinning sidebands from 25kHz MAS.*

Figure 4 shows the experimentally determined losses of Li from the $Li_{1.0}CoO_2$ cathode (determined by using the same approach as described above for cell A) as a function of cycle number for five other similar cells (B through F) cycled at room temperature. A positive correlation exists between the percent of lithium *not* re-intercalated into the cathode at full discharge and the cycle number. The Li loss at higher temperatures is clearly higher: the Li loss for cell A, cycled at 60ºC for only 3000 cycles, is intermediate between that of cell E and F, which have been cycled 6500 and 9000 times, respectively.

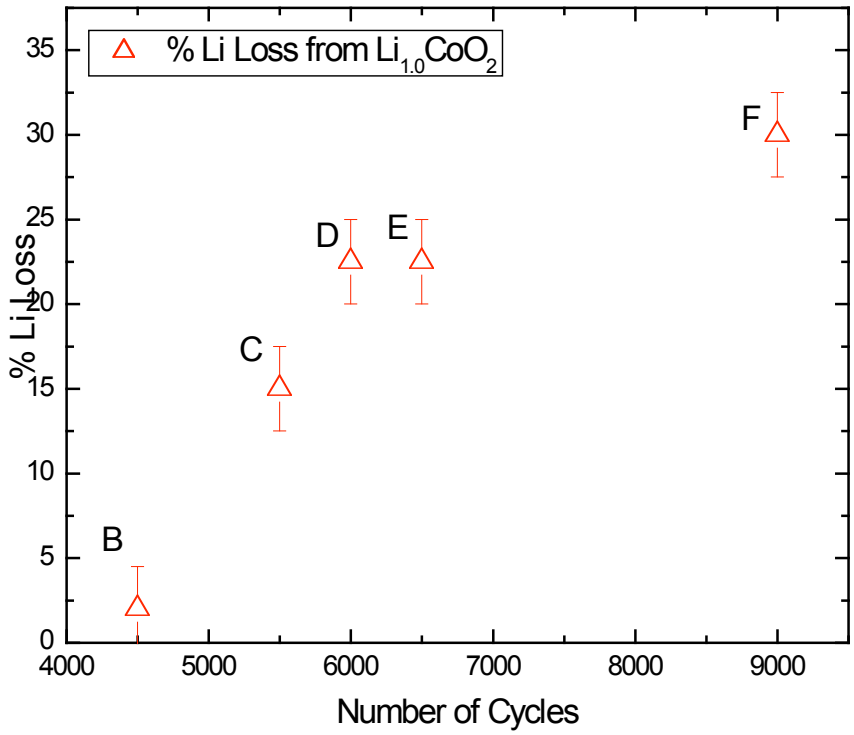

***Figure 4**: Experimentally determined Li loss from $Li_{1.0}CoO_2$ by ^{7}Li MAS NMR spectra for cycled $LiCoO_2$ cathodes.*

The lithium that remains intercalated in the anode can also be directly monitored by via the ^{7}Li NMR spectra of the anode. Figure 5 shows the ^{7}Li MAS NMR spectra of a cycled carbon anode before and after rinsing three times with dimethylcarbonate (DMC). Washing was performed to remove residual electrolyte and salt. The weaker peak at 45ppm, whose intensity remains unchanged after rinsing is assigned to the LiC_6 and/or LiC_{12} phase[iii,iv] which shows that even though the cell was fully discharged, some intercalated lithium remains. A broader resonance, centered near 10ppm is also observed, the intensity of which is noticeably changed after rinsing. This resonance can be deconvoluted into at least three resonances at 0, 8 and 16ppm. The peak near 0ppm is assigned to the SEI and dried electrolyte, consistent with its change of intensity on washing. The shifts of the peaks at 8 and 16ppm appear to be slightly too large to be attributed to any diamagnetic components and on this basis are tentatively assigned to

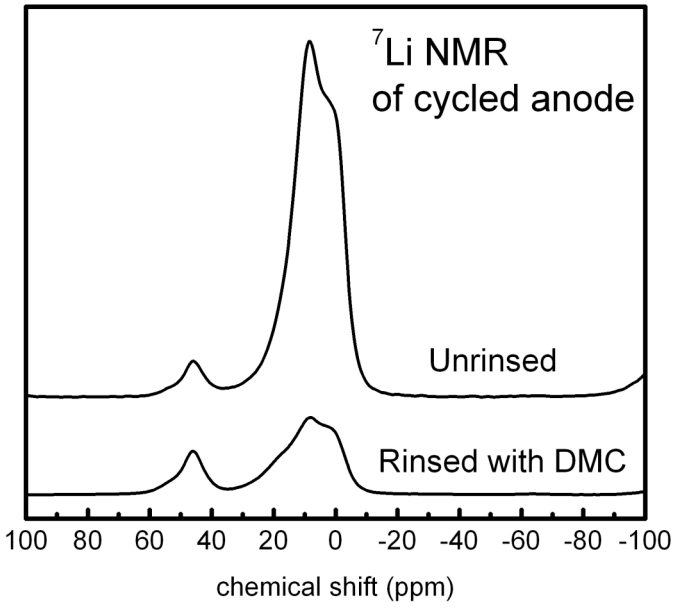

Figure 5: *^{7}Li MAS NMR spectra for the anode of cell A showing the presence of intercalated lithium at 45ppm, before and after rinsing with DMC.*

LiC_x>12.[iii,v] However it is somewhat surprising that the intensities would decrease with rinsing, suggesting that these peaks may be associated with Li^+ either on or near the surface of the carbon particles.

Since it was not possible to further resolve the ^7Li resonances corresponding to LiF in the anode or cathode SEI, ^{19}F NMR was used to identify all the fluorine-containing components. ^{19}F NMR is more sensitive to small changes in the local environment, because the chemical shift range is larger compared to ^7Li and thus components such as LiF are more easily resolved.

Figure 6 shows the ^{19}F MAS NMR spectra for both the cathode and anode taken from cell A. The LiF resonance appears at –200ppm. The resonance at –70ppm is from the $LiPF_6$ in the dried electrolyte. The remaining resonances at –90, and –110ppm are assigned to polyvinylidene fluoride (PVDF), which is used as an electrode binder. Rinsing of the anode with DMC results in a decrease in the integrated intensity of both the dried electrolyte and LiF peaks. However, while the dried electrolyte peak is eliminated, a significant portion of the LiF peak remains. Spectral simulation and integration yield values for the percentage of total ^{19}F signal (excluding dried electrolyte) from LiF content in the cathode, anode, and rinsed anode, respectively for cell A. Normalizing this with the PVDF content (Eq. 1) in each electrode (1:3::cathode:anode) allows for a direct comparison of the amount of LiF formed at each electrode (0.25:3.44:2.16::cathode:unrinsed anode: rinsed anode). As a result, 8.5 times as much LiF is present at the rinsed, and 13 times as much on the unrinsed anode surface than on the unrinsed cathode.

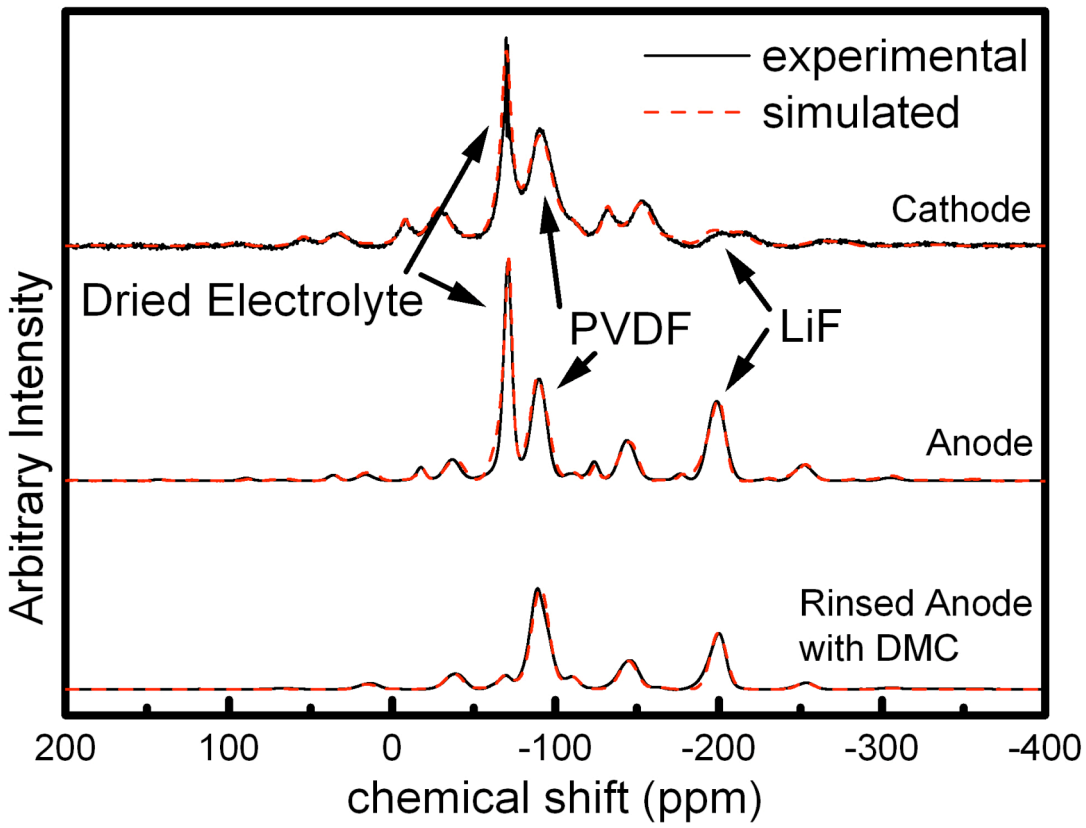

Figure 6: *^{19}F MAS NMR spectra of $LiCoO_2$ cathode and unrinsed and rinsed MCMB anode both from cell A.*

Figure 7 shows the quantitative results from the series of cells cycled at room room temperature from 3.0 to 4.2V for 4500, 5500, 6000, 6500 and 9000 cycles (cells B-F). These were also fully discharged prior to disassembly. The graph shows a positive correlation for the amount of LiF, determined by ^{19}F NMR, at the cathode surface and the percentage Li loss from the cathode (determined by ^{7}Li NMR). Cell F, which was cycled 9000 times and showed a 30% lithium loss from the cathode, as determined by the 89ppm ^{7}Li NMR shifts of the Li_xCoO_2 resonance, contained twice as much LiF as cell C (cycled 5500 times; a 15% lithium loss from the cathode). In all the cells much more LiF was found to be present on the anode as compared to the cathode.

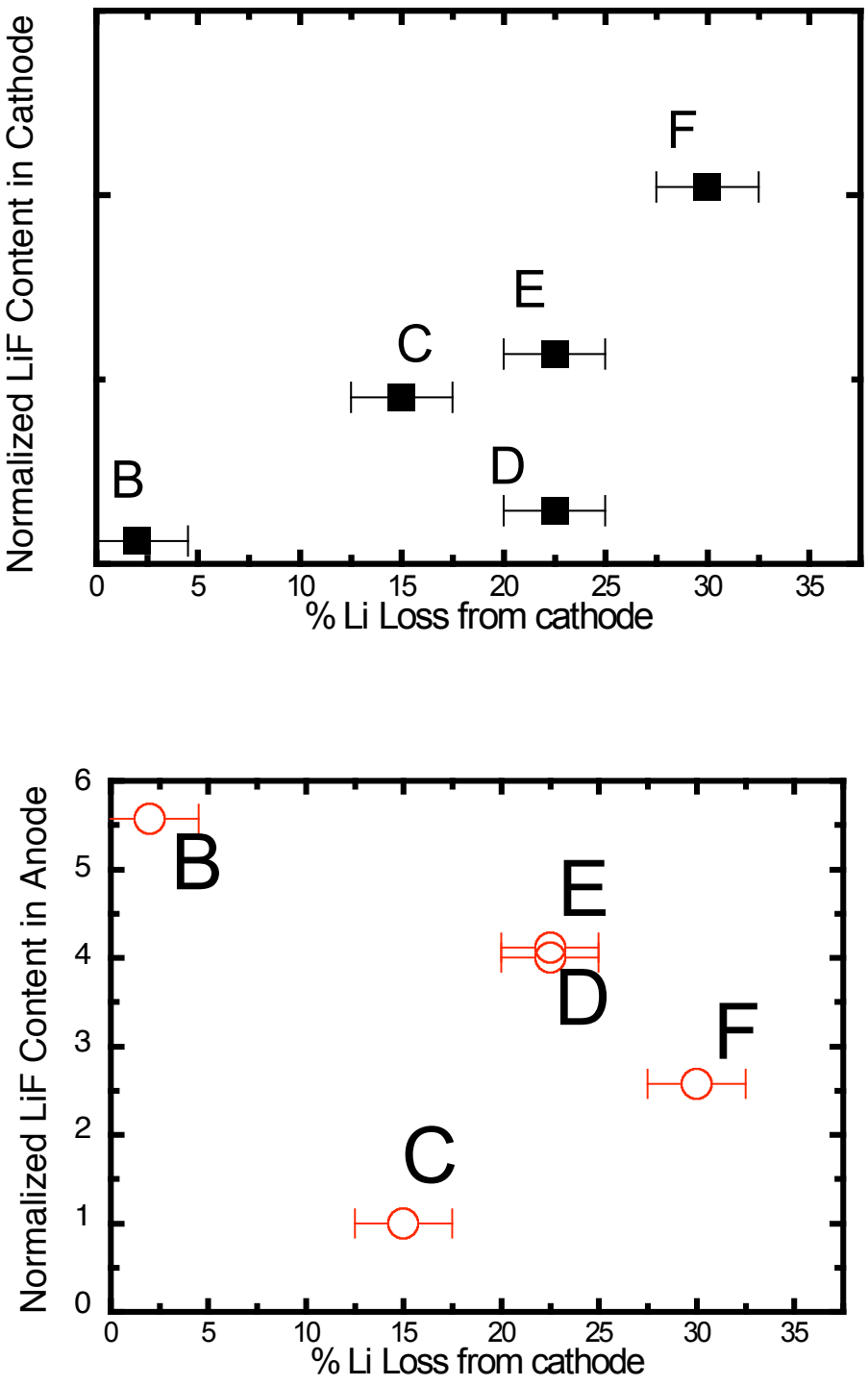

Figure 7: *Comparison of the relative LiF content found on (a) the cathodes and (b) the anodes from cells B, C, D, E and F, using PVDF as a calibration statndard vs. Li loss from the cathode.*

At the moment there is no clear correlation between LiF content on the anode and the percentage of Li loss from the cathode. The anode of cell B contains more LiF than the other anodes that performed to a larger number of cycles. If irreversible loss of lithium was the only mechanism contributing to cell failure, it would be expected that the resultant composition of the cathode of cell B be approximately $Li_{0.8}CoO_2$. However the cathode for cell B shows a very low lithium loss, approximately 2% ($Li_{0.98}CoO_2$) as determined by NMR. This implies that the cell may have failed due to a different mechanism other than the one responsible for the other cell failures. Cell B did contain more Super P carbon added to the MCMB carbon in comparison to the amount used in the other cells. This may suggest that the carbon Super P plays a role in SEI formation, i.e. its higher concentration may result in more LiF in the SEI on the carbonaceous anode surface. The anode for cell F (9000 cycles and 30% lithium loss from cathode) shows a lower concentration of LiF than the anodes with lower cycle numbers. This is another indicator that the dominant reason for cell failure in this case is different.

Temperature clearly affects SEI formation. Cell A cycled at a higher temperature (60ºC) (see Figs. 3 and 5) showed more LiF on both the anode and cathode when compared to the other cells (B - F) cycled at room temperature for a similar extrapolated number of cycles. Interestingly, the results from cell A do not fall on the correlation curve shown in figure 7 for cells B, C, D, E and F, indicating that the high Li loss seen at higher temperatures does not directly correlate with LiF formation.

Conclusions

The results presented in this section show that ^{7}Li NMR spectroscopy of fully discharged $LiCoO_2$ cathodes can be used to estimate the percentage of Li not re-intercalated into the cathode, for cells cycled under a variety of conditions. The lost lithium is incorporated into the SEI at both the anode and cathode and also remains intercalated in the graphitic carbon at the anode. The large ^{19}F chemical shift range allows LiF in the SEI at both the cathode and anode to be identified. Using PVDF as an internal calibration standard enables a direct quantitative comparison of LiF content between the electrodes. In all cells presented, more LiF was formed on the surface of the anode than on the cathode. A positive correlation was established for the amount of LiF formed with both the number of cycles and the percentage of Li lost from the cathode. No apparent correlation was found for LiF versus cycle number for the anodes, suggesting the possibility of different failure mechanisms at each anode.

---

[i] Song, S. W., G. V. Zhuang and P. N. Ross, Jr. "Surface Film Formation on $LiNi_{0.8}Co_{0.15}Al_{0.05}O_2$ Cathodes Using Attenuated Total Reflection IR Spectroscopy." *Journal of the Electrochemical Society* 151.8 (2004): A1162-A1167.

[ii] Menetrier, M., I. Saadoune, S. Levasseur and C. Delmas. "The Insulator-Metal Transition upon Lithium Deintercalation from $LiCoO_2$: Electronic Properties and ^{7}Li NMR Study." *Journal of Materials Chemistry* 9.5 (1999): 1135-1140.

[iii] Imanishi, N., K. Kumai, H. Kokugan, Y. Takeda and O. Yamamoto. "^{7}Li NMR Study of Carbon Fiber and Graphite Anodes for Lithium Ion Batteries." *Solid State Ionics* 107.1-2 (1998): 135-144.

[iv] Smart, M. C., B. V. Ratnakumar, S. Surampudi, Y. Wang, X. Zhang, S. G. Greenbaum, A. Hightower, C. C. Ahn and B. Fultz. "Irreversible Capacities of Graphite in

Low-Temperature Electrolytes for Lithium-Ion Batteries." *Journal of the Electrochemical Society* 146.11 (1999): 3963-3969.

[v] Wang, Y., V. Yufit, X. Guo, E. Peled and S. Greenbaum. "^{7}Li Nuclear Magnetic Resonance Study of Lithium Insertion in Pristine and Partially Oxidized Graphite." *Journal of Power Sources* 94.2 (2001): 230-237.

B. Lithiated Silver Vanadium Oxide Study (SVO)

(In collaboration with Greatbatch; Dr. Tom Reddy, Dr. Faisal Alamgir, Dr. Phil Stallworth, Lina Gonzalez, Amy Colon, Krista Martocci at Hunter College)

Introduction

The primary motivation of this work was to apply ^{7}Li and ^{51}V NMR to reveal atomic level information about the environments of those metal ions in lithiated silver vanadium oxide cathodes. Specifically the goal was to determine the structural changes which occur at several states of lithiation of the discharge product, $Li_xAg_2V_4O_{11}$, with x = 0, 0.71, 2.13 and 5.59, and to elucidate the mechanism of the reduction process. The existence of three separate insertion processes is implied by the electrochemical data on $Li_xAg_2V_4O_{11}$ in which three separate voltage plateaus, (3.2, 2.7, 2.4V) are indicated by the potential plateaus in the discharge curve (figure 1).[i,ii]

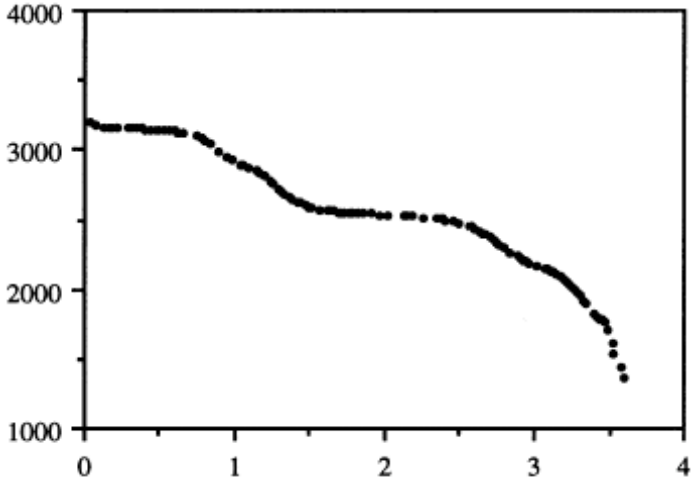

Figure 1: *A typical discharge curve for a lithium silver vanadium oxide cell under constant resistive load; the voltage plateaus indicate stages of ion intercalation; figure taken from Takeuchi, 2001 (ref iii)*

The lithium/silver vanadium oxide (SVO) primary cell is employed for a number of biomedical applications but its principal use is as a power source in implantable cardiac defibrillators (ICDs) which are required to produce 25–40 Joule pulses to paralyze the heart during fibrillation events, following which the normal heart beating rhythm resumes. This function requires a cell capable of producing 1–4A pulses to charge a capacitor in addition to providing the background current of 10–30mA or less for pacing and sensing functions. Silver vanadium oxide [$Ag_2V_4O_{11}$], which belongs to the class of vanadium bronzes (figure 2) and possesses semiconducting properties, has been successfully used as the cathode in this system due to the inherent high rate capability of this material.

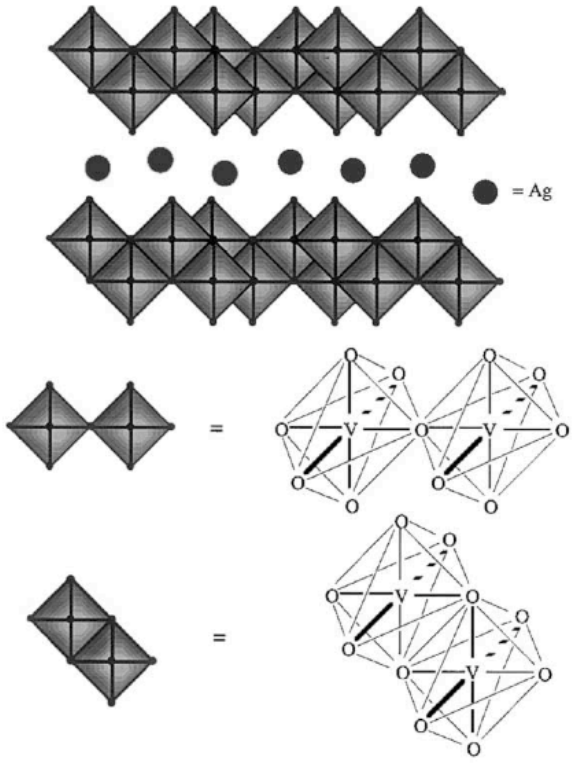

***Figure 2**: δ-$Ag_xV_2O_5$, a layered structure of distorted VO_6 octahedra sharing edges and corners (distortions not shown); image taken Takeuchi, 2001 (ref. iii)*

Electrochemical reduction of SVO is a multistep process which occurs between 3.2 and 2.0 V with the following overall reaction: $Ag_2V_4O_{11} + 7Li = Li_7Ag_2V_4O_{11}$. SVO has a theoretical capacity of 315 mAh/g to a 2.0 V background voltage cutoff. Extensive electrochemical characterization of the Li/SVO system has been carried out by several other groups.[iii,iv,v] Mechanistic studies of this multistep reduction have also been conducted and have identified the formation of silver metal in the early stage of the reaction, through the use of X-ray powder diffraction and scanning electron microscopy/energy-dispersive spectroscopy (SEM/EDS).[vi,vii] However, electrochemical and X-ray diffraction measurements yield only average structural changes related to lithium insertion. The primary motivation of this work was to apply spectroscopic methods that reveal atomic level information about local environments of the metallic ions in the sample, via ^7Li and ^{51}V nuclear magnetic resonance (NMR). The aim was to determine the structural changes which occur at several states of lithiation of the discharge product [$Li_xAg_2V_4O_{11}$] with $x = 0$, 0.71, 2.13, and 5.59 and to elucidate the mechanism of the reduction process.

X-Ray absorption spectroscopy (XAS), or X-Ray Absorption Fine-Structure (XAFS) was also conducted on these samples at the silver and vanadium energies. XAS is a spectroscopic technique that probes the physical and chemical structure of matter at an atomic scale. XAS is element specific, in that X-ray energy is set near the binding energy of a particular core electronic level of a particular atomic species. The peak positions and spectral features of an XAS spectrum can be used to extract chemical and structural parameters such as the oxidation state of a particular ion and its near neighbor environment. Extended absorption near-edge structure (XANES) data was also collected.

XANES, unlike EXAFS, is highly sensitive to the details of the shallow electronic states of the central atom which can shed light on much about the processes occurring over the course of the lithiation. Both the XAFS and XANES studies were performed by other members of the research group therefore the experimental details and results will be discussed only cursorily in this report.

Experimental

Silver vanadium oxide ($Ag_2V_4O_{11}$) was synthesized from silver nitrate and V_2O_5 starting materials.[viii] Experimental hermetic cells were built with lithium anodes and SVO cathodes containing binder and conductive additives. The electrolyte was 1M $LiAsF_6$ in propylene carbonate/1,2–dimethoxyethane solvents (50/50 by volume). Cells were discharged under resistive loads over a 12 month period (at a C-rate of C/8760), and constant current pulses were applied to the cells approximately every 30 days. At regular intervals during the discharge, cells selected for analysis were removed from discharge testing and permitted to equilibrate at open circuit prior to cutting them open to retrieve the cathode component. For the lithiated samples with $x = 0.72$ and 2.13, the cells equilibrated for a total of 20 days, at which time the change in open-circuit voltage was less than 4 mV per day. For the lithiated samples with $x = 5.59$, the cell equilibrated for 10 days, at which time the change in open-circuit voltage was less than 2 mV per day. The cathodes were then rinsed with propylene carbonate and 1,2–dimethoxyethane prior to analysis. The cathode material was removed from the current collector and lightly ground to form a powder. All of these preparations were conducted at the Greatbatch

facility. The samples were sealed and sent to Hunter College for analysis.

^{7}Li and ^{51}V NMR studies were conducted on the four $Li_xAg_2V_4O_{11}$ samples, x = 0, 0.72, 2.13, and 5.59. ^{7}Li (I = 3 /2) NMR measurements were performed on a Varian Unity 500 spectrometer operating at 194.33 MHz and field strength of 11.7T. The spectra were gathered using phase cycled pulse-delay-acquire (one pulse) sequence followed by Fourier transformation of the free- induction decay. The base-line distortions of the spectra resulting from spectrometer dead time were removed using an automated polynomial base-line fitting correction routine. Magic angle spinning (MAS) measurements were performed at 4–12 kHz to remove most of the dipolar broadening. Chemical shifts were reported in parts per million (ppm) and externally referenced to 1M $LiCl_{(aq)}$ at 0 ppm. ^{51}V (I = 7 /2) static NMR spectra, gathered at 79.18 MHz on a Chemagnetics CMX300 spectrometer using a phase cycled two-pulse solid echo sequence, exhibited broad central transitions plus satellite responses of ~250kHz overall width. All spectra were externally referenced to $VOCl_{3(aq)}$. Prior to the NMR measurements, the samples were transferred to tubes or rotor sleeves with hermetic endcaps and sealed in a glovebox under dry Argon.

All of the XAS measurements, taken on samples from the same batch as the NMR experiments, were collected in transmission at the V and Ag K-edges at beamlines X23B and X23A2, respectively, of the National Synchrotron Light Source at Brookhaven National Laboratory. Reference scans of V and Ag foils were collected simultaneously.

Results and Discussion

^{7}Li NMR was conducted on the three samples containing lithium, all of which exhibited at least three isotropic resonances and their spectra are displayed in figure 3. The peaks identified were at least two overlapping peaks near 0 ppm, and an additional peak, shifted downfield into the negative region of the spectrum. This peak pattern is similar to all previously reported ^{7}Li NMR measurements of V_yO_z systems.[ii,ix,x,xi,xii] In the $x = 0.72$ sample a shoulder is clearly visible on the positive side of the center peak.

The existence of three separate insertion processes is implied by electrochemical data on $Li_xAg_2V_4O_{11}$ in which three separate voltage plateaus, (3.2, 2.7, and 2.4 V) are indicated by the potential plateaus in the discharge curve.[i,xiii] It has been previously established that the 3.2 V plateau is associated with Ag reduction and the 2.7 V and 2.4 V

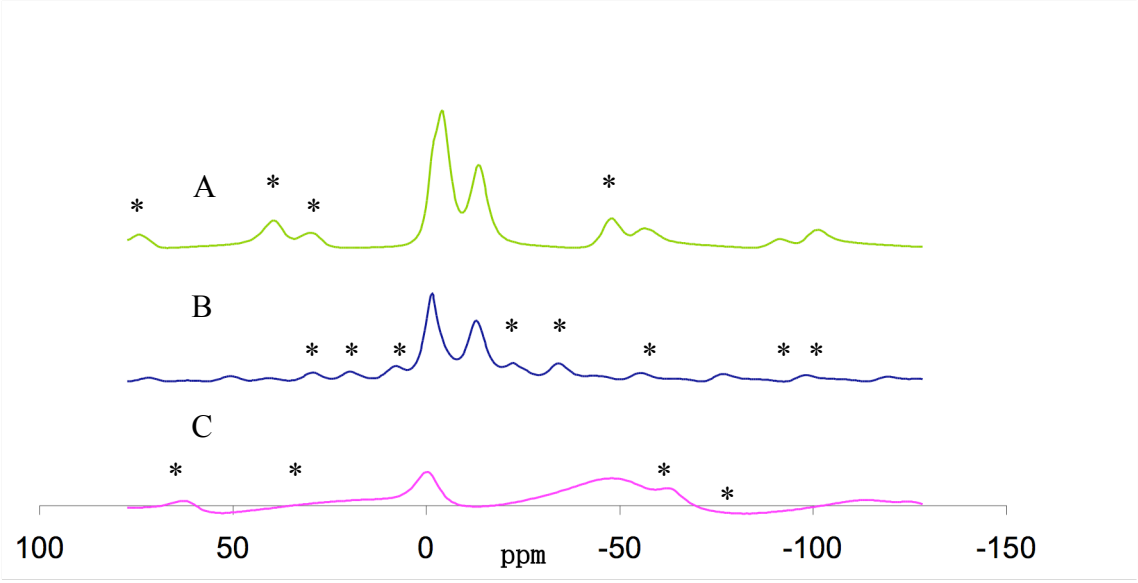

Figure 3: *^{7}Li MAS NMR spectra of SVO cathodes at varying states of discharge: (A) $Li_{0.72}Ag_2V_4O_{11}$, at 8.5kHz spinning speed, (B) $Li_{2.13}Ag_2V_4O_{11}$, at 4 kHz spinning speed, and (C) $Li_{5.59}Ag_2V_4O_{11}$ at 12kHz spinning speed. Spinning sidebands are indicated with asterisks.*

features correspond to V reduction.[i,iii,xiii] The incoming lithium ions simultaneously reduce and displace the Ag^{+} ions which are bound in the oxygen layers of the $Li_xAg_2V_4O_{11}$ structure.[xiv] While these sites are large enough to accommodate atomic silver, in the event that the silver is reduced while the lithium intercalates into a separate site, there exists strong evidence that the silver atoms come out of the host structure and crystallize onto the surfaces of the particles. This evidence is in the form of electrical conductivity measurements, which shows 1000-fold increases for even slightly lithiated SVO cathodes,[iii] SEM/EDS images of silver particles on the surface of the discharged SVO primary particles,[vi] transmission electron microscopy (TEM) images of the same,[vii] XRD studies of discharged cathodes,[i,vii] and XAS measurements.

During the second voltage plateau, the intercalation pathway is assumed to resemble that of $Ag_xV_2O_5$, in which the δ phase of the structure undergoes a phase change to the ε-$Li_xV_2O_5$ with lithium *insertion* in addition to *reduction* of Ag^{+1}. In the third region, also believed to resemble the movement in $Ag_xV_2O_5$, *additional* Li^{+} ions are accommodated in the ε-$Li_xV_2O_5$ structure.[xiii] Integrated intensities are consistent with this hypothesis as the ratio of octahedral to tetrahedral sites in Li=0.72 is 5:3, while in the Li=2.13 sample, the ratio is approximately 11:13. In other words the initial insertion site(s) becomes saturated and the latter site accomodates the remaining ions.

The spectral component near −2.5ppm in the x=0.72 sample is attributed to lithium irreversibly bound in the solid electrolyte interphase (SEI) most likely composed of LiF, Li_2CO_3, and possibly some other lithium-containing breakdown products of the electrolyte on the surface of the material.[xv] Because the elucidation of the overall reduction process involves the question of possible oxygen loss from the cathode, it is

significant to point out that Li_2O is not a likely candidate as an SEI component, as its chemical shift is 2.84ppm, and no detectable resonance is seen in that region in the x = 0.72 sample. As SEI breakdown is typically the greatest after initial cell assembly and early states of discharge, it is presumed that no Li_2O is present. This finding is also significant in that it demonstrates that the reduction and displacement of Ag by Li, discussed below, does not lead to the formation of Li_2O.

The peak near −4ppm is attributed to lithium atoms in the octahedral sites, some of which were formerly occupied by Ag. The lithium atoms in the octahedral sites are further away from the vanadium lattice points than those in the tetrahedral coordination. This is evidenced by the fact that as the lithium content is increased in the three samples, this peak does not exhibit any additional chemical shift. Therefore, as vanadium ions are reduced at higher intercalation levels, these lithium ions remain relatively unaffected by these changes in the vanadium oxidation states. This peak does, however, exhibit slight broadening upon maximum intercalation (x = 5.59), as discussed below. (Slight changes in the widths of the x = 0.72 and 2.13 samples are attributed to differences in the spinning speeds, as spin rate is inversely proportional to the widths of the signals.) The second voltage plateau is associated with lithium intercalation in addition to reduction of Ag^{+1}, and the −4ppm peak is assigned to this intercalated lithium site, although it is not possible to exclude contributions from the first plateau.

The third peak (at approximately −14ppm in the x = 0.72 and 2.13 samples and at −54ppm in the x = 5.59 sample) represents the lithium ions intercalated in the positions nearest the vanadium ions. It is hypothesized that these are tetrahedral sites as reported for δ-$Li_xV_2O_5$,[xvi] (see figure 4) and are associated with the third plateau region in which

additional Li^+ ions are accommodated in the structure, presumably after all (or most) of the silver has been reduced. Regarding this resonance, two effects are seen; an increase in the negative shift as well as a significant broadening of the intercalated component. The shifting and broadening are attributed to the increase in the number of V^{4+} and/or V^{3+} ions with increasing Li content. This effect is consistent with previously reported studies of lithium intercalated into vanadate structures.[ix,xvii,xviii,xix] This increase in broadening

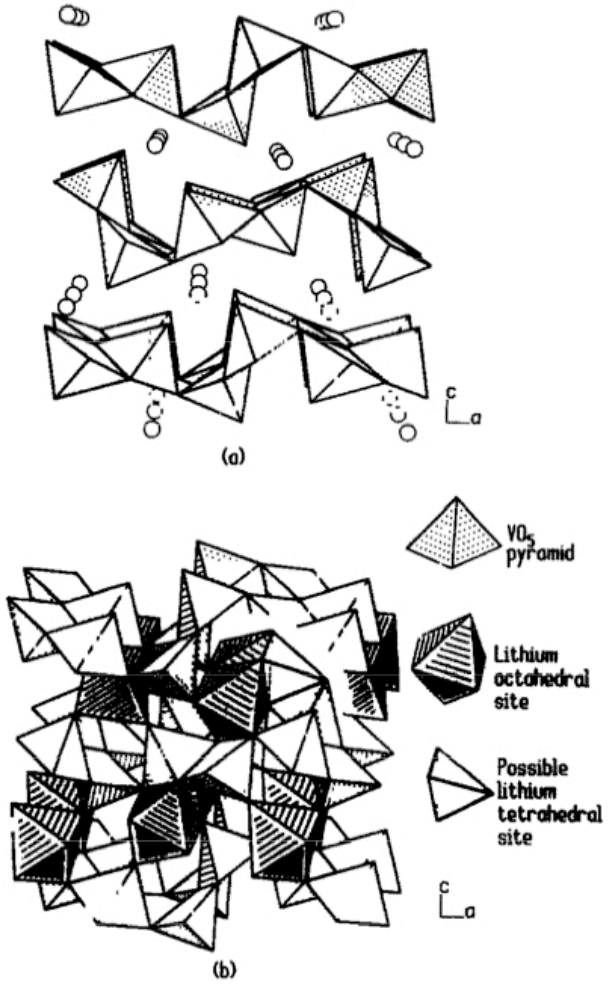

Figure 4: *Structure of the γ-$Li_xV_2O_5$ phase showing the puckering of the $(V_2O_5)_x$ layers (a) and the possible tetrahedral site available for lithium intercalation beyond x=1 (b); image taken from Cocciantelli, 1992 (ref. xvii)*

was the most drastic between the $x = 2.13$ and $x = 5.59$ samples, suggesting that in the Li = 0.72 sample most, if not all, of the vanadium is in the +5 oxidation state. This delay in the shift until higher Li insertion supports the hypothesis that most of the silver ions are reduced prior to the reduction of the vanadium (V^{5+}) ions, however not necessarily all of them. Although the transition from Ag to V reduction as a function of lithiation could have been examined more definitively with more samples around the Li = 2 range, it is possible that there is, in fact, no clear transition, in that there is some degree of parallel rather than purely serial reduction of both metal ions. This hypothesis was also confirmed by XAS data that was collected on the same samples.

Considering the ionic radii of Li vs Ag (0.6 and 1.2 Å, respectively) it would be expected that at higher levels of silver displacement during the discharge process, a collapse in the structure would be evident. It has been suggested that loss of Ag from the SVO structure is responsible for the decrease in the *c*-axis of the crystal, which in turn allows a reduction in the distance between V_4O_{11} slabs.[iv,xx] The large broadening and line shift in the $x = 5.59$ sample thus arises from two factors, reduced Li–V distances upon decrease in the *c*-axis, and reduction of diamagnetic V^{5+} to paramagnetic V^{4+} and V^{3+}. This phenomenon has been noted in other systems as well.[xxi,xxii,xxiii]

It is interesting to note the distinctions between this study and that of Holland et al.[x] in which ^{7}Li NMR of $Li_xV_2O_5$ xerogels at different stages of lithiation are compared. The same general trend is noticed in the peaks: in particular, the downfield peak undergoes significant shifting and broadening with increased lithiation. If it was supposed that during the insertion mechanism all of the Ag^{+1} was reduced first, then the structure would have the general formula $Li_2V_4O_{11}$, which could be compared to Li(x ≈ 1 (actually

0.98). However in their study, the sample is broadened and shifted more than the current sample, Li=2.13. Considering that in V_2O_5 there is no elongation of the c-axis (c=3.56Å)[xxiv] due to silver atoms between the oxygen layers, the lithium atoms are located closer to the vanadium centers, and would explain why the shift and broadening is seen at lower lithium values.

An overall decrease in the integrated areas is seen in the successively discharged samples (from $x = 2.13$ to $x = 5.59$, as compared to $x = 0.72$). This may provide evidence of the presence of V^{3+} in these cathodes, as the presence of these reduced vanadium ions is known to broaden nearby lithium signals significantly.[xxv]

^{51}V NMR plays a much different role than does ^{7}Li as a nuclear probe. Due to a nuclear spin of $7/2$, ^{51}V NMR exhibits large quadrupolar broadening effects that prevent the dissection of the spectra into several peaks. Nevertheless, the quadrupole interaction is an extremely sensitive probe of the short-range structural environment of the nucleus. The spectra of all four samples are displayed in figure 5. Here the horizontal scale is expressed in frequency units rather than ppm. $Ag_2V_4O_{11}$ shows somewhat more distinct quadrupolar satellites than the $x = 0.72$ sample. However, because the quadrupole satellites do not notably decrease in intensity or definition, it is concluded that the electronic symmetry about the nuclei is not significantly altered. Therefore, it is likely that this is the effect of the lithium ions simply displacing the Ag ions while preserving the overall structure without significant distortion in the first phase of discharge. The $x = 2.13$ sample shows a severe loss in structural order which has been previously reported to happen in this discharge range.[v]

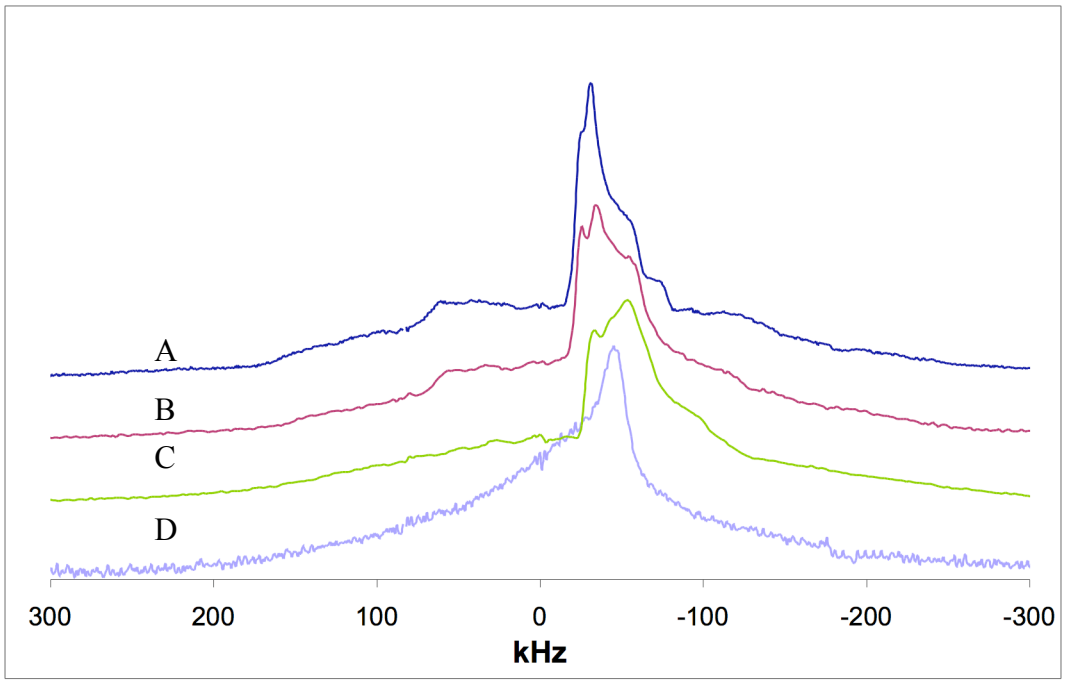

Figure 5: *^{51}V Quadrupolar echo NMR spectra of SVO cathodes at varying states of discharge, normalized to average intensity for comparison: (A) $Ag_2V_4O_{11}$ (B) $Li_{0.72}Ag_2V_4O_{11}$, (C) $Li_{2.13}Ag_2V_4O_{11}$, and (D) $Li_{5.59}Ag_2V_4O_{11}$*

As the large magnetic fields localized on paramagnetic ions precludes observation of an NMR signal from the nuclei of these ions, the remaining signal seen in the $x = 5.59$ sample is likely the result of a V_2O_5 impurity or electrochemically inaccessible regions of the original SVO cathode material. As all samples were prepared from the same batch of starting material, they all exhibit this spectral component, although it is masked by the other vanadium atoms in the +5 oxidation state in all but the $x = 5.59$ sample.

The XAFS results indicate corresponding conclusions.[xxvi] The silver nearest neighbor environment is apparently quite strongly affected by the amount of lithium added. The silver is seen to segregate from the SVO bulk upon even the lowest lithiation level, to form metallic fcc Ag, as seen clearly via comparison to the Ag foil reference. A

slight decrease in the calculated coordination number at the higher lithation levels suggested either defects in the segregated Ag regions, or surface Ag atoms. An increase in ordering of the particles is also seen in the increase in amplitude of the Ag-Ag peak. The XANES data further indicates that even at the highest level of lithiation (x=5.59), some Ag still exists in the +1 oxidation state, suggesting remaining electrochemically-isolated regions of SVO. The XANES data from the vanadium edge is also illuminating of the changes in oxidation state upon lithiation, including the formation of previously hypothesized[x] co-existing V^{+4} and V^{+5} states.

Conclusions

Spectroscopic analyses of the local environments of all three metal ions in lithiated SVO reveal details not readily available from electrochemical and X-ray diffraction studies. In particular, the picture of strictly serial reduction, first Ag, then V, should be modified.

The NMR results prove that there is no observable Li_2O, either as a component of the SEI or as a result of Li reduction of Ag^+, and that there are two distinct sites associated with intercalated Li. This is consistent and supportive of the XAS analyses which indicated that Ag reduction is initiated by $x = 0.72$ and proceeds to $x \leq 5.59$, at which point, ~95% of the Ag appears to have been reduced. The XAS data also indicated that the reduction of the Ag occurs via a phase separation from the starting structure to fcc Ag, but the segregated Ag is not in the equilibrium state with static disorder and defects remaining in the structure. The NMR and XAS data indicate that the V reduction

also commences by $x = 0.72$ and proceeds monotonically to $x = 5.59$. Over this range, V appears to go from V^{5+} to V^{3+} with associated structural changes. The local vanadium structure in $Li_{0.72}Ag_2V_4O_{11}$ is a more ordered form than that in SVO, but the vanadium environment becomes disordered at the higher lithium content. There is also evidence for residual V^{5+} in the $x = 5.59$ sample, attributable to either an impurity or electrochemically inaccessible SVO particles.

---

[i] West, K. and A.M. Crespi. "Lithium Insertion into Silver Vanadium Oxide, Ag2V4O11."*Journal of Power Sources* 54.2 (1995): 334-337.

[ii] Hirschinger, J., T. Mongrelet, C. Marichal, P. Granger, J. M. Savariault, E. Deramond and X. Galy. "Lithium (^{6}Li and ^{7}Li) NMR in High-Temperature Phases of Lithium Vanadium Oxide Bronzes ($Li_xV_2O_5$; $0.2<x<1$)." *Journal of Physical Chemistry* 97 (1993): 10301-10311.

[iii] Takeuchi, K. J., A. C. Marschilok, S. M. Davis, R. A. Leising and E. S. Takeuchi. "Silver Vanadium Oxides and Related Battery Applications." *Coordination Chemisty Reviews* 219-221 (2001): 283-310.

[iv] Crespi, Y., P. M. Skarstad, H. W. Zandebergen and J. Schoonman. *Proceedings of the Symposium on Lithium Batteries*, ed. E. S. Surampudi and V. Koch 93-94 (1993): 98-105.

[v] Ramasamy, R. P., C. Feger, T. Strange and B. N. Popov. "Discharge Characteristics of Silver Vanadium Oxide Cathodes." *Journal of Applied Electrochemistry* 36.4(2006): 487-497.

[vi] Gleason, N. R., R. A. Leising, M. Palazzo, E. S. Takeuchi and K. J. Takeuchi. *Talk # 248: Microscopic Study of the First Voltage Plateau in the Discharge of SVO and the Consequences on Electronic Conductivity.* 208th Meeting of the Electrochemical Society Session D2 – Rechargeable Lithium and Lithium-Ion Batteries/Battery/Energy Technology. Los Angeles, CA: 2005.

[vii] Crespi, A. M., P. M. Skarstad and H. W. Zandbergen. "Characterization of Silver Vanadium Oxide Cathode Material by High-Resolution Electron Microscopy." *Journal of Power Sources* 54.1(1995): 68-71.

[viii] Takeuchi, E. S. and R. A. Leising. "Melt Impregnation of Mixed Metal Oxide." US

Patent 6413669. 2 July 2002. (a); E. S. Takeuchi and R. A. Leising. “Synthetic Method for Preparation of a Low Surface Area, Single Phase Silver Vanadium Oxide.” US Patent 6566007. 20 May 2003. (b).

[ix] Vijayakumar, M., S. Selvasekarapandian, K. Nakamura, T. Kanashiro and R. Kesavamoorthy. "^{7}Li MAS NMR and Vibrational Spectroscopic Investigations of $Li_xV_2O_5$ (x=1.0, 1.2 and 1.4)." *Solid State Ionics* 167.1-2 (2004): 41-47.

[x] Holland, G. P., D. A. Buttry and J. L. Yarger. "^{7}Li NMR Studies of Electrochemically Lithiated V_2O_5 Xerogels." *Chemistry of Materials* 14.9 (2002): 3875-3881.

[xi] Stallworth, P. E., F. S. Johnson, S. G. Greenbaum, S. Passerini, J. Flowers, W. Smyrl and J. J. Fontanella. "Magnetic Resonance Studies of Chemically Intercalated $Li_xV_2O_5$ (x=1.16 and 1.48)." *Solid State Ionics* 146.1-2 (2002): 43-54.

[xii] Nakamura, K., D. Nishioka, Y. Michihiro, M. Vijayakumar, S. Selvasekarapandian and T. Kanashiro. "^{7}Li and ^{51}V NMR Study on Li^+ Ionic Diffusion in Lithium Intercalated $Li_xV_2O_5$." *Solid State Ionics* 177.1-2 (2006): 129-135.

[xiii] Kawakita, J., H.Sasaki, M.Eguchi, T.Miura and T.Kishi. "Characteristics of [delta]-$Ag_yV_2O_5$ as a Lithium Insertion host." *Journal of Power Sources* 70.1 (1998): 28-33.

[xiv] Rozier P. and J. Galy. "$Ag_{1.2}V_3O_8$ Crystal Structure: Relationship with $Ag_2V_4O_{11-y}$ and Interpretation of Physical Properties." *Journal of Solid State Chemistry* 134.2 (1997): 294-301.

[xv] Peled, E. "The Electrochemical-Behavior of Alkali and Alkaline-Earth Metals in Non-Aqueous Battery Systems - the Solid Electrolyte Interphase Model." *Journal of the Electrochemical Society* 126.12 (1979): 2047-2051.

[xvi] Cocciantelli, J. M., K. S. Suh, J. Senegas, J. P. Doumerc and M. Pouchard. "^{7}Li NMR of Electrochemically Inserted $Li_xV_2O_5$." *Journal of Physics and Chemistry of Solids* 53.1 (1992): 57-59.

[xvii] Cocciantelli, J. M., K. S. Suh, J. Senegas, J. P. Doumerc, J. L. Soubeyroux, M. Pouchard and P. Hagenmuller. (1992). "^{7}Li NMR in Electrochemically Intercalated [gamma] - $Li_xV_2O_5$ Bronzes ($0.95<x<1.9$)." *Journal of Physics and Chemistry of Solids* 53(1): 51-55.

[xviii] Garcia-Alvarado, F. and J. M. Tarascon. “Lithium Intercalation in $Ag_2V_4O_{11}$.” *Solid State Ionics* 73.3-4 (1994): 247-254.

[xix] Kuwabara, K., M. Itoh and K. Sugiyama. “Ionic-Electronic Mixed Conduction in $Li_xV_2O_5$.” *Solid State Ionics* 20.2 (1986): 135-139.

[xx] Zandbergen, H. W., A. M. Crespi, P. M. Skarstad and J. F. Vente. "Two Structures of $Ag_{2-x}V_4O_{11}$, Determined by High Resolution Electron Microscopy." *Journal of Solid State Chemistry* 110.1 (1994): 167-175.

[xxi] Pan, C., Y. J. Lee, B. Ammundsen and C. P. Grey. "^{6}Li MAS NMR Studies of the Local Structure and Electrochemical Properties of Cr-doped Lithium Manganese and Lithium Cobalt Oxide Cathode Materials for Lithium-Ion Batteries." *Chemistry of Materials* 14.5 (2002): 2289-2299.

[xxii] Menetrier, M., I. Saadoune, S. Levasseur and C. Delmas. "The Insulator-Metal Transition upon Lithium Deintercalation from $LiCoO_2$: Electronic Properties and ^{7}Li NMR Study." *Journal of Materials Chemistry* 9.5 (1999): 1135-1140.

[xxiii] Levasseur, S., M. Menetrier and C. Delmas. "Combined Effects of Ni and Li doping on the Phase Transitions in Li_xCoO_2 - Electrochemical and ^{7}Li Nuclear Magnetic Resonance Studies." *Journal of the Electrochemical Society* 149.12 (2002): A1533-A1540.

[xxiv] Chakrabarti, A., R. Druzinic, K. Hermann, M. Petersen, F. Wagner and M. Witko. "Geometric and Electronic Structure of Vanadium Pentoxide: A Density Functional Bulk and Surface Study." *Physical Review B* 59.16 (1999): 10583-10590.

[xxv] Stallworth, P. E., S. Kostov, M. L. denBoer, S. G. Greenbaum and C. Lampe-Onnerud. "X-ray Absorption and Magnetic Resonance Spectroscopic Studies of $Li_xV_6O_{13}$." *Journal of Applied Physics* 83.3 (1998): 1247-1255.

[xxvi] Leifer, N. D., A. Colon, K. Martocci, S. G. Greenbaum, F. M. Alamgir, T. B. Reddy, N. R. Gleason, R. A. Leising and E. S. Takeuchi. *Journal of The Electrochemical Society* 154.6 (2007): A500-A506.

C. The CFx Project

(In collaboration with Hong Gan at Greatbatch Inc., Dr. Thomas Reddy at Rutgers University, Valencia Johnson & Rakefet Ben-Ari at Hunter College)

Introduction

This ongoing project is a study of chemically discharged CF_x cathodes. In practice, Li/CF_x is a primary battery system in which lithium metal serves as the anode against fluorinated graphite in the presence of an electrolyte. Upon discharge, the lithium ions are oxidized while the fluorine is reduced, producing LiF, which precipitates on the remaining carbon structure. Certain facts about the mechanism of discharge of this system are known, such as the increase in conductivity of the CF_x that occurs as the battery is discharged.[i] However, the structure of the CF_x cathode during and after discharge, the mechanism of the de-fluorination process, and the exact location and form of the LiF remain unresolved.

The primary objective of this study was to investigate three types of fluorinated graphite materials in order to determine any chemical and/or structural distinctions between them as such, and as they undergo lithiation. Electrochemical studies on these different types of CF_x have indicated significant differences in electrochemical performance, including varying degrees of instability. Ultimately the aim is to correlate these findings with electrochemical data collected on the same materials in order to more fully understand the discharge mechanisms. The three starting CF materials were: CF_x F, which is fiber-based; CF_x G, which is graphite-based, and CF_x D, which is petroleum

coke-based. These three compounds are of nominally the same composition, i.e. $(CF)_x$, $x \approx 1$, but result from different preparation routes.

Each starting compound was subjected to chemical reduction in n-butyllithium under identical conditions to achieve several levels of lithiation, followed by EPR, ^{19}F NMR and ^{13}C NMR analyses. Both the solid powders and the filtrates were studied. Though it is appreciated that chemical lithiation is only a relatively crude model for electrochemical reduction, in part because of the very rapid, highly exothermic, and far-from-equilibrium nature of the reaction compared to relatively slow discharge rates characteristic of CF_x batteries, it does provide a useful means to characterize the samples in a timely manner. Therefore, although the spectroscopic details may differ somewhat between chemically and electrochemically reduced samples, it is expected that the main reaction species and the trends observed in their formation will be similar. Additionally the reactants were added very slowly, in titration-like fashion, in order to allow the reaction to proceed steadily and the chemical reaction was closely monitored for drastic changes in temperature.

Experimental

Three different types of carbon: an amorphous coke, a fibrous graphite and a standard graphite were fluorinated at high temperatures (>450^{o}C) to provide starting materials CF_x D, CF_x F and CF_x G, respectively. These starting materials were provided for analysis and subsequent lithiation, along with the CF_x standard electrode 'mixes', which contained 91.1% CF_x starting material, 5% carbon black and 3.9% PTFE binder.

The starting materials were chemically lithiated in an effort to simulate electrochemically cycling on a shorter time scale. All of the starting materials were reduced by a 2.5 M n-Butyl Lithium (nBL) solution in hexane. The depth of discharge (DoD) was controlled by adjusting the n-Butyl Lithium:CF_x mole ratio. The chemical procedure was as follows: 15 mL of hexane was added to 1g CF_x in a reaction vessel to obtain the CF_x suspension. The vessel was closed and stirred at a moderate rate. Once the powders were thoroughly wetted with hexane, varying amounts of nBL were added at the rate of 1-2 mL/hr. and the solution was stirred for 48 hours until reaction completion. The solution was then filtered, washed three times with hexane, and dried overnight under vacuum at room temperature. All procedures were carried out under controlled atmosphere in an Argon-filled glove box.

For the EPR experiments all samples were packed in air into quartz EPR tubes and run under identical parameters on a Bruker EMX Spectrometer. EPR data is typically reported as a derivative absorption peak therefore an integration procedure was necessary to obtain peaks that could be deconvoluted into separate components. The spectra were doubly integrated to provide a measure of the intensity of the signal, and quantify the number of paramagnetic centers and/or radical species by comparison to a known standard, $VOSO_4 \cdot nH_2O$, (n~5).

^{13}C and ^{19}F direct observe MAS NMR was conducted on all three starting materials, G (graphitic carbon), F (carbon fiber) and D (amorphous coke), in addition to the lithiated materials. ^{19}F was also conducted on the liquid effluents from the lithiation process for some samples. The ^{13}C NMR was conducted at high field (500MHz) in a 11.7T magnet in a Doty low C/F background NMR probe, and the samples were spun at

various speeds, from 8-12kHz. The ^{19}F experiments were conducted using a 300MHz Varian NMR spectrometer at various speeds, from 18-25kHz. For these experiments a 90_x-180_y pulse echo sequence was used to minimize the probe background signal. An aqueous solution of lithium trifluoromethylsulfonate (LiTf) was used as an external reference for fluorine, at -77.8ppm relative to the common reference ($CFCl_3$ at 0ppm) and TMS (0ppm) was used for carbon. All NMR spectral data was processed using Mestre-C, a standard NMR data processing software.

Results & Discussion

All samples show intense EPR signals in the region of g ~ 2 (figure 1) which is typical for free radicals and many paramagnetic species. Significant differences in the lineshapes of the EPR spectra of the starting materials were seen that changed with temperature (figure 1). These differences are indicative of variations in electronic structure and interactions in the samples. At room temperature CF_x G indicates the broadest (110G) and most intense signal while those of CF_x F and D are narrower (~50G). In the low temperature measurements (77K), the CF_x G line narrows, and broad, clear splitting patterns are seen in samples D and F. The total integrated areas of the low temperature spectra was measured and compared with a standard in order to quantify the number of paramagnetic centers in each sample. In addition, the single integrations of the low temperature data appeared to be composed of an overlap of a narrow and a broad line. Spectral deconvolutions of these integrated spectra were conducted in order to get a ratio of these two features. This data is presented in table 1.

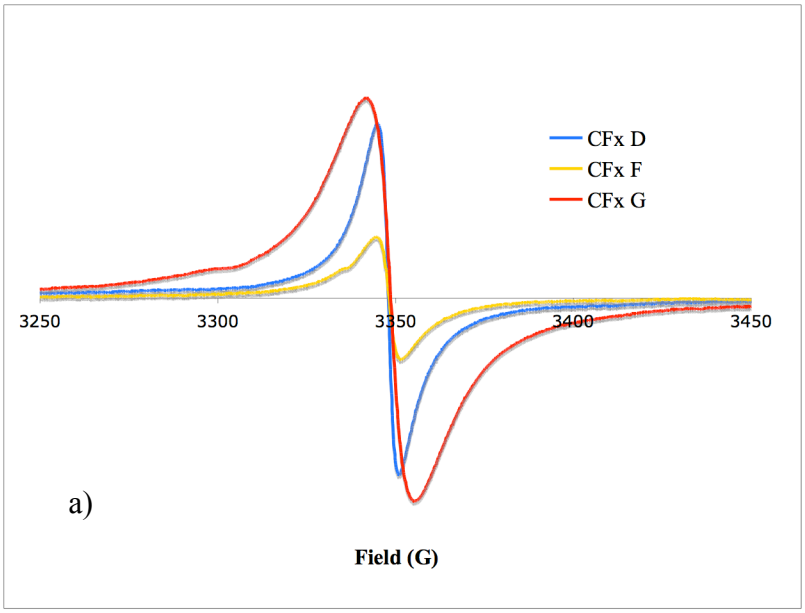

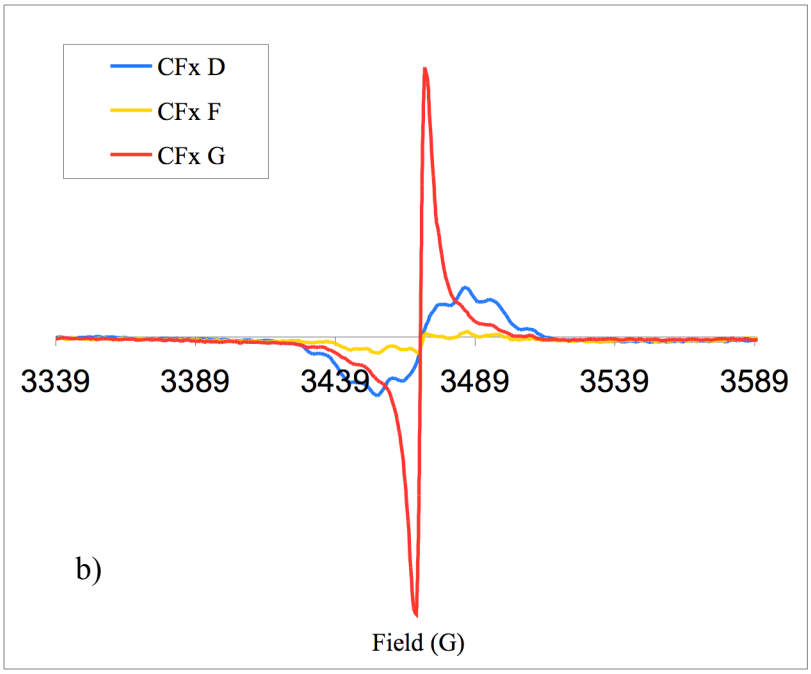

Figure 1: *EPR Spectra of starting materials CF_x D, CF_x F and CF_x G, at room temperature (a) and at 77K (b)*

The large narrow signal seen in sample G at low temperature indicates many highly mobile (delocalized) paramagnetic centers.[ii] At high (room) temperatures, the signal

width in G broadens significantly. This is most likely due to (highly motionally sensitive) shortened T_1 electron relaxation times, in accord with the Heisenberg Uncertainty Principle, which can be stated as $\Delta E \Delta t \geq \frac{\hbar}{2}$. As the lifetime of the spin states decreases, there will be a corresponding uncertainty in the energy of the state, and as $\Delta E = g_e m_B B_0$, this will correspond to an uncertainty in the resonant field, B_o. The narrower signals seen at room temperatures in samples D and F are suggestive of more delocalized spin carriers, but the signals are still rather broad at both low and high temperatures, suggesting this width is due to electron dipole-dipole and exchange interactions between paramagnetic centers, in turn suggesting that these centers are clustered, rather than randomly distributed throughout the sample.[iii] The well-defined splitting patterns seen at low temperatures additionally supports this hypothesis, as these are a result of hyperfine interactions with nearby fluorine nuclei (I=1/2), thereby implying more localized spin carriers. The relative intensities of the signals remain constant at low temperatures. The ratios of spins per volume and spins per gram were obtained from the double integrated intensity (DIN) of the spectra (table 1). CF_x D and G contain on the order of 10^{19} spins per gram, while sample CF_x F contains approximately one order of magnitude less.

Sample	**# spins/gram**	**Overall peak-to-peak Linewidths, ΔH_{pp}, in Gauss (G)**		**Ratio of areas of the broad to narrow lines in deconvolution (at 77K)**
		RT	77K	77K
CFxD	1.289×10^{19}	50	32	7:1
CFxF	1.582×10^{18}	55	32	16:1
CFxG	1.979×10^{19}	110	4	3:1
$VOSO_4 \cdot nH_2O$	2.380×10^{21}	--	--	--

Table 1: *Quantitiative EPR data from the low temperature (77K) measurements*

A simple line deconvolution illustrates that the integrated spectra are clearly composed of both broad and narrow peaks that correspond to the two types of spins, the ratios of which can be determined by the ratio of the relative integrated peak areas. (table 1). CF_x F appears to contain significantly greater ratio of the broad component, implying a greater percentage of localized spins.

^{19}F NMR was conducted at the lower field (300MHz) due to the capability of higher MAS speeds (20-25kHz) on that instrument. Spectra for the starting materials D, F and G are shown in figure 2. Generally, for homonuclear dipolar coupling, optimal spinning speeds should be at least as great as half of the width of the spectral envelope, which, for ^{19}F, due to its strong dipolar interactions, is usually quite large. This properly separates out the sidebands from actual resonances. The width of all of the fluorine peaks is attributed mainly to the large homonuclear dipolar coupling between the fluorine nuclei. So at higher speeds, the main covalent C-F resonance, seen at approximately -184ppm, narrows significantly. This allowed for the detection of a second component in the vicinity in the form of a prominent shoulder at approximately -166ppm. When the lines deconvolutions were performed additional peak(s) from -171 to -178ppm were necessary to include in order to properly fit the spectra. These peaks have been identified as typical of fluorine in graphite intercalation compounds (GICs) with C/F ratios of 4-6;[iv] that is, a more ionic, or semi-ionic C-F interaction.[v] The many small peaks seen in the region between -110 and -125ppm,[vi] (or -116 to -120ppm)[vii] are characteristic of $–CF_2$ sites. The differences in the CF_2 shifts are suggestive of different immediate environments, e.g. bulk vs. edge sites. Additionally, some intensity is seen in the region from -40 to -80ppm, which is where $-CF_3$ groups would resonate, however the intensities

of these resonances are too low to reliably quantify. Upon lithiation (see figure 3), the

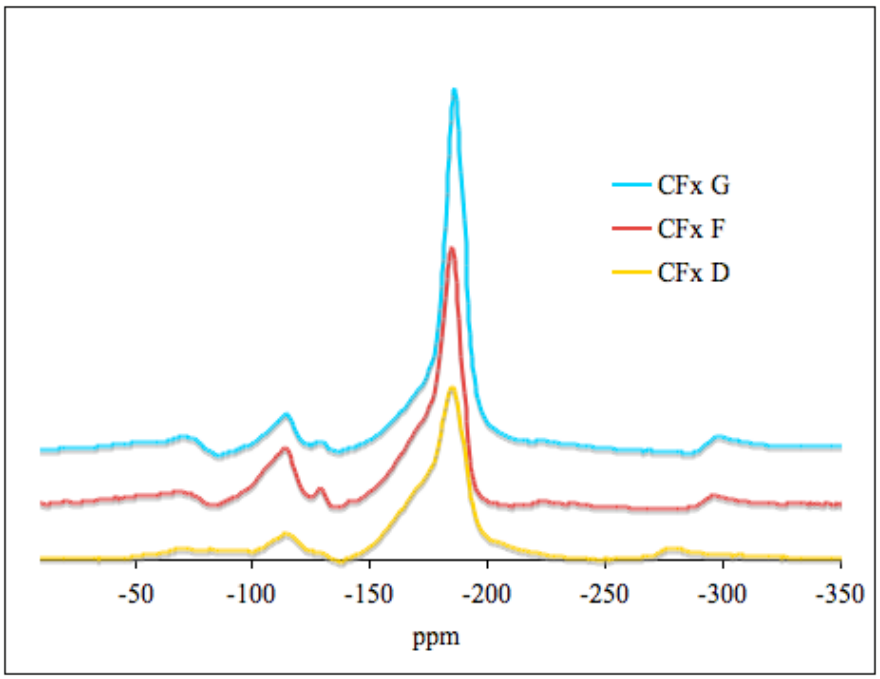

Figure 2: *^{19}F NMR of Starting Materials CFx D, F and G on 300MHz spectrometer at 26-32kHz spinning speeds*

LiF resonance is seen near -200ppm. Spectral deconvolutions were conducted to properly quantify the ratios of these resonances for all lithiation levels for all three sample materials (see figures 4a-c).

The successive lithiation process can be tracked in the spectra through the obvious decrease in the C-F intensity and the accompanying increase in the LiF signal. Other trends were made evident through the line deconvolutions, such as the reduction order of the different types of fluorine in the bulk. There appear to be approximately four different types of carbon-fluorine interactions, from covalent to semi-ionic/ionic. It is clear that the

D and F starting materials contain more semi-ionic species than does G. (30%, 40%, and 18%, respectively). This is significant for two reasons. One is that the starting material

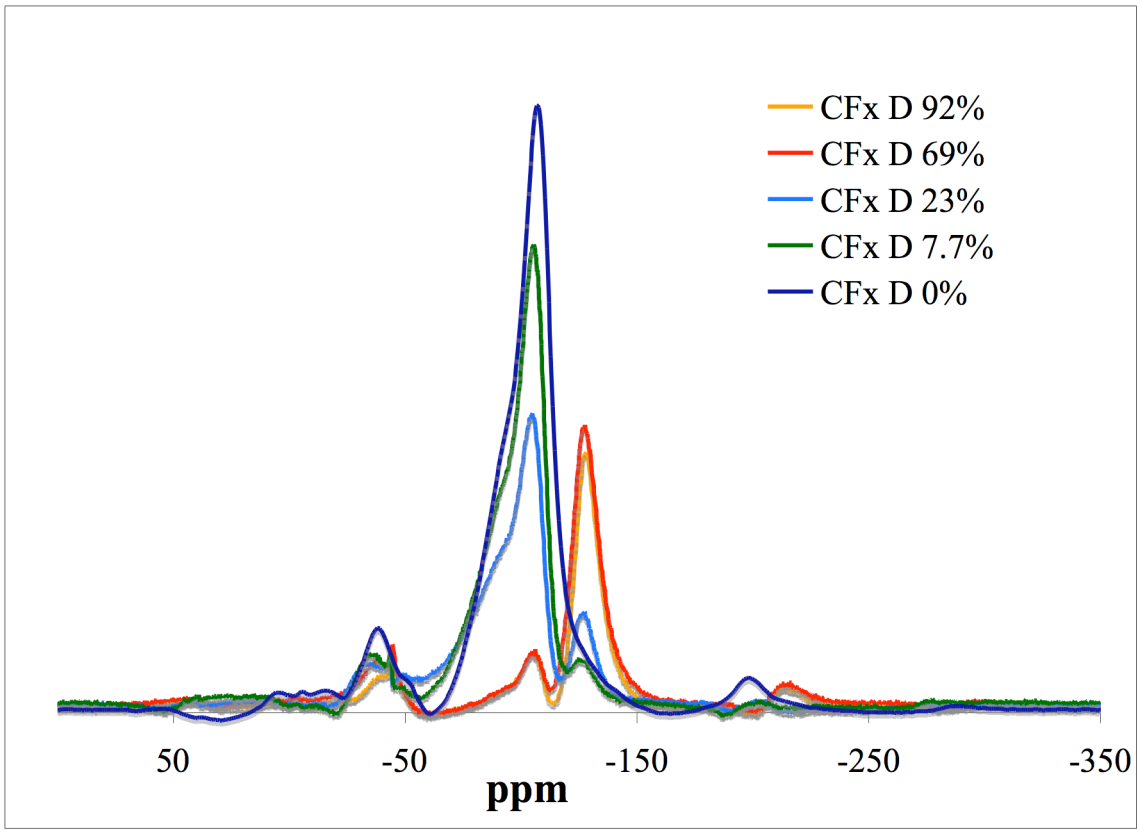

Figure 3: *^{19}F NMR of lithiated CFx D Series, 23kHz spinning speeds*

were fluorinated at temperatures >450^{o}C, and are therefore considering high temperature (HT) CF compounds; the C-F interactions in such compounds are expected to be almost, if not completely, covalent.[viii] Furthermore, with respect to electrochemical behavior, Root et al. claimed that ionic C_xF compounds tend to exhibit higher reduction potentials when compared to their covalent analogs.[viii] As far as the trend over the course of the lithiation, it appears through the deconvolutions that in F the covalent fluorines are

reduced at a faster rate than the semi-ionic fluorines in the initial stages (up to 23%). Then there is a drastic reduction in the semi-ionic fluorines in the 69% level. A similar pattern is seen in D, although the starting material appears to lose some CF_2 intensity, and perhaps due to some re-structuring of the layers over the course of the reaction, it appears more semi-ionic interactions are indicated in the first level of lithiation compared to the starting material. In G it also seems that the covalent fluorines are reduced preferentially in the first stage, along with some restructuring of C-F interactions, however the semi-ionic fluorines are greatly reduced at the 23% level and are completely gone by 69%. In D and F some ionic fluorine intensity remains even at the 69% level.

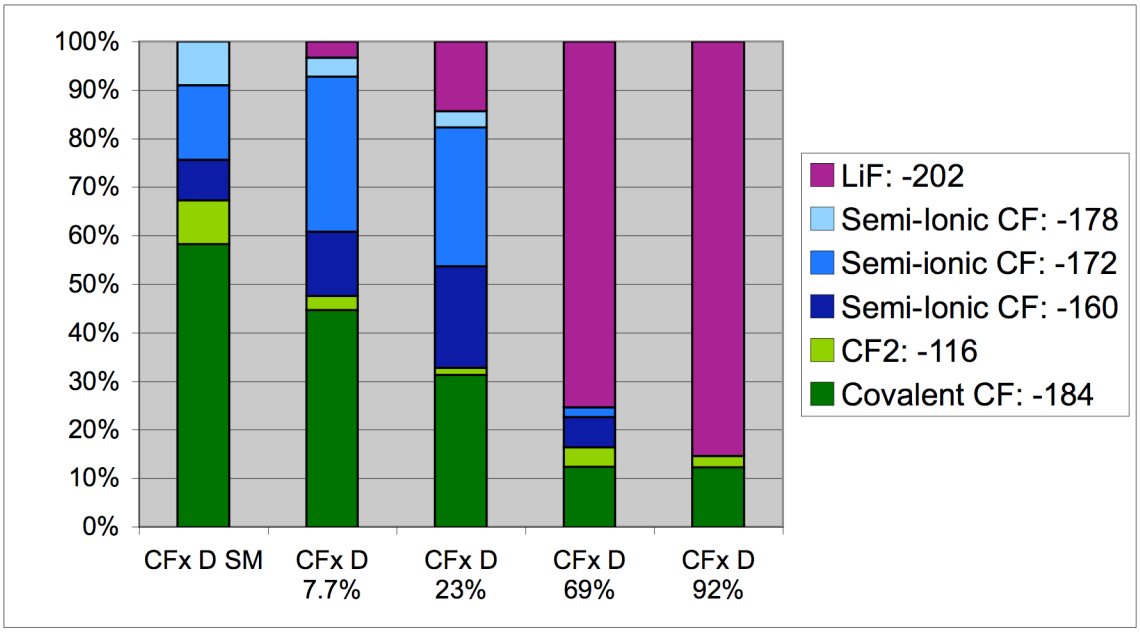

Figure 4a: *^{19}F NMR (300MHz) Comparative Quantitative Line Deconvolutions of lithiated CFx D*

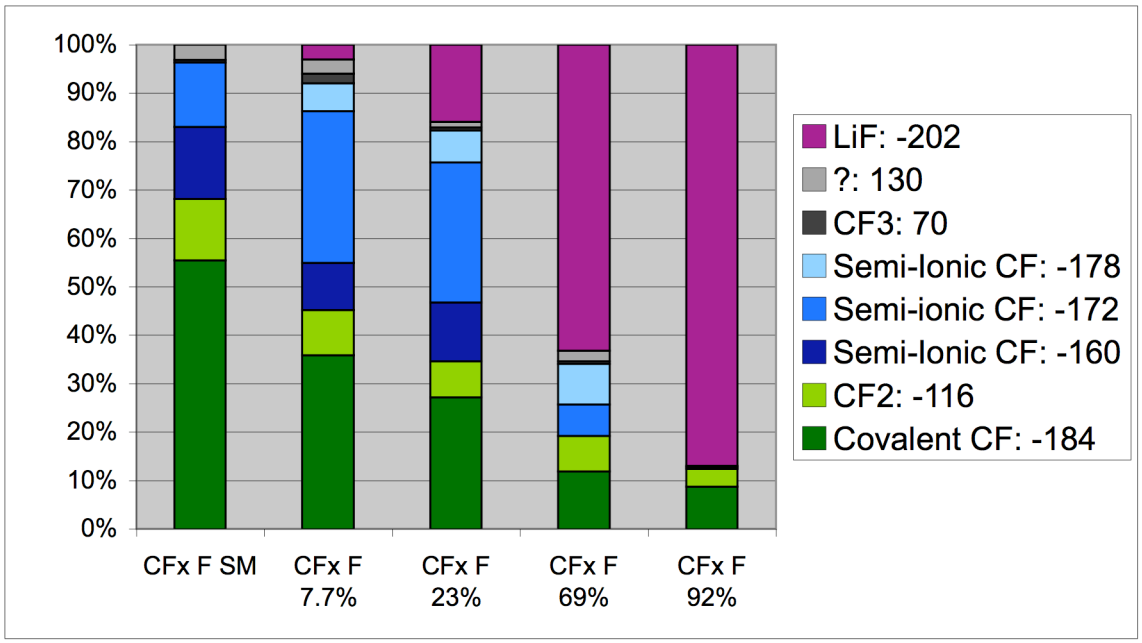

Figure 4b: *^{19}F NMR (300MHz) Comparative Quantitative Line Deconvolutions of lithiated CFx F*

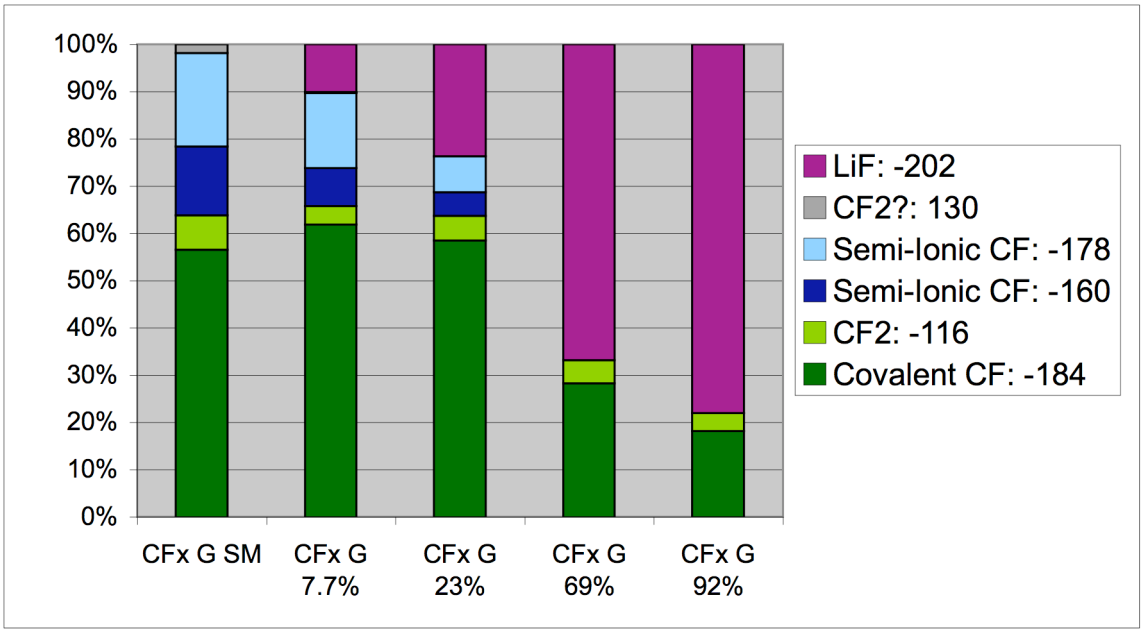

Figure 4c: *^{19}F NMR (300MHz) Comparative Quantitative Line Deconvolutions of lithiated CFx G*

In series G, the production of LiF maximizes near 80%. This implies that the LiF-producing reaction does not go to completion. The question remains whether the remainder of the n-BuLi stays unreacted, and simply volatilizes off of the surface, or whether a different reaction takes place, such as lithium reacting with the carbons in the structure. For this reason ^{7}Li MAS NMR experiments of the samples and the sample filtrates is the next logical step in this study, as Li-C interactions may be discernible from other lithium signals via NMR. The main CF peak in D and F samples is close to 10% of the signal at the 92% lithiation. This is indication that the reaction in these samples does basically go to completion, as expected.

The existence of $–CF_2$ sites in and of itself, in samples which were nominally fully fluorinated (CF_1), implies the existence of fluorine-free graphitic regions.[ix,x] Further evidence of these is in the ^{13}C NMR data of these same samples, in which $–CF_2$ and $–CF_3$ resonances can be identified. Another phenomenon common to all three samples is the persistence of these CF_2 resonances throughout the lithiation. In fact any perceived reduction in that group of resonances, except perhaps in the first stage of lithiation of D, is small enough to be within measurement error. This is consistent with the hypothesis by Delabarre et al. that the CF_2 groups are electrochemically inactive.[xi] A significant difference in the samples is that in CF_x D and G 3-5% of the fluorine is in $>CF_2$ groups. This number is greater by approximately a factor of two for CF_x F.

A very small resonance near -70ppm is seen in sample F. This peak is in the $-CF_3$ region and remains throughout the lithiation process. This is also consistent with the hypothesis by Delabarre for $–CF_3$ groups as these were also deemed to be electrochemically inactive.

A peak near -130ppm is seen in the F and G starting materials. It is 'consumed' immediately in G, but remains up until the last level of lithiation in F. This peak is in the CF_2 region, but clearly in a different configuration from the CF_2 resonance at -115ppm. Further studies (relaxation and/or cross-polarization) would be necessary to provide more information.

^{19}F NMR was also conducted on the liquid filtrate from the lithiation of the following samples: G 7.7%, G 23%, F 23% and F 92%. The NMR was conducted within two days of the lithiation process in order to detect any short-lived intermediates. No signal was seen, indicating that no soluble fluorine-containing species remained in the filtrate.

Upon close examination, there appears to be a slight shift in the LiF peak near 200ppm. An initial hypothesis was that this shift could be a result of a change in LiF particle size. Additional investigations into this hypothesis were conducted, including a ^{19}F NMR study of different sized particles of ball-milled LiF, and high speed MAS to reduce the uncertainty in spectral line position. No shifts were discernible in these spectra; this shift is presumed to be experimental artifact.

The ^{13}C MAS NMR spectra were collected on the 500MHz spectrometer at spinning speeds of 10-20kHz. The spectra of sample D are shown in figure 5. Due to the long relaxation times of carbon nuclei in these materials, most other studies conduct ^{13}C NMR via cross-polarization by the fluorine, which shortens the relaxation time considerably. However, cross-polarization data is not accurately quantifiable, as resonances are excited unequally. In this study directly observed ^{13}C NMR was conducted. Though due to this low abundance of ^{13}C nuclei, and a relatively low

gyromagnetic ratio, the directly observed carbon signal is quite weak, necessitating thousands of scans for a decent signal-to-noise. However due to time constraints dictated by the long T_1 times (90-200s), this was not possible for all of the samples therefore signal-to-noise was low which increases the error margin in the associated spectral deconvolutions (figure 6a-c). Additionally sample G 7.7% appears to be an outlier; it is presumed that the error lay in the chemical reaction, i.e. the lithiation process did not go to completion.

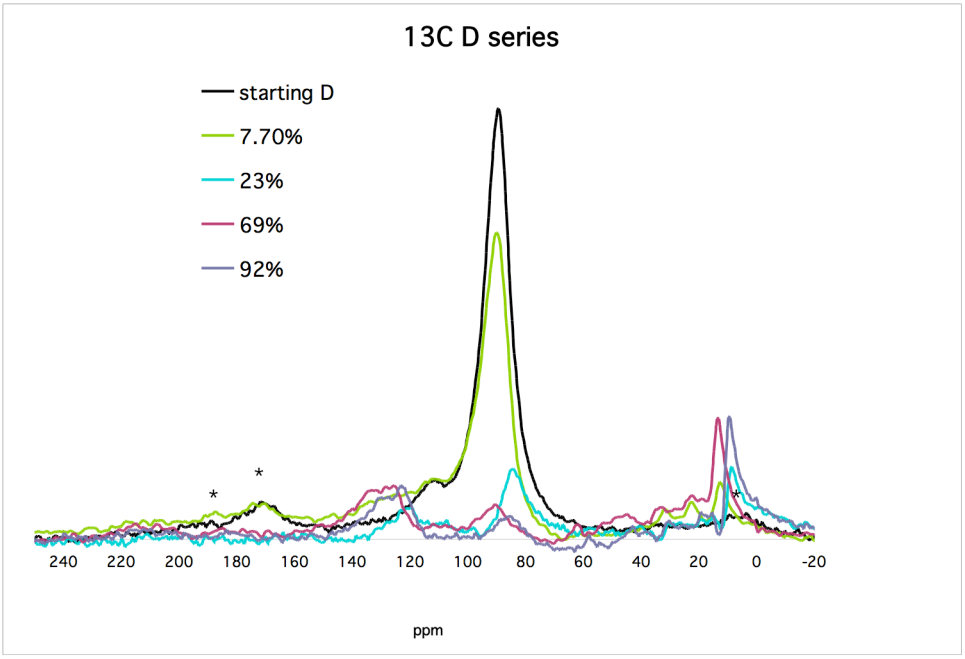

Figure 5: *^{13}C NMR Spectra of Lithiated CFx D Series*

Several peaks are seen in the starting and lithiated materials, most of which are readily identifiable. The covalent CF peak resonates at 88ppm. According to Sato, in a study of semi-ionic CF materials, the ^{13}C chemical shift of a carbon in a semi-ionic/ionic interaction with fluorine is near 89ppm.[v] Therefore this peak would not be

distinguishable from the covalent resonance. A clear resonance is visible near 109ppm in all D and F samples. Shifts in this regions are assigned to some type of $>CF_2$ group.[vi] As seen in the ^{19}F NMR data, this resonance appears to decrease slightly, but does not disappear, even at the 92% lithiation level.

A small resonance near 34ppm is seen in sample D and remains constant throughout the lithiation process. Resonances in this vicinity are identified as 'sp^3' carbon, e.g. ^{13}C in diamond resonates at 35ppm.[xii]

A small resonance is seen near 43ppm in all of the samples. They exhibit different trends, however. The 43ppm shift increase in intensity throughout the lithiation in D and F; this same shift appears in the starting material of G yet appears to decrease in that sample. It is presumed that this is also an 'sp^3' type of interaction, suggestive perhaps of $-C_xH_y$ groups at the particle edges.

Two peaks near 125ppm and 136ppm begin to appear over the course of the lithiation. These peaks have been identified as graphitic carbon, the former considered 'bulk graphitic' (C_b) (two or more bonds away from CF) and the latter considered 'interfacial graphitic' (C_i) (less than two bonds away from CF).[xiii,xiv] Samples F and G appear to contain graphitic domains in their starting material. As some amount of CF_2 is seen in F, this is not in discord with the presumed 1:1 CF ratio. In sample G, the existence of the graphite at the outset, with no recognizable CF_2 or CF_2 resonances, implies a C:F ratio of greater than 1:1. As the lithiation progresses, more bulk

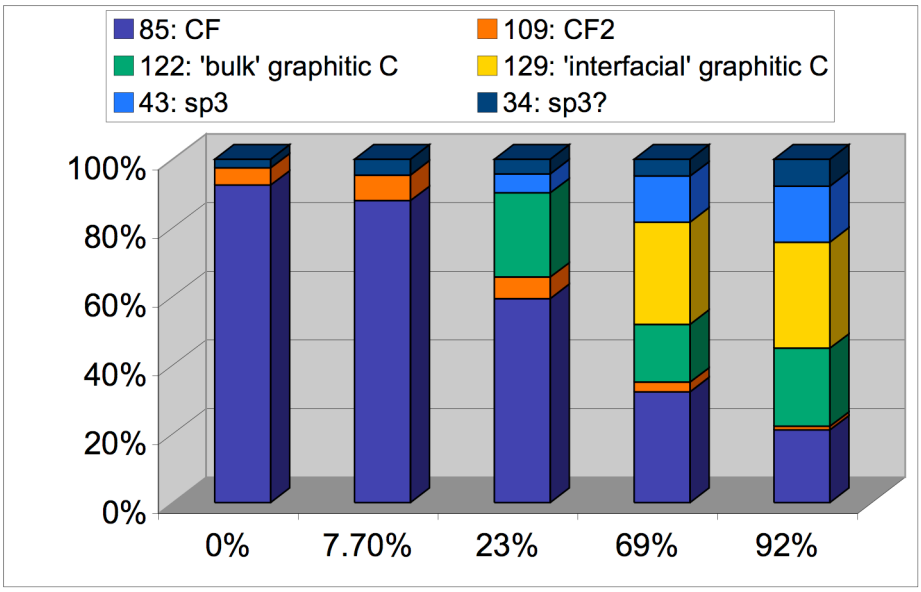

Figure 6a: *^{13}C NMR (500MHz) Comparison of Quantitative Spectral Deconvolutions of CFx D*

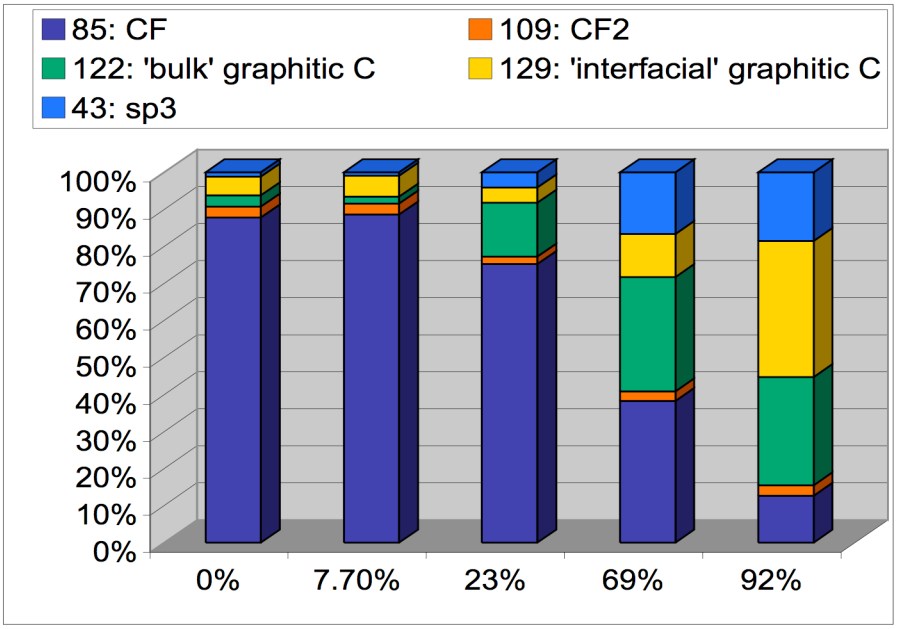

Figure 6b: *^{13}C NMR (500MHz) Comparison of Quantitative Spectral Deconvolutions of CFx F*

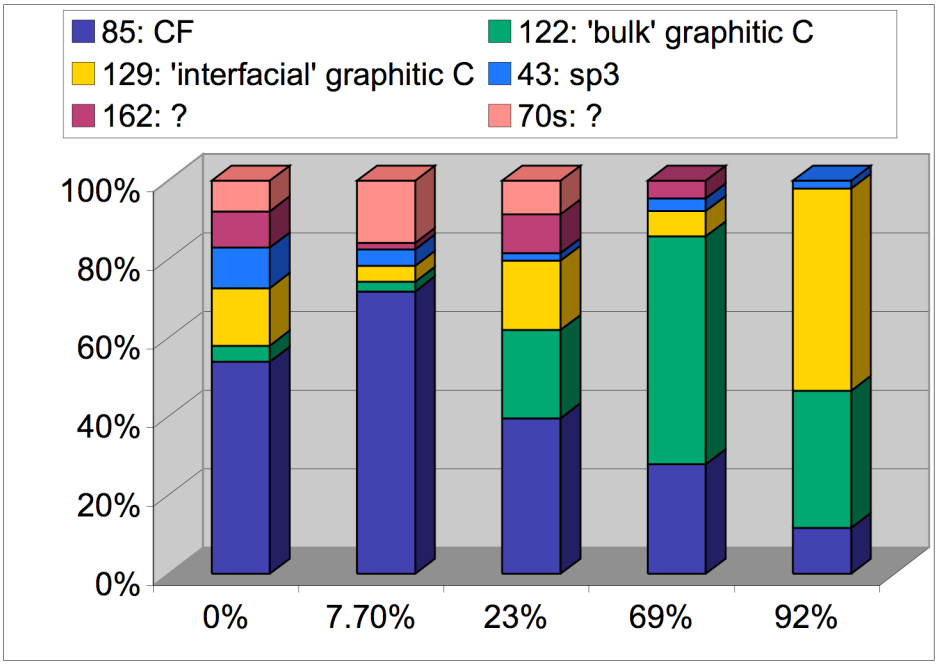

Figure 6c: *^{13}C NMR (500MHz) Comparison of Quantitative Spectral Deconvolutions of CFx G*

than interfacial graphite is seen in both D and F. This suggests that the initial graphitic domains are larger, and perhaps more localized near the surfaces of the particles (i.e. not close to the remaining C-F regions). By the 69% lithiation in both, the interfacial components are more significant, implying the creation of a greater number of smaller graphitic domains within the particles. In sample G at 69% the bulk graphitic carbon is quite large, suggesting that this data is erroneous. If it is accurate this would imply that the graphitic domains are large and continuous; the subsequent increase in the interfacial component in the 92% sample would then suggest that these regions are broken up into smaller subdomains. The overall increase in graphitic domains in general is also confirmed in the XRD data taken of these samples at different stages of lithiation. A

reflection near 26°, which increases continuously with increasing lithiation, is assigned to to graphite in a recent study of similar compounds.[xv]

A simple calculation to monitor the F:C ratio over the course of the lithiation is indicated in equation 1, below:[xiv]

$$\frac{F}{C} = \frac{CF + 2CF_2}{C_i + C_b + CF + CF_2} \qquad \textit{Equation 1.}$$

These results are displayed graphically in figure 7. Though some source of error is expected due to the poor signal-to-noise of the ^{13}C NMR spectra, samples D and F indicate reasonable trends while the same data from sample G remains inconclusive. Samples D and F both indicate an F:C ratio close to one initially, and this does not significantly decrease until the second state of lithiation at 23%. As the semi-ionic intensity is included in that of the covalent because of the spectral overlap, the fact that this ratio changes only slightly could be supportive of the ^{19}F data which seemed to indicate less that the production of LiF (and the accompanying removal of F from the bulk) was the major event, and rather that the first stage of lithiation mostly induced a re-arrangment of the C-F atoms in the main structure.

The set of peaks in the region 10-32ppm (see figure 5) likely arise from nBL, hexane and/or derivatives of these compounds, as this is where they are known to resonate.[xvi,xvii] As the species alone are volatile, and therefore not likely to remain on the surfaces over time, in addition to the fact that these resonances increase in intensity with increasing lithiation, it is highly probable that these compounds are intercalating into the graphite layers. Sample D does not indicate any of the 30ppm resonance. This could be evidence of different intercalation phenomena, perhaps due to differences in lattice spacing/size of intercalate. Evidence of intercalation is also seen in FTIR data taken of

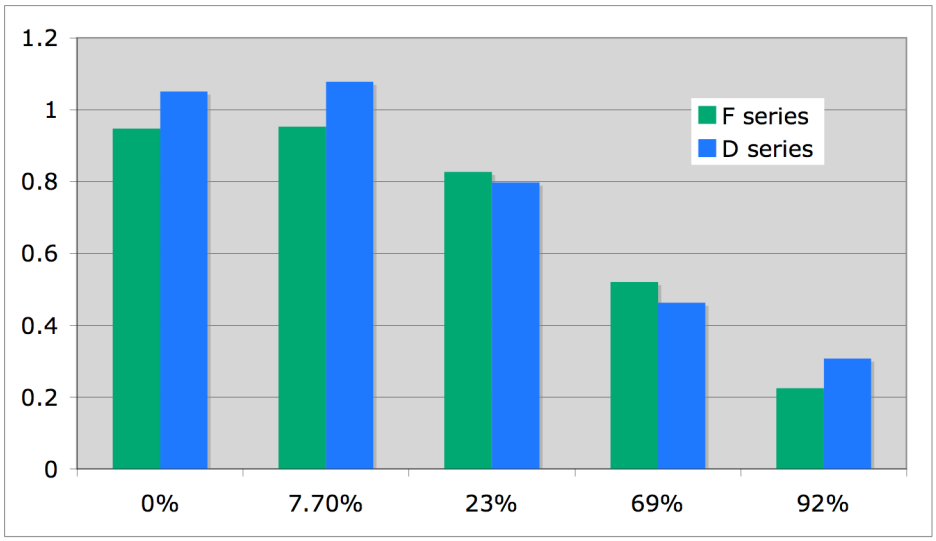

Figure 7: *F/C ratio throughout lithiation of all series: D, F and G*

the lithiated samples in which vibrational modes characteristic of organic solvents are seen, and in the XRD studies, in which a reflection near 21° is seen to gradually increase. According to the study of intercalated fluorinated graphites referenced earlier by Delabarre et al., this reflection near 21° corresponds to species intercalated into the graphite layers.[xi] Additionally, as is clear in the quantitative deconvolutions in figure 8a-c, the resonances do not increase evenly, strongly suggesting intercalation of the hexane and/or nBL derivatives. (These resonances are not included in the ^{13}C NMR deconvolution graphs, in order to accurately compare the fates of structural carbon alone.)

a)

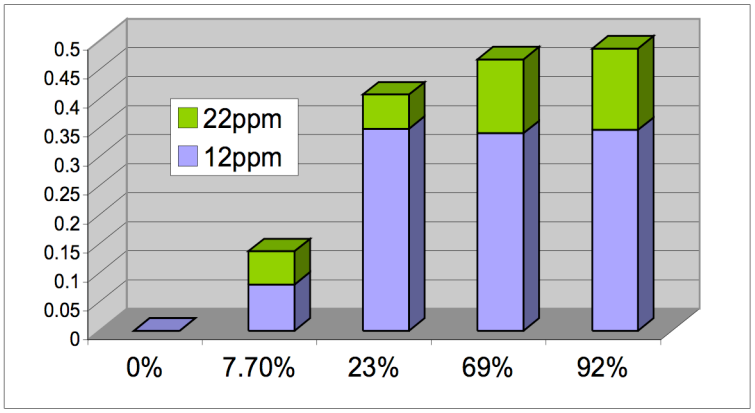

b)

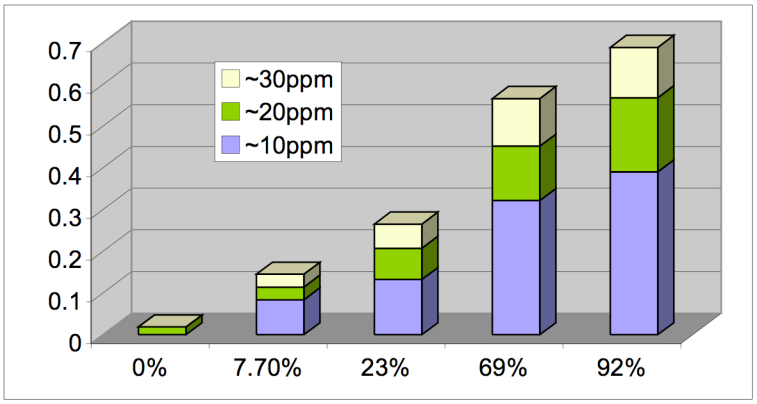

c)

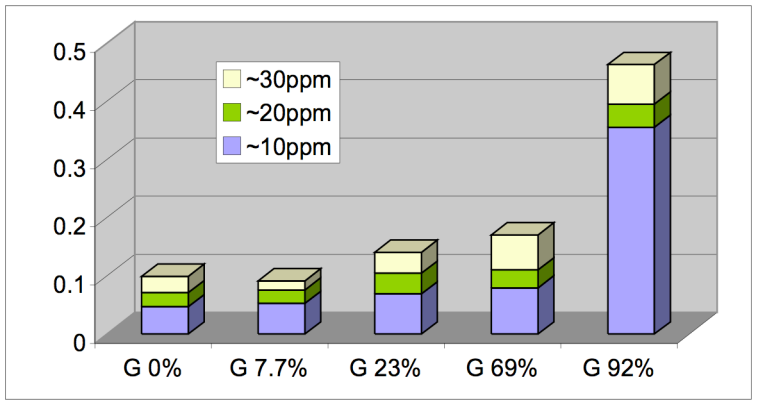

Figure 8: *^{13}C NMR (300MHz) of solvent derivative species in (a) CFx D, (b) CFx F, and (c) CFx G.*

Conclusions

The data collected provided several new insights into structural and chemical differences in these materials. Clear differentiations in the starting materials were seen in

the EPR data including the presence of structural defects (i.e. dangling bonds), at low temperatures. The graphite-based material had a spin density almost 50% higher than the petroleum coke-based sample and about one order of magnitude higher than the graphite fiber. The detection and quantification of several semi-ionic/ionic C-F interactions, in addition to the expected covalent CF interactions was novel and interesting, as high temperature (>450^{o}C) CF_x compounds have previously been presumed to be composed only of the latter. It was also then possible to track the order of reduction of the different fluorines over the course of the lithiation, and determined that in samples F and D the covalent fluorine are reduced *in advance* of the semi-ionic species. In sample G the ionic interactions disappear more quickly, and are entirely consumed by the 69% lithiation level. It was also evident in both the ^{19}F and the ^{13}C NMR that at least one type of CF_2 species remained as such throughout the entire lithiation process, either indicating electrochemically isolated regions, or an electrochemically inactive bonding configuration. In addition there appears to be a greater amount of LiF production in samples F and D compared to sample G at the highest DOD (nominally 92%). It was also confirmed that there is some amount of intercalation of the solvent and/or solvent breakdown products into the bulk structure that increased with successive lithiation.

Further studies will include ^{7}Li NMR of the sample filtrates, particularly at end stages of lithiation to determine whether any unreacted lithium species remain in solution. ^{7}Li NMR will also be performed on the samples themselves to monitor whether any direct Li-C bonding or lithium intercalation has taken place unexpectedly. ^{19}F-^{13}C cross-polarization experiments will also be an excellent supplement to the data already collected, shedding light on the differences in C-F bond lengths as these slight variations

in distances correspond to different optimal contact times. These will be conducted in tandem with relaxation studies on these same resonances, as the T_1 times for fluorine are reported to decrease in more ionic-type C-F interactions (660ms vs. 53ms), as the T_2 times increase (0.026ms vs. 0.036ms).[iii] Detailed EPR data (including deconvolutions and quantitation of spins) will also be collected on the lithiated materials.

---

[i] Watanabe, N. "Two Types of Graphite Fluorides, $(CF)_n$ and $(C_2F)_n$, and Discharge Characteristics and Mechanisms of Electrodes of $(CF)_n$ and $(C_2F)_n$ in Lithium Batteries." *Solid State Ionics* 1.1 (1980): 87-110.

[ii] Dubois, M., K. Guerin, J. P. Pinheiro, Z. Fawal, F. Masin and A. Hamwi. "NMR and EPR Studies of Room Temperature Highly Fluorinated Graphite Heat-Treated Under Fluorine Atmosphere." *Carbon* 42.10 (2004): 1931-1940.

[iii] Panich, M., A. I. Shames and T. Nakajima. "On Paramagnetism in Fluorinated Graphite: EPR and Solid State NMR Study." *Journal of Physics and Chemistry of Solids* 62.5 (2001): 959-964.

[iv] Panich, A. M., T. Nakajima and S. D. Goren. "^{19}F NMR Study of C-F Bonding and Localization Effects in Fluorine-Intercalated Graphite." *Chemical Physics Letters* 271.4-6 (1997): 381-384.

[v] Sato, Y., K. Itoh, R. Hagiwara, T. Fukunaga and Y. Ito. "On the So-Called "Semi-Ionic" C-F Bond Character in Fluorine-GIC." *Carbon* 42.15 (2004): 3243-3249.

[vi] Krawietz, T. R. and J. F. Haw. "Alkali Metal Oxides, Peroxides and Superoxides: A Multinuclear MAS NMR Study." *Chemical Communications* 102.45 (1998): 2151-2152.

[vii] Weigert, F. J. and R. J. J. Karel. “A Fluorine NMR Database.” *Journal of Fluorine Chemistry* 37 (1987): 125-149.

[viii] Root, M. J., R. Dumas, R. Yazami and A. Hamwi. “The Effect of Carbon Starting Materials on Carbon Fluoride Synthesized at Room Temperature.” *Journal of the Electrochemical Society* 148.4 (2001): A339-A345.

[ix] Giraudet, J., M. Dubois, K. Guerin, J. P. Pinheiro, A. Hamwi, W. E. E. Stone, P. Pirotte and F. Masin. "Solid-State ^{19}F and ^{13}C NMR of Room Temperature Fluorinated Graphite and Samples Thermally Treated Under Fluorine: Low-Field and High-Resolution Studies." *Journal of Solid State Chemistry* 178.4 (2005): 1262-1268.

[x] Homer, J. and L. F. Thomas. "The Nuclear Magnetic Resonance Spectra of *cis*- and *trans*-Perfluorodecalin." *Proceedings of the Chemical Society* (1961): 139-140.

[xi] Delabarre, C. M., Dubois, K. Guerin, Z. Fawal and A. Hamwi. "Room Temperature Graphite Fluorination Process Using Chlorine as Catalyst." *Journal of Physics and Chemistry of Solids* 67 (2006): 1157-1161.

[xii] Guerin, K., J. P. Pinheiro, M. Dubois, Z. Fawal, F. Masin, R. Yazami and A. Hamwi "Synthesis and Characterization of Highly Fluorinated Graphite Containing sp^2 and sp^3 Carbon." *Chemistry Materials* 16 (2004): 1786-1792.

[xiii] Mallouk, T., B. L. Hawkins, M. P. Conrad, K. Zilm, G. E. Maciel and N. Bartlett. "Raman, Infrared and N.M.R. Studies of the Graphite Hydrofluorides $C_xF_{1-\delta}(HF)_\delta$ ($2 \leq x \leq 5$)." *Philisophical Transactions of the Royal Society of London. Series A, Math & Physical Sciences* 314:1528 (1985): 179-187.

[xiv] Hagaman, E. W. and D. K. Murray. "Solid State ^{13}C and ^{19}F NMR Characterization of Fluorinated Charcoal." *Energy & Fuels* 12 (1998): 399-408.

[xv] Guerin, K., M. Dubois and A. Hamwi. "Electrochemical Discharge Mechanism of Fluorinated Graphite Used as Electrode in Primary Lithium Batteries." *Journal of Physics and Chemistry of Solids: Proceedings of the 13th International Symposium on Intercalation Compounds* 67.5-6 (2006): 1173-1177.

[xvi] Feist, P. "Carbon Chemical Shifts." *University of Colorado at Boulder :: Chemistry and Biochemistry Website*. 2003. University of Colorado at Boulder. Oct 2008 <http://orgchem.colorado.edu/hndbksupport/nmrtheory/carbonchemshift.html>.

[xvii] Reich, H. J. *C-13 Chemical Shifts*. 2008. Department of Chemistry at the University of Wisconsin. Oct 2008 <http://www.chem.wisc.edu/areas/reich/Handouts/nmr-c13/cdata.htm>.

D. ^{13}C Solid State NMR Study of Carbon Anodes Cycled in Isotopically Enriched Electrolytes

(In collaboration with In-Q-Tel, Prof. Clare P. Grey at Stony Brook University, Prof. Prakash at University of Southern California, Dr. Marshall Smart at Jet Propulsion Laboratories, and Luz Sanchez at Hunter College/JPL, and Boris Itin at the New York State Structural Biology Center)

Introduction

A considerable amount research has been conducted in an attempt to elucidate a complete chemical and physical model of the SEI. Several review articles have attempted to summarize what has been learned thus far.[i,ii,iii,iv,v] It is general presumed that the bulk of the SEI formed on the cathode surface is composed of semi-organic and inorganic species, while that found on the carbonaceous anode is primarily composed of organic species. Unfortunately the elemental make-up of organic compounds themselves impose limitations on the utility of NMR for use in such investigations: the hydrogen nucleus has a very small chemical shift range, rendering the signals indistinguishable from one another in a the solid state; and the non-zero spin isotopes of carbon and oxygen are extremely low in natural abundance.

In this study the limitation on the carbon nucleus was addressed by isotopically enriching the electrolytes used with ^{13}C so that the corresponding breakdown products would be NMR-detectable. The sensitivity of the NMR probe at the field used in this study (750MHz) is such that a minimum of ~10^{18} NMR-active nuclei are needed to

produce a detectable signal. A directly observed ^{13}C NMR study of the SEI formed from unenriched materials would not be distinguishable from the graphitic electrode, or carbon-containing additives in the electrodes. The electrolyte used was a mixture of ethylene dicarbonate and diethyl carbonate, both enriched on the carbonate position (figure 1).

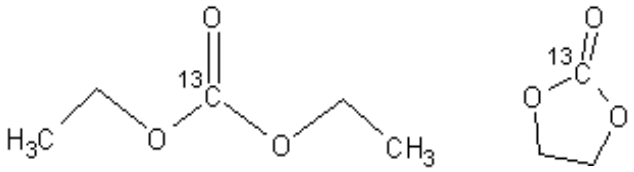

a. b.

Figure 1: *^{13}C enriched solvent compounds (a) diethyl carbonate & (b) ethylene carbonate*

Experimental

Relevant experimental parameters for all of the samples are given in table 1. All of the enrichments were conducted by Prof. Prakash at USC, and cell assembly/cycling was conducted by Dr. Smart and Ms. Sanchez at JPL, after which the samples were sealed and sent to Hunter College for analysis at the NYSBC.

For all cells in this study, the cathode used was commercially available $LiCoO_2$ and the anode was graphitic mesocarbon microbeads (MCMB), both fabricated with 5 wt % polyvinylidene difluoride (PVDF) binder, and 0.5% super P graphite to improve conductivity between the particles. Enriched ethylene carbonate and diethylene carbonate were synthesized using 99% ^{13}C enriched K_2CO_3 as a precursor. The solvents were then diluted to 25% enrichment and used to make 1M $LiPF_6$ for use in the electrochemical

cells. The cells were assembled using double-sided coated electrodes in a flooded electrolyte/cylindrical cell design and were equipped with pseudo lithium metal reference electrodes to monitor the cell electrochemistry.

Electrochemical measurements were made using an EG&G Potentiostat/Galvanostat interfaced with an IBM PC, using Softcorr 352. A Solartron 1255 Frequency Response Analyzer was used with this potentiostat for impedance measurements, with M388 software. Charge-discharge measurements and cycling tests were performed with an Arbin battery cycler. The cycling tests were done at current densities of 0.25 mA/cm2 (~ C/12 rate) and 0.50 mA/cm2 (~ C/6 rate) for charge and discharge, respectively. The cells were charged to 4.10V, followed by a tapered charge period at constant potential for three hours, and discharged to 2.75V, with 15 minutes of interval between the charge/discharge steps. The cells were soaked at different high temperatures (55^{o}, 60^{o}, 65^{o} and 70^{o}C) in the fully charged state for ten days at each temperature, and were subjected to various electrochemical measurements to determine their available capacities and individual electrode kinetics at different temperatures. For comparison, two cells were only stored at 60^{o}C only. In order to investigate the effects of the high temperature exposure to the SEI, and hence on the individual electrode kinetics, a number of electrochemical characterization techniques were employed, including: DC Tafel and micro- (or linear) polarization, and electrochemical impedance spectroscopy (EIS). All of these techniques were performed before and after each storage period. After performing the electrical performance measurements and in-situ electrochemical characterization of the samples, electrode samples were retrieved for ex-situ measurements.

For the NMR analysis, the electrode material was scraped from the foil backing inside an Argon-filled glove box and packed into 4mm zirconia rotors. Due to the electrical conductivity of graphite, the pure samples could not, as such, be spun stably at high speeds in the NMR magnets due to the induced eddy currents. The samples were therefore diluted with insulating, inert materials. For sample SG4A (table 2), Teflon® was accidentally used for the dilution, which itself served as an internal chemical shift reference, at 111ppm. For all the rest of the samples, dry Al_2O_3 was used instead.

The ^{13}C MAS NMR spectra were acquired at 188.1 MHz on a Bruker 750MHz system. The data were collected using both a single $\pi/2$ pulse, and a $\pi/2$-τ-π-τ Hahn echo sequence with variable recycle delays between scans at a 10-15 kHz spinning speed. ^{1}H decoupling and ^{1}H-^{13}C cross-polarization experiments were also conducted. ^{13}C chemical shifts are quoted relative to TMS as an external reference.

Sample	EC:DEC ratio	Enriched compound	Storage Temperatures
SG1A	25:75	EC	55^o, 60^o, 65^o, 70^o
SG2A	50:50	EC	55^o, 60^o, 65^o, 70^o
SG4A	75:25	EC	55^o, 60^o, 65^o, 70^o
SG7A	25:75	DEC	55^o, 60^o, 65^o, 70^o
SG9A	75:25	DEC	55^o, 60^o, 65^o, 70^o
SG10A	75:25	DEC	60^o
SG13A	75:25	EC	60^o

Table 1: *Sample experimental information for cells with reported NMR data - including solvent ratios, solvent enrichment and sample storage temperatures*

The sensitivity and amount of SEI necessary for detection is an important consideration in this study. The natural abundance of ^{13}C nuclei is 1.108%. This low abundance, combined with other atomic properties, makes the relative sensitivity of ^{13}C,

~3000 times less sensitive than the standard, ^{1}H. Through enrichment (and subsequent dilution) the concentration of ^{13}C nuclei in the precursor electrolyte compounds is 25 times stronger than this. (Though this increased abundance only applied to the carbonyl carbon, as indicated in figure 1). Typical measurements on the Bruker 750MHz wide bore solids probe used in this study give a signal-to-noise (S/N) of 50:1 for a 70Hz linewidth (~$3.3x10^{7}$ integrated area) from one scan of a rotor packed with 40mg of un-enriched glycine. Our measurements had a typical S/N of 25:1 for a 3-4kHz linewidth (~$2.1x10^{8}$ integrated area) after 4000 scans of a rotor packed with 20mg of the cycled anode material. The biggest source of error in this calculation is the approximation of the thickness of the SEI, and how much of the enriched carbon remained in a detectable (i.e. solid) state. Lei et al. include a brief summary of experimental methods and results regarding the thickness of the SEI;[vi] estimates range from 10s-100s of nm. Estimates of anode particle size range from 10-20μm, making the volume of the SEI approximately 5-25% of the total electrode mass.

The presence of 8% PVdF in the anode is another measure of the quantities of electrolyte-derived species seen. PVdF makes up 8% of the sample mass, and unenriched, 0.08% of carbons, by mass, translating into approximately $1.6x10^{19}$ ^{13}C nuclei in the PVdF. The PVdF signal is not seen in any of the samples, thereby offering a lower limit to the sensitivity of this method; any species in abundances less than this were not detectable.

Results and Discussion

^{13}C NMR was attempted on both the anodes and the cathodes. The data collected on the cathodes reveals only a background signal from the super-P carbon additive in the electrode. No individual signals from the electrolyte or its breakdown products were seen. In contrast, the spectra taken of the anode samples were very clear. The remainder of this section will focus on the anode data.

Given the inherent sensitivity limitations in solid state NMR, and the implied quantities of electrolyte-derived product necessary to produce a signal, the detection of strong, clear signals is itself quite significant.

All seven anode samples in this study, regardless of temperature, EC:DEC ratios, and EC vs. DEC enrichment exhibited clearly distinguishable peaks at approximately 110, 115-120, 125 and 135ppm (see figure 2). Spectra of some of the samples contained smaller peaks at 85, 95, 100 and 149ppm; only sample SG09A deviated from this format. Figure 3 indicates the ratios of peak areas for all of the resonances in each of these seven samples. Sample SG09A was investigated in a different probe at a higher magnetic field (21.1T), so it is assumed that it is mostly due to this increase in field, this sample exhibited a very small peak close to 170ppm; additional intensity in the 95-120ppm range could be attributed to the increase in the field, or to a carbon background signal in the probe. Sample SG09A data will be not be discussed in detail in this report, as its analysis has been suspended until confirmation of the background signal has been made.

Decoupling experiments were conducted (^{1}H-^{13}C) on several of the samples. No effect on the signal was noticed, suggesting, as expected, that the carbon atoms detected

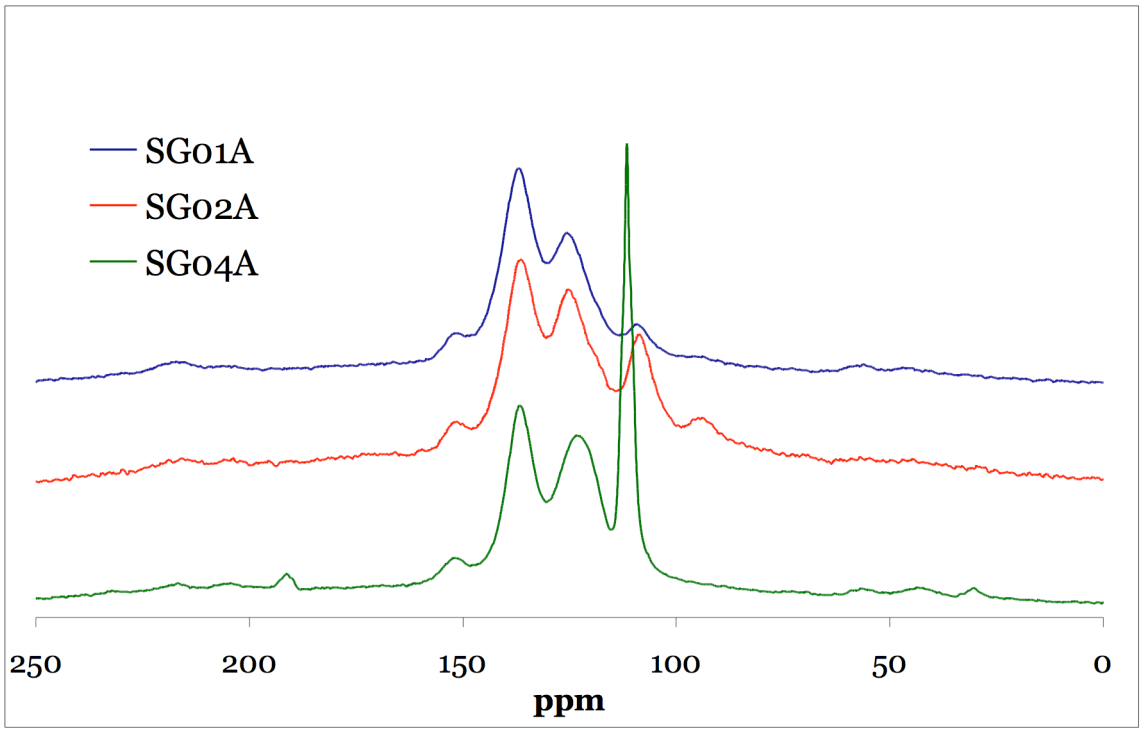

Figure 2: *^{13}C MAS NMR of anodes SG01, SG02 and SG04 with a 20s delay between scans and 1.5-4k scans*

in the samples were not directly bonded to protons.

Initially the most notable characteristic of the ^{13}C NMR spectral data was the absence of any distinguishable spectral peaks in the typical carbonyl range, (155-210ppm) where at least some carbonyl-containing breakdown products are expected to resonate.[vii] (except for a small resonance seen in sample 9A). This range includes the carbonyl signal of both electrolyte species EC (155.9ppm) and DEC (155.4ppm).[viii] Many of the most commonly suggested components whose breakdown mechanisms preserve their carbonyl group fall into this chemical shift range as well. These compounds, identified mostly via XPS and FTIR, include: lithium ethandiol biscarbonate, $(LiOC^{*}O_2CH_2)_2$,[ix,x] at 157ppm;[ix] lithium methyl carbonate, $CH_3OC^{*}O_2Li$,[ii,xi] at

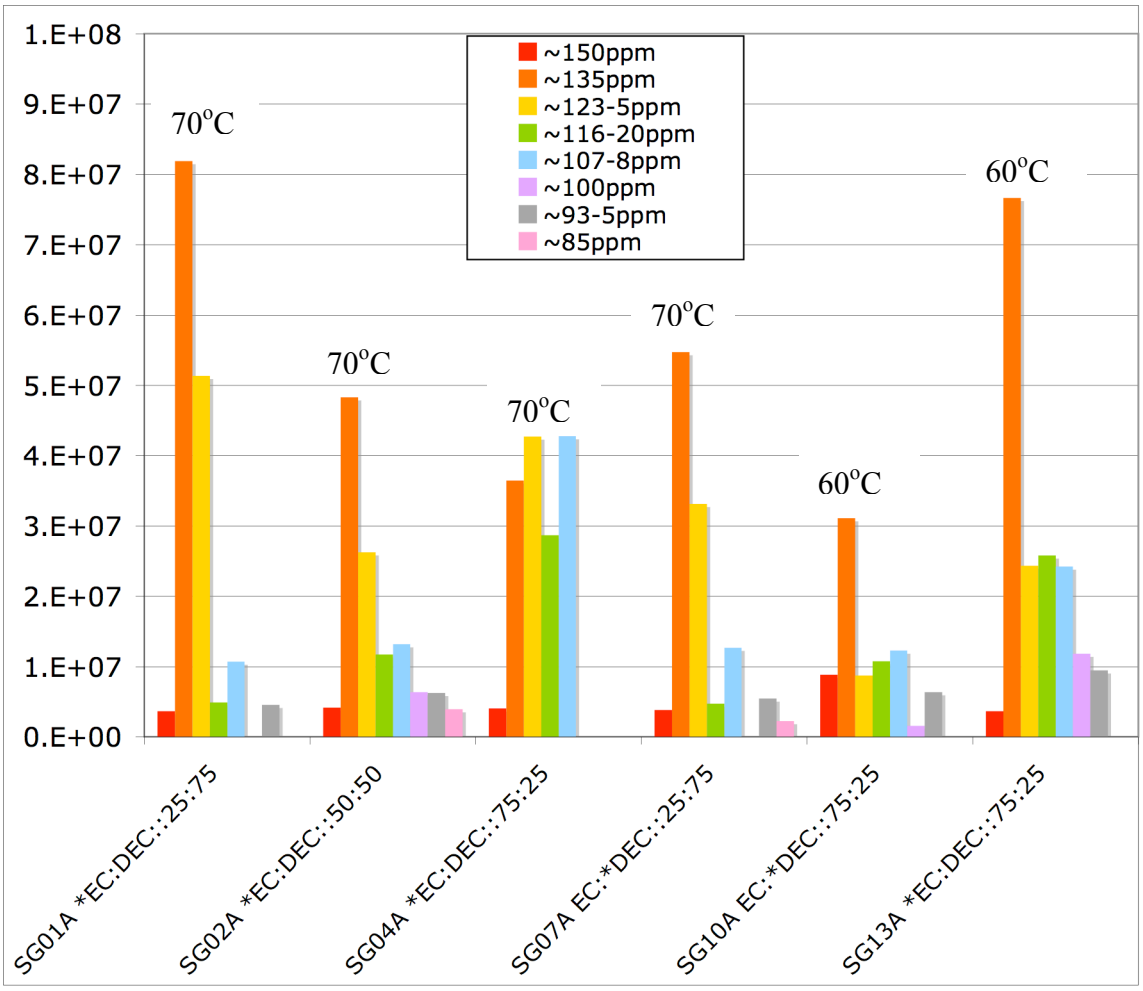

Figure 3: *Quantitative comparison of integrated peaks; asterisk indicates which of the electrolytes was enriched (all enrichments were of the carbonyl carbon); final temperatures at which the cells were stored are listed above the graphs.*

161.9ppm;[xii] lithium ethyl carbonate, $CH_3CH_2OC^*O_2Li$,[ii,xiii] at 163.6ppm;[xii] lithium oxalate $(LiO_2C)_2$,[xiv] at 173.5ppm;[viii] generic lithium alkyl carbonates, e.g. RCH_2OCO_2Li,[xiv] ranging from 160-164ppm;[viii,xii] $(CH_2OCO_2H)_2$,[ii] at ~155ppm;[xv] H_2CO_3,[ii,xvi] at 166.3ppm;[xv] formate, HCO_2H,[xvi] at 166ppm,[viii] oxalate, $(HOCO)_2$,[xvi] at 162ppm;[xv] possibly Li_2C_2[xvii] at 195ppm;[xi] transesterification products, in the range 150-160ppm;[xv,xii,viii] and more complex carbonate compounds and oligomers of the original

solvents,[xviii,xix] in the range 160-170ppm.[xv,xii,viii]

Some of the above-referenced studies claim that these carbonate-containing compounds of the form $ROCO_2Li$ are found on anode surfaces, even in $LiPF_6$-containing systems. However most of the studies in which $LiPF_6$ is used as the electrolyte do not report these types of compounds, the most commonly offered reason being the interactions with the salt breakdown product, HF.[ii,xvii,xx,xxi,xxii] In particular, lithium carbonate, Li_2CO_3 (~168ppm[xxiii]) is suggested in several studies as a dominant component of the SEI in other systems, but in the presence of $LiPF_6$ has been presumed to be unstable.[xxi,xxii] Gireaud et al. specifically explained the difficulty of identifying lithium bis-carbonates via FT-IR due to the chemical and electrochemical instability of this species.[xiii] Additionally, Kawamura et al. presuppose a $C_2H_5OCO_2PF_4$ product, but then conclude, due to experimental analysis, its subsequent breakdown into CO_2 etc.[xxiv] Also, Aurbach et al. proposed in a 1996 study that any carbonate products would be soluble in the electrolyte, therefore not detectable in the solid state SEI.[xxv] Zhuang et al. confirmed this as they detected some of these types of compounds via solution state NMR of the collected electrolyte from cycled cells.[ix]

It is significant that no resonances are seen in this region of any of the spectra (with exception of samle 9, where a very small signal is detected). One possible suggestion is that these particular oft-claimed reduction products are either not being formed at all, or being formed in quantities below the sensitivity threshold of NMR.

Another less likely explanation is that nearby species (e.g. Li^+ or PF_6^-) interacting with the carbonyl groups induces a severe shift in the resonance frequencies (figure 4, b and c). There are a few examples of this phenomenon in the literature. One is the study

conducted by Golden et al., who claim that a 20ppm shift of the carbonyl carbon in poly(vinylene) carbonate occurs as a result of complexation with lithium, as the extra shifted peak was only seen when the solid polymer was synthesized in the presence of lithium ions.[xxvi] Another is a ~16ppm shift in methyl isobutyrate vs. lithioisobutyrate;[xxvii] this compound is described as a 'metalated ester'. A similar phenomenon is described by a complexing, or clustering phenomenon of the electrolyte/electrolyte-derived species around the lithium cation (see figure 4, pathway a), as suggested by the DFT calculations of Wang et al.[xxviii] This complexing could possibly affect the immediate environment of the ^{13}C nucleus, resulting in a chemical shift. One study claimed 20ppm shifts due to such molecular aggregation, (though in the liquid state); e.g. a tetramer of phenyllithium vs. the monomer of the same.[xxix] We believe that it is unlikely that the lithium interaction as such is responsible for the shift in the present data. Part of the reason why is that in all of these examples, the unshifted, lithium-free parent resonances are seen in the experimental data along with the lithium-complexed species, which is not the case in this study.

Such an effect has been reported by many other groups as well, however none as severe as the three previous examples. Most of the shifts reported for complexation/associative effects on chemical shifts are much less severe (>5ppm).[xxx,xxxi,xxxii,xxxiii] A few groups even reported slight upfield shifts as a result of the same types of interactions.[xxxiv]. The simple lithiation of a species (e.g. lithium lactate vs. lactic acid) results in shifts of only 2-7ppm.[viii]

Another interesting feature of the data in general was that there *was* such a strong signal at all. It is inarguable that the original (enriched) carbonyl carbons from the

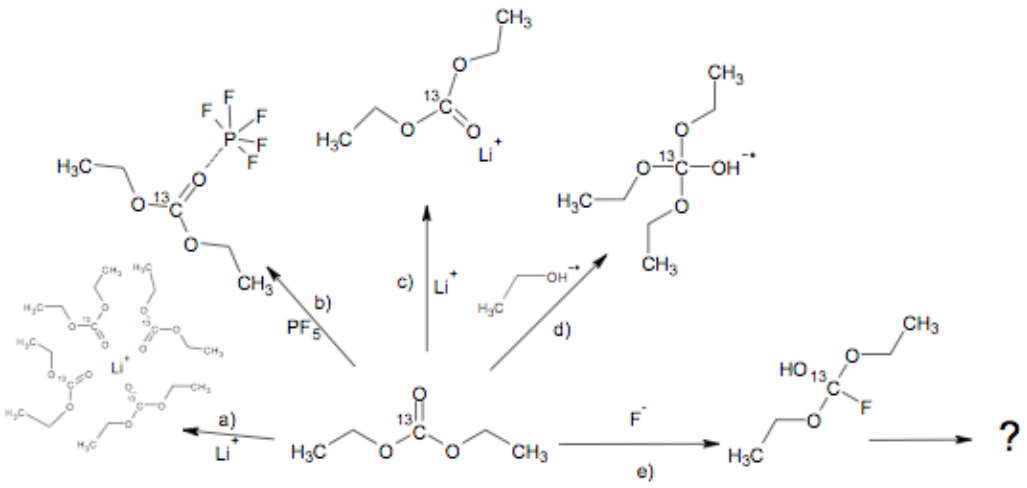

Figure 4: *Different hypothetical fates of the enriched carbonate carbon in the original DEC electrolyte (center of figure) provide possible explanations for unexpected ^{13}C chemical shifts measured. These reactions/interactions include: (a) electrolyte complexations about cation centers; (b),(c) formation of delocalized charges on the carbonate due to association with PF_5 or Li^+ centers causing extreme chemical shifts; (d) free radicals generated by other degredation mechanisms (not shown here) attack carbonyl carbon, generating new 'poly-oxyspiro' compounds (a pathway also suggested by Wang et al.); (e) fluorination of carbonate carbon, subsequent to the breakdown of the $LiPF_6$ salt.*

solvents either remain in some configuration in solid form on the surface of the anode, or, less likely, intercalated into the anode. (This is true of both solvents, as cells with enriched EC and those with enriched DEC both indicated strong ^{13}C signals.) However most of the previously proposed solvent breakdown pathways result in the creation of CO_2, whose carbon atom is likely to originate from the (enriched) carbonyl carbon. Several groups have detected CO_2 gasses via mass spectroscopy of the evolved vapors in cycled cells.[xxxv, xxxvi, xxxvii, xxxviii] The only reasonable conclusion is that the CO_2-creating

mechanisms are not unique, or CO_2 is a reaction intermediate, as suggested by Imhof et al.[xxxix] Though in one comparative study of CO_2 generation in a variety of electrolyte solutions, the $LiPF_6$-containing mixtures evolved the least amount of gas, several of the above-referenced studies used $LiPF_6$ as the salt.[xl]

Throughout all of the research done thus far regarding the SEI, with few exceptions, the fate of the carbonyl carbon in both the EC and DEC molecules is thought to be either consumed in the formation of CO or CO_2, or remain in its original carbonate form, with perhaps some slight molecular rearrangements (e.g. $LiCH_2CH_2OCO_2)_2$). The evidence provided by this report clearly indicates that if CO_2 is indeed generated by the breakdown of the electrolyte components, this pathway describes just one of several other possible fates for these compounds. That is, the CO_2 production is either not a final or not a unique decomposition scheme, since clearly some of the central carbonyl carbons terminate in a non-volatilized, solid form in volumes detectable via NMR. This implies volumes of $\sim 10^{18}$ and greater, as explained above.

Another interesting feature of the collected data is *where* the resonances are located. The carbon chemical shift range is well established and not too many species resonate in this chemical shift range. One conclusion is evident and that is the disruption of the carbonyl bond to create species that retain the carbon atom, but result in different chemical configurations than those previously suggested (with some exceptions). This disruption is likely initiated by species formed from electrolyte or salt breakdown (figure 2, pathways d,e). There are several pieces of evidence to suggest this reaction route. Many studies have already suggested the creation of radical species during the initial breakdown of the EC and DEC compounds.[xviii] Additionally the coordination of the

carbonyl oxygen with the PF_5 molecule makes the carbonyl carbon susceptible to nucleophilic attack, as suggested by Sasaki et al.[xli] The charge densities of the carbonyl carbons in EC and DEC had the highest positive values of +0.444 & +0.501, respectively. Therefore the radical species likely attacks the carbonyl carbon, and subsequent rearrangement of the resulting compound into the formation of binary, tertiary and/or quaternary ethers is presumed. These compounds all have chemical shifts in the 100-135ppm range (figure 3), in very good correspondence with the data collected in this report. A reaction mechanism of this type has already been suggested, as one of several possible pathways, by Wang et al. as a result of DFT calculations.[xxviii]

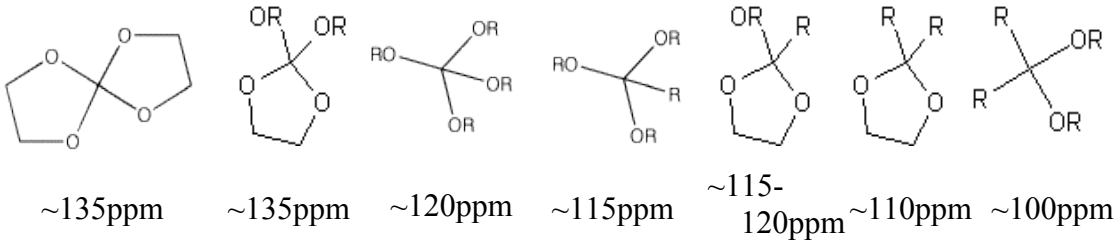

Figure 5: *Possible breakdown products of solvent components with their approximate chemical shifts, where R=H, -CH_3, -CH_2CH_3, etc.*

This suggestion, though different from many previous SEI investigations, can be reconciled with FT-IR and XPS reasonably well. C1s and O1s peaks in the XPS of the suggested carbonates could likely arise from binary, tertiary and/or quaternary ethers. O1s energies of 531-3eV are expected for both carbonyl and ethereal oxygens.[xxv, xlii] Zhuang et al. report slightly higher values of 535eV for carbonyl oxygen, and 537-538eV for O single-bonded to carbon.[xliii] However these energies are also reported to exhibit

slight shifts in the presence of lithium. C1s energies of 287-290eV are reportedly typical for carbonates and 286-290eV for alkoxy/ethereal carbons.[xxv, xli, xliv] Again the data from Zhuang et al. is slightly shifted: 292-294eV for carbonyl carbon and 290eV for carbon single bonded to oxygen.[xliii] Even the energies for $-CF_2$ and $-CF_3$ are in close range: 292eV and 294eV, respectively.[xlii] As for FT-IR data of carbonates, several sample spectra of suggested carbonates were compared to those of ethers and many of the same stretches could be reconciled with these alternatively proposed compounds.[xlv]

An alternative breakdown pathway that should be considered assigns a larger role in the process to the $LiPF_6$ and its derivatives. The evidence that compelled a further examination of fluorine-containing breakdown products is in the chemical shifts and dipolar splitting patterns of such compounds. Many possibly relevant fluorine-containing compounds were found to resonate in this region: $F_2{}^*C{=}O$, 133ppm;[xv] $^*CF_3CHF^*CF_3$, 120ppm;[xv] $^*CF_3CH_2{}^*CF_3$, 123.5ppm;[xv] $CH_3CH_2CH_2{}^*CF_2CH_2CH_3$, 125ppm[xv] etc. Figure 6 depicts a possible carbon-containing $O_xP_yF_z$ compound that has resonances due to J-coupling at 114, 120, 125 and 130ppm.[xv] These shifts correspond very well with the data collected herein.

Many studies at least make mention of the likelihood of some fluorine-containing breakdown products in the SEI. First of all there is general concurrence on the following equilibrium reaction: $LiPF_6 \Leftrightarrow LiF + PF_5$. The subsequent reaction, in the presence of trace water ($LiPF_6$ has typical impurities of 15ppm H_2O[xlvi]) is presumed to be: $PF_5 + H_2O \Leftrightarrow PF_3O + HF$. However besides the oft-mentioned generic OP_xF_y compounds, there have been few proposals of specific fluorine-containing final-stage breakdown products. One GC-MS study suggested the presence of $C_3H_3F_3$, $C_4H_3F_3$ and

$C_2H_4OF_2P$.[xlvii] An initial reduction of the PF_6^-/PF_5 to form Li_xPF_y is proposed along with a subsequent reaction with the organic solvent molecules to form these organofluoro-phosphorous compounds, though no details of this secondary reaction were described. Herstedt et al. suggest that it is ether-carbonate breakdown products which react with PF_5 to form the breakdown products listed in the previous study by Aurbach et al.[xlviii] Sloop et. al clearly demonstrate that once PF_5 is generated from $LiPF_6$, it reacts with the solvents, but no specific details are elucidated from that study either.[xlix] Ravdel et al. suggest PF_5 and OPF_3 as active initiators of the solvent decomposition at elevated temperatures.[xxxvii] However their study focuses on the gaseous and liquid states, via GC-

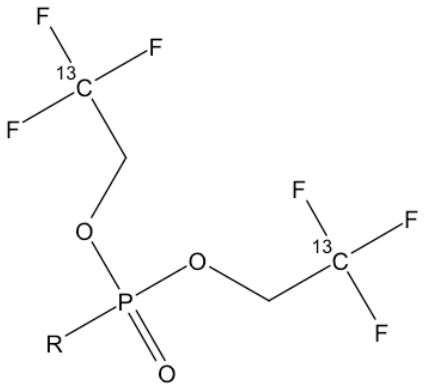

Figure 6: *^{13}C NMR resonances in this molecule, due to J-coupling, are seen at 114, 120, 125 & 130ppm (ref. viii)*

MS and liquid state ^{19}F and ^{31}P NMR. Their results suggest the presence of $OPF_2(OCH_3)$, diethylether, OPF_3, fluoroethane, $OPF_2(OEt)$ and $OPF(OEt)_2$. Kawamura et al. used

differential scanning calorimetry (DSC) to determine that $LiPF_6$ in DEC produces C_2H_5F, PF_3O, PF_4OH and $C_2H_5OCOOPF_4$ at high temperatures.[xxiv]

The remaining issue to address is determining a suitable degradation mechanism of the salt/electrolyte components that would produce such compounds, ensuring the conservation of the (enriched) carbonyl carbon in the product(s). There is a strong likelihood that the mechanism would be initiated by an attack of the carbonyl carbon by a fluorine ion, or fluorine-containing species. This could be followed by subsequent fluorine replacements on one or more of the carbon bond sites.

Conclusions

An initial conclusion of this study was the lack of a significant concentration of organics found at the cathode. This is consistent with previous conjectures on the chemical make-up of the SEI. The most significant conclusion of this study is the proposal that previously conjectured carbonate-containing breakdown products (lithium biscarbonate in particular) are either present in very low quantities, or do not survive at all in the solid component of the SEI in a $LiPF_6$-containing system. Although all previous experimental data supporting their existence has not been completely reconciled, a first attempt at re-interpreting the XPS and FT-IR data shows favorable results. Further work along these lines would be useful to confirm these conclusions.

Instead, the pathway suggested is an attack on the carbonyl carbon by the radical compounds produced from the first stages of solvent degradation. It is likely that the dominant products in this type of system are a combination of a variety of mainly

quaternary & tertiary ethers, in addition to some fluorine-containing alkoxy compounds. A follow-up project involving the enrichment of other carbons in the electrolytes would significantly complement this work, rounding out the characterization of the SEI.

---

[i] Aurbach, D., A. Zaban, Y. Ein-Eli, I. Weissman, O. Chusid, B. Markovsky, M. Levi, E. Levi, A. Schechter and E. Granot. "Recent Studies on the Correlation Between Surface Chemistry, Morphology, Three-Dimensional Structures and Performance of Li and Li-C Intercalation Anodes in Several Important Electrolyte Systems." *Journal of Power Sources* 68.1 (1997): 91-98.

[ii] Aurbach, D. "Review of Selected Electrode-Solution Interactions Which Determine the Performance of Li and Li Ion Batteries." *Journal of Power Sources* 89.2 (2000): 206-218.

[iii] Leifer, N. and S. G. Greenbaum. "Spectroscopic Analysis of SEI Formation in Lithium-Ion Batteries." *Advanced Materials and Methods for Lithium Ion Batteries*. Edited. S. S. Zhang. Kerala, India: Transworld Research Network, 2007.

[iv] Blomgren, G. E. "Liquid Electrolytes for Lithium and Lithium-Ion Batteries." *Journal of Power Sources: Selected papers presented at the 11th International Meeting on Lithium Batteries* 119-121 (2003): 326-329.

[v] Xu, K. "Nonaqueous Liquid Electrolytes for Lithium-Based Rechargeable Batteries." *Chemical Reviews* 104.10 (2004): 4303-4417.

[vi] Lei, J. L., L. J. Li, R. Kostecki, R. Muller and F. McLarnon. "Characterization of SEI Layers on $LiMn_2O_4$ Cathodes with In-Situ Spectroscopic Ellipsometry." *Journal of the Electrochemical Society* 152.4 (2005): A774-A777.

[vii] Reich, H. J. *C-13 Chemical Shifts*. 2008. Department of Chemistry at the University of Wisconsin. Oct 2008 <http://www.chem.wisc.edu/areas/reich/Handouts/nmr-c13/cdata.htm>.

[viii] Saito, T., K.Hayamizu, M.Yanagisawa and O.Yamamoto. *Spectral Database for Organic Compounds, SDBS*. 2008. National Institute of Advanced Industrial Science and Technology. Sept 2008 <http://riodb01.ibase.aist.go.jp/sdbs/cgi-bin/cre_index.cgi?lang=eng>.

[ix] Zhuang, G. V., K. Xu, H. Yang, J. R. Jow and P. N. Ross, Jr. "Lithium Ethylene Dicarbonate Identified as the Primary Product of Chemical and Electrochemical Reduction of EC in 1.2 M $LiPF_6$/EC:EMC Electrolyte." *Journal of Physical Chemistry B* 109.37 (2005): 17567-17573.

[x] Gireaud, L., S. Grugeon, S. Pilard, P. Guenot, J. M. Tarascon and S. Laruelle. "Mass Spectrometry Investigations on Electrolyte Degradation Products for the Development of Nanocomposite Electrodes in Lithium Ion Batteries." *Analytical Chemistry* 78 (2006): 3688-3698.

[xi] Duncan, T. M. "A Study of the ^{13}C Chemical-Shift Anisotropy in Metal Acetylides." *Inorganic Chemistry* 28.13 (1989): 2663-2668.

[xii] Gubernator, Klaus. *Chemgate Spectroscopy Search Engine*. 2008. Wiley Vch. Nov 2008 <http://chemgate.emolecules.com/index.php>.

[xiii] Gireaud, L., S. Grugeon, S. Laruelle, S. Pilard and J. M. Tarascon."Identification of Li Battery Electrolyte Degradation Products Through Direct Synthesis and Characterization of Alkyl Carbonate Salts." *Journal of the Electrochemical Society* 152.5 (2005): A850-A857.

[xiv] Zhao, L. W., I. Watanabe, T. Doi, S. Okada and J. Yamaki. "TG-MS Analysis of Solid Electrolyte Interphase (SEI) on Graphite Negative-Electrode in Lithium-Ion Batteries." *Journal of Power Sources* 161.2 (2006): 1275-1280.

[xv] Pouchert, J. and C. Behnke. *The Aldrich Library of NMR Spectra*. 1993.

[xvi] Sloop, S. E., J. B. Kerr and K. Kinoshita. "The Role of Li-Ion Battery Electrolyte Reactivity in Performance Decline and Self-Discharge." *Journal of Power Sources* 119 (2003): 330-337.

[xvii] Eshkenazi, V., E. Peled, L. Burstein and D. Golodnitsky. "XPS Analysis of the SEI Formed on Carbonaceous Materials." *Solid State Ionics* 170.1-2 (2004): 83-91.

[xviii] Moshkovich, M., M. Cojocaru, H. E. Gottlieb and D. Aurbach. "The Study of the Anodic Stability of Alkyl Carbonate Solutions by In-Situ FTIR Spectroscopy, EQCM, NMR and MS." *Journal of Electroanalytical Chemistry* 497.1-2 (2001): 84-96.

[xix] Yazami, R. "Surface Chemistry and Lithium Storage Capability of the Graphite-Lithium Electrode." *Electrochimica Acta* 45.1-2 (1999): 87-97.

[xx] Aurbach, D. "Electrode-Solution Interactions in Li-Ion Batteries: A Short Summary and New Insights." *Journal of Power Sources* 119 (2003): 497-503.

[xxi] Aurbach, D. and E. Zaban. “Impedance Spectroscopy of Nonactive Metal Electrodes at Low Potentials in Propylene Carbonate Solutions.” *Journal of the Electrochemical Society* 141:7 (1994): 1808-1819.

[xxii] Ein-Eli, Y., B. Markovsky, D. Aurbach, Y. Carmeli, H. Yamin and S. Luski. "The Dependence of the Performance of Li-C Intercalation Anodes for Li-Ion Secondary Batteries on the Electrolyte Solution Composition." *Electrochimica Acta* 39.17 (1994): 2559-2569.

[xxiii] ^{13}C NMR conducted on premises, referenced to TMS at 0ppm.

[xxiv] Kawamura, T., A. Kimura, M. Egashira, S. Okada and J.-I. Yamaki. "Thermal Stability of Alkyl Carbonate Mixed-Solvent Electrolytes for Lithium Ion Cells." *Journal of Power Sources* 104.2: (2002): 260-264.

[xxv] Aurbach, D., I. Weissman, A. Schechter and H. Cohen. "X-ray Photoelectron Spectroscopy Studies of Lithium Surfaces Prepared in Several Important Electrolyte Solutions. A Comparison with Previous Studies by Fourier Transform Infrared Spectroscopy." *Langmuir* 12.16 (1996): 3991-4007.

[xxvi] Golden, J. H., B. G. M. Chew, D. B. Zax, F. J. DiSalvo, J. M. J. Frechet and J.-M. Tarascon. "Preparation of Propylene Carbonate Acrylate and Poly(propylene carbonate acrylate) Electrolyte Elastomer Gels. ^{13}C NMR Evidence for Li^{+}-Cyclic Carbonate Interaction." *Macromolecules* 28.9 (1995): 3468-3470.

[xxvii] Vancea, L. and S. Bywater. "^{13}C NMR Studies on Anion Pairs Related to Acrylate Polymerization. 2.) Dimer Models." *Macromolecules* 14 (1981): 1776-1778.

[xxviii] Wang, Y. X., S. Nakamura, M. Ue and P. B. Balbuena. "Theoretical Studies to Understand Surface Chemistry on Carbon Anodes for Lithium-Ion Batteries: Reduction Mechanisms of Ethylene Carbonate." *Journal of the American Chemical Society* 123.47 (2001): 11708-11718.

[xxix] Jackman, L. M. and L. M. Scarmoutzos. “Structure of Phenyllithium in Solution.” *Journal of the American Chemical Society* 106.16 (1984): 4627-4629.

[xxx] Matsubara, K., R. Kaneuchi and N. Maekita. "^{13}C NMR Estimation of Preferential Solvation of Lithium Ions in Non-Aqueous Mixed Solvents." *Journal of the Chemical Society, Faraday Transactions* 94 (1998): 3601-3605.

[xxxi] Reddy, V. P., M. C. Smart, K. B. Chin, B. V. Ratnakumar, S. Surampudi, J. Hu, P. Yan and G. K. S. Prakash. "^{13}C NMR Spectroscopic, CV and Conductivity Studies of Propylene Carbonate-Based Electrolytes Containing Various Lithium Salts." *Electrochemical and Solid-State Letters* 8.6 (2005): A294-A298.

[xxxii] Sankaram, M. B. and K. R. K. Easwaran. "CD and NMR Studies on the Interaction of Lithium Ion with Valinomycin and Gramicidin-S." *Biopolymers* 21 (1982): 1557-1567.

[xxxiii] Rao, C. P., P. Balaram and C. N. R. Rao. (1980). "^{13}C Nuclear Magnetic Resonance Studies of the Binding of Alkali and Alkaline Earth Metal Salts to Amides." *Journal Chemical Society, Faraday Transactions* 76: 1008-1013.

[xxxiv] Wang, H. L., H.-M. Kao, M. Digar and T. C. Wen. "FTIR and Solid State ^{13}C NMR Studies on the Interaction of Lithium Cations with Polyether Poly(urethane Urea)." *Macromolecules* 34 (2001): 529-537.

[xxxv] Cattaneo, E. and J. Ruch. "Anodic Stability of Propylene Carbonate on Manganese Dioxide Electrodes." *Journal of Power Sources*, 44.1-3 (1993): 341-347.

[xxxvi] Yoshida, H., T. Fukunaga, T. Hazama, M. Terasaki, M. Mizutani and M. Yamachi. "Degradation Mechanism of Alkyl Carbonate Solvents Used in Lithium-Ion Cells During Initial Charging." *Journal of Power Sources* 68.2 (1997): 311-315.

[xxxvii] Ravdel, B., K. M. Abraham, R. Gitzendanner, J. DiCarlo, B. Lucht and C. Campion. "Thermal Stability of Lithium-Ion Battery Electrolytes." *Journal of Power Sources* 119-121 (2003): 805-810.

[xxxviii] Zhao, L. W., I. Watanabe, T. Doi, S. Okada and J. Yamaki. "TG-MS Analysis of Solid Electrolyte Interphase (SEI) on Graphite Negative-Electrode in Lithium-Ion Batteries." *Journal of Power Sources* 161.2 (2006): 1275-1280.

[xxxix] Imhof, R. and P. Novak. "In-Situ Investigation of the Electrochemical Reduction of Carbonate Electrolyte Solutions at Graphite Electrodes." *Journal of The Electrochemical Society* 145.4 (1998): 1081-1087.

[xl] Arakawa, M. and J.-i. Yamaki."Anodic Oxidation of Propylene Carbonate and Ethylene Carbonate on Graphite Electrodes." *Journal of Power Sources* 54.2 (2001): 250-254.

[xli] Sasaki, T., T. Abe, J. Iriyama, M. Inaba and Z. Ogumi. "Formation Mechanism of Alkyl Dicarbonates in Li-Ion Cells." *Journal of Power Sources* 150 (2005): 208-215.

[xlii] Andersson, A. M., M. Herstedt, A. G. Bishop and K. Edstrom. "The Influence of Lithium Salt on the Interfacial Reactions Controlling the Thermal Stability of Graphite Anodes." *Electrochimica Acta* 47.12 (2002): 1885-1898.

[xliii] Zhuang, G., Y. Chen and P. N. Ross, Jr. "The Reaction of Lithium with Dimethyl Carbonate and Diethyl Carbonate in Ultrahigh Vacuum Studied by X-ray

Photoemission Spectroscopy." *Langmuir* 15 (1999): 1470-1479.

[xliv] Yang, Y.-Y., J.-P. Wan, T.-S. Chung, P. K. Pallathadka, S. Ng and J. Heller. "POE-PEG-POE Triblock Copolymeric Microspheres Containing Protein: I. Preparation and Characterization." *Journal of Controlled Release* 75.1-2 (2001): 115-128.

[xlv] Pouchert, C., *The Aldrich Library of FT-IR Spectra*.1985.

[xlvi] Linden, D. and T. B. Reddy. *Handbook of Battery Materials*, 3rd ed. New York: McGraw-Hill, 2001.

[xlvii] Aurbach, D., B. Markovsky, A. Rodkin, M. Cojocaru, E. Levi and H.-J. Kim. "An Analysis of Rechargeable Lithium-Ion Batteries After Prolonged Cycling." *Electrochimica Acta* 47.12 (2002): 1899-1911.

[xlviii] Herstedt, M., D. P. Abraham, J. B. Kerr and K. Edstrom. "X-ray Photoelectron Spectroscopy of Negative Electrodes from High-Power Lithium-Ion Cells Showing Various Levels of Power Fade." *Electrochimica Acta* 49.28 (2004): 5097-5110.

[xlix] Sloop, S. E., J. K. Pugh, S. Wang, J. B. Kerr and K. Kinoshita. "Chemical Reactivity of PF_5 and $LiPF_6$ in Ethylene Carbonate/Dimethyl Carbonate Solutions." *Electrochemical and Solid State Letters* 4.4 (2001): A42-A44.

VI. Conclusion

The usefulness and variety of the application of solid state NMR spectroscopy to the study of lithium ion batteries is well illustrated by the studies presented in this thesis. The studies illustrate different ways that this technique can be used to elucidate different quantitative and qualitative information in battery systems. The following is a summary of the conclusions from each study.

The first study, on the inorganic components of the SEI layer, showed that ^{7}Li NMR of fully discharged $LiCoO_2$ cathodes could be used to estimate the percentage of Li not re-intercalated into the cathode. ^{19}F NMR was also used to quantify the LiF formed on the electrode surfaces, indicating more of this substance in the anodic SEI compared to the cathodic layer. A positive correlation was also established for the amount of LiF formed with both the number of cycles and the percentage of Li lost from the cathode.

The second study, which involved multinuclear NMR studies of lithiated SVO materials, revealed details not readily available from electrochemical and X-ray diffraction studies. The ^{7}Li NMR results include no observable Li_2O, either as a component of the SEI or as a result of Li reduction of Ag^{+}, as well as a clear indication of two distinct sites associated with intercalated Li. Both the ^{7}Li and the ^{51}V NMR revealed information on the order of reduction of the vanadium, which commences by $x = 0.72$ and proceeds monotonically to $x = 5.59$. Over this range, V appears to go from V^{5+} to V^{3+} with associated structural changes. The local vanadium structure in $Li_{0.72}Ag_2V_4O_{11}$ is a more ordered form than that in SVO, but the vanadium environment becomes disordered at the higher lithium content. There is also evidence in the ^{51}V NMR of residual V^{5+} in the $x = 5.59$ sample, attributable to either an impurity or electrochemically inaccessible

SVO particles.

The third study, which included both EPR and ^{7}Li and ^{19}F NMR, offers several new insights into structural and chemical differences in a variety of starting and lithiated CF_x materials. Clear differentiations in the starting materials were seen in the EPR data including the presence of structural defects and differences in spin densities. The detection and quantification of several semi-ionic/ionic C-F interactions, in addition to the expected covalent CF interactions was novel and interesting, as high temperature CF_x compounds have previously been presumed to be composed only of the latter. It was also possible to track the order of reduction of the covalent vs. ionic fluorines over the course of lithiation. It was also evident in both the ^{19}F and the ^{13}C NMR that at least one type of CF_2 species remained as such throughout the entire lithiation process, either indicating electrochemically isolated regions, or an electrochemically inactive bonding configuration. At the highest depth of discharge different amounts of LiF were measured, indicating differences in reaction completion. Lastly, the ^{13}C NMR clearly indicated that some amount of intercalation of the solvent and/or solvent breakdown products into the bulk structure increased with successive lithiation.

The fourth study, an investigation of the organic part of the SEI, indicated several conclusions. One expected conclusion was the lack of a significant concentration of organic compounds found in the cathodic SEI. A more significant and unexpected conclusion was that previously conjectured carbonate-containing breakdown products are either present in very low quantities, or do not survive at all in the solid component of the SEI in a $LiPF_6$-containing system. Instead, the pathway suggested is an attack on the carbonyl carbon by the radical compounds produced from the first stages of solvent

degradation, proceeding into a variety of mainly quaternary & tertiary ethers and/or fluorine-containing alkoxy compounds.

Overall half of the work herein focuses on the elucidation of both the inorganic and organic SEI. In the second half of the work presented, atomic and electronic rearrangement are monitored in cycled battery electrodes. In all cases NMR was successfully used to further the understanding of battery technology, information which will be used in the continued pursuit of better functioning systems.

VII. Bibliography

Alcantara, M. Jaraba, P. Lavela, J. L. Tirado, E. Zhecheva and R. Stoyanova. "Changes in the Local Structure of $LiMg_yNi_{0.5-y}Mn_{1.5}O_4$ Electrode Materials During Lithium Extraction." *Chemistry of Materials* 16 (2004): 1573-1579.

Andersson, A. M., M. Herstedt, A. G. Bishop and K. Edstrom. "The Influence of Lithium Salt on the Interfacial Reactions Controlling the Thermal Stability of Graphite Anodes." *Electrochimica Acta* 47.12 (2002): 1885-1898.

Arakawa, M. and J.-i. Yamaki."Anodic Oxidation of Propylene Carbonate and Ethylene Carbonate on Graphite Electrodes." *Journal of Power Sources* 54.2 (2001): 250-254.

Aurbach, D. "Electrode-Solution Interactions in Li-Ion Batteries: A Short Summary and New Insights." *Journal of Power Sources* 119 (2003): 497-503.

Aurbach, D. "Review of Selected Electrode-Solution Interactions Which Determine the Performance of Li and Li Ion Batteries." *Journal of Power Sources* 89.2 (2000): 206-218.

Aurbach, D., K. Gamolsky, B., Y. Gofer, M. Schmidt and U. Heider. "On the Use of Vinylene Carbonate (VC) as an Additive to Electrolyte Solutions for Li-Ion Batteries." *Electrochimica Acta* 47.9 (2002): 1423-1439.

Aurbach, D., B. Markovsky, M. D. Levi, E. Levi, A. Schechter, M. Moshkovich and Y. Cohen. "New Insights into the Interactions Between Electrode Materials and Electrolyte Solutions for Advanced Nonaqueous Batteries." *Journal of Power Sources* 81-82 (1999): 95-111.

Aurbach, D., B. Markovsky, A. Rodkin, M. Cojocaru, E. Levi and H.-J. Kim. "An Analysis of Rechargeable Lithium-Ion Batteries After Prolonged Cycling." *Electrochimica Acta* 47.12 (2002): 1899-1911.

Aurbach, D., B. Markovsky, A. Rodkin, E. Levi, Y. S. Cohen, H. J. Kim and M. Schmidt. "On the Capacity Fading of $LiCoO_2$ Intercalation Electrodes: The Effect of Cycling, Storage, Temperature and Surface Film Forming Additives." *Electrochimica Acta* 47.27 (2002): 4291-4306.

Aurbach, D., I. Weissman, A. Schechter and H. Cohen. "X-ray Photoelectron Spectroscopy Studies of Lithium Surfaces Prepared in Several Important Electrolyte Solutions. A Comparison with Previous Studies by Fourier Transform Infrared Spectroscopy." *Langmuir* 12.16 (1996): 3991-4007.

Aurbach, D. and A. Zaban. "Impedance Spectroscopy of Lithium Electrodes: Part 1. General Behavior in Propylene Carbonate Solutions and the Correlation to Surface Chemistry and Cycling Efficiency." *Journal of Electroanalytical Chemistry* 348 (1993): 155-179.

Aurbach, D. and E. Zaban. "Impedance Spectroscopy of Nonactive Metal Electrodes at Low Potentials in Propylene Carbonate Solutions." *Journal of the Electrochemical Society* 141:7 (1994): 1808-1819.

Aurbach, D., A. Zaban, Y. Ein-Eli, I. Weissman, O. Chusid, B. Markovsky, M. Levi, E. Levi, A. Schechter and E. Granot. "Recent Studies on the Correlation Between Surface Chemistry, Morphology, Three-Dimensional Structures and Performance of Li and Li-C Intercalation Anodes in Several Important Electrolyte Systems." *Journal of Power Sources* 68.1 (1997): 91-98.

Balasubramanian, M., H. S. Lee, X. Sun, X. Q. Yang, A. R. Moodenbaugh, J. McBreen, D. A. Fischer and Z. Fu. "Formation of SEI on Cycled Lithium-Ion Battery Cathodes: Soft X-Ray Absorption Study." *Electrochemical and Solid-State Letters* 5.1 (2002): A22-A25.

Blomgren, G. E. "Liquid Electrolytes for Lithium and Lithium-Ion Batteries." *Journal of Power Sources: Selected papers presented at the 11th International Meeting on Lithium Batteries* 119-121 (2003): 326-329.

Boyle, T. J., D. Ingersoll, T. M. Alam, C. J. Tafoya, M. A. Rodriguez, K. Vanheusden and D. H. Doughty. "Rechargeable Lithium Battery Cathodes. Nonaqueous Synthesis, Characterization and Electrochemical Properties of $LiCoO_2$." *Chemistry of Materials* 10.8 (1998): 2270-2276.

Callaghan, Paul. *Principles of NMR Spectroscopy*. Oxford: Clarendon Press, 1991.

Campion, C. L., W. Li, W. B. Euler, B. L. Lucht, B. Ravdel, J. F. DiCarlo, R. Gitzendanner and K. M. Abraham. "Suppression of Toxic Compounds Produced in the Decomposition of Lithium-Ion Battery Electrolytes." *Electrochemical and Solid-State Letters* 7.7 (2004): A194-A197.

Carewska, M., S. Scaccia, F. Croce, S. Arumugam, Y. Wang and S. G. Greenbaum. "Electrical Conductivity and ^6Li, ^7Li NMR Studies of $Li_{1+y}CoO_2$." *Solid State Ionics* 93.3-4 (1997): 227-237.

Carlier, D., M. Menetrier and C. Delmas. "^7Li MAS NMR Study of Electrochemically Deintercalated $Li_xNi_{0.30}Co_{0.70}O_2$ Phases: Evidence of Electronic and Ionic Mobility and Redox Processes." *Journal of Materials Chemistry* 11.2 (2001): 594-603.

Cattaneo, E. and J. Ruch. “Anodic Stability of Propylene Carbonate on Manganese Dioxide Electrodes.” *Journal of Power Sources*, 44.1-3 (1993): 341-347.

Chakrabarti, A., R. Druzinic, K. Hermann, M. Petersen, F. Wagner and M. Witko. "Geometric and Electronic Structure of Vanadium Pentoxide: A Density Functional Bulk and Surface Study." *Physical Review B* 59.16 (1999): 10583-10590.

Chevallier, F., S. Gautier, J. P. Salvetat, C. Clinard, E. Frackowiak, J. N. Rouzaud and F. Béguin. "Effects of Post-Treatments on the Performance of Hard Carbons in Lithium Cells." *Journal of Power Sources* 97-98 (2001): 143-145.

Cocciantelli, J. M., K. S. Suh, J. Senegas, J. P. Doumerc and M. Pouchard. "^{7}Li NMR of Electrochemically Inserted $Li_xV_2O_5$." *Journal of Physics and Chemistry of Solids* 53.1 (1992): 57-59.

Cocciantelli, J. M., K. S. Suh, J. Senegas, J. P. Doumerc, J. L. Soubeyroux, M. Pouchard and P. Hagenmuller. (1992). "^{7}Li NMR in Electrochemically Intercalated [gamma] - $Li_xV_2O_5$ Bronzes ($0.95<x<1.9$)." *Journal of Physics and Chemistry of Solids* 53(1): 51-55.

Crespi, A. M., P. M. Skarstad and H. W. Zandbergen. "Characterization of Silver Vanadium Oxide Cathode Material by High-Resolution Electron Microscopy." *Journal of Power Sources* 54.1 (1995): 68-71.

Crespi, Y., P. M. Skarstad, H. W. Zandebergen and J. Schoonman. *Proceedings of the Symposium on Lithium Batteries*, ed. E. S. Surampudi and V. Koch 93-94 (1993): 98-105.

Delabarre, C. M., Dubois, K. Guerin, Z. Fawal and A. Hamwi. "Room Temperature Graphite Fluorination Process Using Chlorine as Catalyst." *Journal of Physics and Chemistry of Solids* 67 (2006): 1157-1161.

Dubois, M., K. Guerin, J. P. Pinheiro, Z. Fawal, F. Masin and A. Hamwi. "NMR and EPR Studies of Room Temperature Highly Fluorinated Graphite Heat-Treated Under Fluorine Atmosphere." *Carbon* 42.10 (2004): 1931-1940.

Duer, Melinda. *Introduction to Solid State NMR Spectroscopy* Boston: Wiley-Blackwell Publishers, 2005.

Duncan, T. M. "A Study of the ^{13}C Chemical-Shift Anisotropy in Metal Acetylides." *Inorganic Chemistry* 28.13 (1989): 2663-2668.

Ein-Eli, Y., B. Markovsky, D. Aurbach, Y. Carmeli, H. Yamin and S. Luski. "The Dependence of the Performance of Li-C Intercalation Anodes for Li-Ion Secondary Batteries on the Electrolyte Solution Composition." *Electrochimica*

Acta 39.17 (1994): 2559-2569.

Endo, E., M. Ata, K. Sekai and K. Tanaka. "Spin Trapping Study of Gradual Decomposition of Electrolyte Solutions for Lithium Secondary Batteries." *Journal of the Electrochemical Society* 146.1 (1999): 49-53.

Endo, E., M. Ata, K. Tanaka and V. Sekai. "Electron Spin Resonance Study of the Electrochemical Reduction of Electrolyte Solutions for Lithium Secondary Batteries." *Journal of the Electrochemical Society* 145.11 (1998): 3757-3764.

Eshkenazi, V., E. Peled, L. Burstein and D. Golodnitsky. "XPS Analysis of the SEI Formed on Carbonaceous Materials." *Solid State Ionics* 170.1-2 (2004): 83-91.

Feist, P. "Carbon Chemical Shifts." *University of Colorado at Boulder Chemistry and Biochemistry Website*. 2003. University of Colorado at Boulder. Oct 2008 <http://orgchem.colorado.edu/hndbksupport/nmrtheory/carbonchemshift.html>.

Garcia-Alvarado, F. and J. M. Tarascon. "Lithium Intercalation in $Ag_2V_4O_{11}$." *Solid State Ionics* 73.3-4 (1994): 247-254.

"Gaston Nerada Lithium Battery Products FAQ." *Gaston Nerada Lithium Battery Products*. Gaston Nerada Int'l Ltd. Dec 2009 <http://www.gaston-narada.com/tech-certificates.html>.

Giraudet, J., M. Dubois, K. Guerin, J. P. Pinheiro, A. Hamwi, W. E. E. Stone, P. Pirotte and F. Masin. "Solid-State ^{19}F and ^{13}C NMR of Room Temperature Fluorinated Graphite and Samples Thermally Treated Under Fluorine: Low-Field and High-Resolution Studies." *Journal of Solid State Chemistry* 178.4 (2005): 1262-1268.

Gireaud, L., S. Grugeon, S. Laruelle, S. Pilard and J. M. Tarascon."Identification of Li Battery Electrolyte Degradation Products Through Direct Synthesis and Characterization of Alkyl Carbonate Salts." *Journal of the Electrochemical Society* 152.5 (2005): A850-A857.

Gireaud, L., S. Grugeon, S. Pilard, P. Guenot, J. M. Tarascon and S. Laruelle. "Mass Spectrometry Investigations on Electrolyte Degradation Products for the Development of Nanocomposite Electrodes in Lithium Ion Batteries." *Analytical Chemistry* 78 (2006): 3688-3698.

Gleason, N. R., R. A. Leising, M. Palazzo, E. S. Takeuchi and K. J. Takeuchi. *Talk # 248: Microscopic Study of the First Voltage Plateau in the Discharge of SVO and the Consequences on Electronic Conductivity.* 208th Meeting of the Electrochemical Society Session D2 – Rechargeable Lithium and Lithium-Ion Batteries/Battery/Energy Technology. Los Angeles, CA: 2005.

Golden, J. H., B. G. M. Chew, D. B. Zax, F. J. DiSalvo, J. M. J. Frechet and J.-M.

Tarascon. "Preparation of Propylene Carbonate Acrylate and Poly(propylene carbonate acrylate) Electrolyte Elastomer Gels. ^{13}C NMR Evidence for Li^+-Cyclic Carbonate Interaction." *Macromolecules* 28.9 (1995): 3468-3470.

Grey, C. P. and S. G. Greenbaum. "Nuclear Magnetic Resonance Studies of Lithium-Ion Battery Materials." *MRS Bulletin* 27.8 (2002): 613-618.

Grey, C. P. and Y. J. Lee. "Lithium MAS NMR Studies of Cathode Materials for Lithium-Ion Batteries." *Solid State Sciences* 5.6 (2003): 883-894.

Gubernator, Klaus. *Chemgate Spectroscopy Search Engine*. 2008. Wiley Vch. Nov 2008 <http://chemgate.emolecules.com/index.php>.

Guerin, K., M. Dubois and A. Hamwi. "Electrochemical Discharge Mechanism of Fluorinated Graphite Used as Electrode in Primary Lithium Batteries." *Journal of Physics and Chemistry of Solids: Proceedings of the 13th International Symposium on Intercalation Compounds* 67.5-6 (2006): 1173-1177.

Guerin, K., M. Menetrier, A. Fevrier-Bouvier, S. Flandrois, B. Simon and P. Biensan. "A ^7Li NMR Study of a Hard Carbon for Lithium-Ion Rechargeable Batteries." *Solid State Ionics* 127.3-4 (2000): 187-198.

Guerin, K., J. P. Pinheiro, M. Dubois, Z. Fawal, F. Masin, R. Yazami and A. Hamwi "Synthesis and Characterization of Highly Fluorinated Graphite Containing sp^2 and sp^3 Carbon." *Chemistry Materials* 16 (2004): 1786-1792.

Haeberlen, Ulrich. *High Resolution NMR in Solids Selective Averaging* New York: Academic Press, 1976.

Hagaman, E. W. and D. K. Murray. "Solid State ^{13}C and ^{19}F NMR Characterization of Fluorinated Charcoal." *Energy & Fuels* 12 (1998): 399-408.

Herstedt, M., D. P. Abraham, J. B. Kerr and K. Edstrom. "X-ray Photoelectron Spectroscopy of Negative Electrodes from High-Power Lithium-Ion Cells Showing Various Levels of Power Fade." *Electrochimica Acta* 49.28 (2004): 5097-5110.

Hirschinger, J., T. Mongrelet, C. Marichal, P. Granger, J. M. Savariault, E. Deramond and X. Galy. "Lithium (^6Li and ^7Li) NMR in High-Temperature Phases of Lithium Vanadium Oxide Bronzes ($Li_xV_2O_5$; $0.2<x<1$)." *Journal of Physical Chemistry* 97 (1993): 10301-10311.

Holland, G. P., D. A. Buttry and J. L. Yarger. "^7Li NMR Studies of Electrochemically Lithiated V_2O_5 Xerogels." *Chemistry of Materials* 14.9 (2002): 3875-3881.

Homer, J. and L. F. Thomas. “The Nuclear Magnetic Resonance Spectra of *cis*- and *trans*-Perfluorodecalin.” *Proceedings of the Chemical Society* (1961): 139-140.

Imanishi, N., K. Kumai, H. Kokugan, Y. Takeda and O. Yamamoto. "^{7}Li NMR Study of Carbon Fiber and Graphite Anodes for Lithium Ion Batteries." *Solid State Ionics* 107.1-2 (1998): 135-144.

Imhof, R. and P. Novak. "In-Situ Investigation of the Electrochemical Reduction of Carbonate Electrolyte Solutions at Graphite Electrodes." *Journal of The Electrochemical Society* 145.4 (1998): 1081-1087.

Jackman, L. M. and L. M. Scarmoutzos. “Structure of Phenyllithium in Solution.” *Journal of the American Chemical Society* 106.16 (1984): 4627-4629.

Kawakita, J., H.Sasaki, M.Eguchi, T.Miura and T.Kishi. "Characteristics of [delta]-$Ag_yV_2O_5$ as a Lithium Insertion host." *Journal of Power Sources* 70.1 (1998): 28-33.

Kawamura, T., A. Kimura, M. Egashira, S. Okada and J.-I. Yamaki. "Thermal Stability of Alkyl Carbonate Mixed-Solvent Electrolytes for Lithium Ion Cells." *Journal of Power Sources* 104.2: (2002): 260-264.

Kerlau, M., J. A. Reimer and E. J. Cairns. "Investigation of Particle Isolation in Li-Ion Battery Electrodes Using ^{7}Li NMR Spectroscopy." *Electrochemistry Communications* 7.12 (2005): 1249-1251.

Kosova, N. and E. Devyatkina. “Soft Mechanochemical Synthesis: Preparation of Cathode Materials for Rechargeable Lithium Batteries.” *Les Annales de Chimie – Science des Matériaux* 27.6(2002): 77-90.

Krawietz, T. R. and J. F. Haw. "Alkali Metal Oxides, Peroxides and Superoxides: A Multinuclear MAS NMR Study." *Chemical Communications* 102.45 (1998): 2151-2152.

Kuwabara, K., M. Itoh and K. Sugiyama. “Ionic-Electronic Mixed Conduction in $Li_xV_2O_5$.” *Solid State Ionics* 20.2 (1986): 135-139.

Lee, Y. J., S. H. Park, C. Eng, J. B. Parise and C. P. Grey. "Cation Ordering and Electrochemical Properties of the Cathode Materials $LiZn_xMn_{2-x}O_4$, $0 < x < 0.5$: A ^{6}Li Magic-Angle Spinning NMR Spectroscopy and Diffraction Study." *Chemistry of Materials* 14.1 (2002): 194-205.

Lee, Y. J., F. Wang, S. Mukerjee, J. McBreen and C. P. Grey. "^{6}Li and ^{7}Li Magic Angle Spinning Nuclear Magnetic Resonance and In-Situ X-Ray Diffraction Studies of the Charging and Discharging of $Li_xMn_2O_4$ at 4V." *Journal of the Electrochemical Society* 147.3 (2000): 803-812.

Lei, J. L., L. J. Li, R. Kostecki, R. Muller and F. McLarnon. "Characterization of SEI Layers on $LiMn_2O_4$ Cathodes with In-Situ Spectroscopic Ellipsometry." *Journal of the Electrochemical Society* 152.4 (2005): A774-A777.

Leifer, N. D., A. Colon, K. Martocci, S. G. Greenbaum, F. M. Alamgir, T. B. Reddy, N. R. Gleason, R. A. Leising and E. S. Takeuchi. *Journal of The Electrochemical Society* 154.6 (2007): A500-A506.

Leifer, N. and S. G. Greenbaum. "Spectroscopic Analysis of SEI Formation in Lithium-Ion Batteries." *Advanced Materials and Methods for Lithium Ion Batteries*. Edited. S. S. Zhang. Kerala, India: Transworld Research Network, 2007.

Letellier, M., F. Chevallier, F. Beguin, E. Frackowiak and J.-N. Rouzaud. "The First In-Situ ^7Li NMR Study of the Reversible Lithium Insertion Mechanism in Disorganised Carbons." *Journal of Physics and Chemistry of Solids* 65.2-3 (2004): 245-251.

Levasseur, S., M. Menetrier and C. Delmas. "Combined Effects of Ni and Li doping on the Phase Transitions in Li_xCoO_2 - Electrochemical and ^7Li Nuclear Magnetic Resonance Studies." *Journal of the Electrochemical Society* 149.12 (2002): A1533-A1540.

Levasseur, S., M. Menetrier and C. Delmas. "On the Dual Effect of Mg Doping in $LiCoO_2$ and Li^{1+}[delta]-CoO_2: Structural, Electronic Properties and ^7Li MAS NMR Studies." *Chemistry of Materials* 14.8 (2002): 3584-3590.

Levasseur, S., M. Menetrier, E. Suard and C. Delmas. "Evidence for Structural Defects in Non-Stoichiometric HT-$LiCoO_2$: Electrochemical, Electronic Properties and ^7Li NMR Studies." *Solid State Ionics* 128.1-4 (2000): 11-24.

Li, J., K. Naga, Y. Ohzawa, T. Nakajima, A. I. Shames and A. M. Panich. "Effect of Surface Fuorination on the Electrochemical Behavior of Petroleum Cokes for Lithium Ion Battery." *Journal of Fluorine Chemistry* 126 (2005): 265-273.

Li, W., C. Campion, B. Lucht, B. Ravdel, J. DiCarlo and K. M. Abraham. "Additives for Stabilizing $LiPF_6$-Based Electrolytes Against Thermal Decomposition." *Journal of the Electrochemical Society* 152.7 (2005): A1361-A1365.

Linden, D. and T. B. Reddy. *Handbook of Battery Materials*, 3rd ed. New York: McGraw-Hill, 2001.

"Lithium Battery." *Wikipedia*. 2008. Wikimedia Foundation, Inc.. 28 Jan 2009 <http://en.wikipedia.org/wiki/Lithium_battery>.

Mallouk, T., B. L. Hawkins, M. P. Conrad, K. Zilm, G. E. Maciel and N. Bartlett.

"Raman, Infrared and N.M.R. Studies of the Graphite Hydrofluorides $C_xF_{1-\delta}(HF)_\delta$ ($2 \leq x \leq 5$)." *Philisophical Transactions of the Royal Society of London. Series A, Math & Physical Sciences* 314:1528 (1985): 179-187.

Matsubara, K., R. Kaneuchi and N. Maekita. "^{13}C NMR Estimation of Preferential Solvation of Lithium Ions in Non-Aqueous Mixed Solvents." *Journal of the Chemical Society, Faraday Transactions* 94 (1998): 3601-3605.

Matsuta, S., Y. Kato, T. Ota, H. Kurokawa, S. Yoshimura and S. Fujitani. "Electron Spin Resonance Study of the Reaction of Electrolytic Solutions on the Positive Electrode for Lithium-Ion Secondary Batteries." *Journal of the Electrochemical Society* 148.1 (2001): A7-A10.

Menetrier, M., I. Saadoune, S. Levasseur and C. Delmas. "The Insulator-Metal Transition upon Lithium Deintercalation from $LiCoO_2$: Electronic Properties and ^{7}Li NMR Study." *Journal of Materials Chemistry* 9.5 (1999): 1135-1140.

Menetrier, M., C. Vaysse, L. Croguennec, C. Delmas, C. Jordy, F. Bonhomme and P. Biensan. "^{7}Li and ^{1}H MAS NMR Observation of Interphase Layers on Lithium Nickel Oxide Based Positive Electrodes of Lithium-Ion Batteries." *Electrochemical and Solid State Letters* 7.6 (2004): A140-A143.

Moshkovich, M., M. Cojocaru, H. E. Gottlieb and D. Aurbach. "The Study of the Anodic Stability of Alkyl Carbonate Solutions by In-Situ FTIR Spectroscopy, EQCM, NMR and MS." *Journal of Electroanalytical Chemistry* 497.1-2 (2001): 84-96.

Nagy, Zoltan. *Electrochemistry Dictionary*. 2008. Case Western Reserve University. Dec 2008 <http://electrochem.cwru.edu/ed/dict.htm>.

Nakamura, K., D. Nishioka, Y. Michihiro, M. Vijayakumar, S. Selvasekarapandian and T. Kanashiro. "^{7}Li and ^{51}V NMR Study on Li^+ Ionic Diffusion in Lithium Intercalated $Li_xV_2O_5$." *Solid State Ionics* 177.1-2 (2006): 129-135.

Nakamura, K., M. Yamamoto, K. Okamura, Y. Michihiro, I. Nakabayashi and T. Kanashiro. "NMR Investigation on the Motion of Li^+ Defects in $LiCoO_2$ and $LiNiO_2$." *Solid State Ionics* 121.1-4 (1999): 301-306.

Ota, H. Y. S., A. Inoue and S. Yamaguchi. "Analysis of Vinylene Carbonate Derived SEI Layers on Graphite Anode." *Journal of the Electrochemical Society* 151 (2004): A1659-A1669.

Pan, C., Y. J. Lee, B. Ammundsen and C. P. Grey. "^{6}Li MAS NMR Studies of the Local Structure and Electrochemical Properties of Cr-doped Lithium Manganese and Lithium Cobalt Oxide Cathode Materials for Lithium-Ion Batteries." *Chemistry of Materials* 14.5 (2002): 2289-2299.

Panich, A. M., T. Nakajima and S. D. Goren. "^{19}F NMR Study of C-F Bonding and Localization Effects in Fluorine-Intercalated Graphite." *Chemical Physics Letters* 271.4-6 (1997): 381-384.

Panich, M., A. I. Shames and T. Nakajima. "On Paramagnetism in Fluorinated Graphite: EPR and Solid State NMR Study." *Journal of Physics and Chemistry of Solids* 62.5 (2001): 959-964.

Peled, E. "The Electrochemical-Behavior of Alkali and Alkaline-Earth Metals in Non-Aqueous Battery Systems - the Solid Electrolyte Interphase Model." *Journal of the Electrochemical Society* 126.12 (1979): 2047-2051.

Peled, E., D. Golodnitsky and G. Ardel. "Advanced Model for Solid Electrolyte Interphase Electrodes in Liquid and Polymer Electrolytes." *Journal of the Electrochemical Society* 144.8 (1997): L208-L210.

Peled, E., D. Golodnitsky, G. Ardel and V. Eshkenazy. "The SEI Model -- Application to Lithium-Polymer Electrolyte Batteries." *Electrochimica Acta* 40.13-14 (1995): 2197-2204.

Pouchert, C., *The Aldrich Library of FT-IR Spectra*.1985.

Pouchert, J. and C. Behnke. *The Aldrich Library of NMR Spectra*. 1993.

Ramasamy, R. P., C. Feger, T. Strange and B. N. Popov. "Discharge Characteristics of Silver Vanadium Oxide Cathodes." *Journal of Applied Electrochemistry* 36.4 (2006): 487-497.

Randolph, Curtis. "Glossary of Technical Battery Terminology." *Green Batteries*. 2008. Responsible Energy Corporation. Dec 2008 <http://www.greenbatteries.com/batteryterms.html>.

Rao, C. P., P. Balaram and C. N. R. Rao. (1980). "^{13}C Nuclear Magnetic Resonance Studies of the Binding of Alkali and Alkaline Earth Metal Salts to Amides." *Journal Chemical Society, Faraday Transactions* 76: 1008-1013.

Ratnakumar, B. V., M. C. Smart and S. Surampudi. "Effects of SEI on the Kinetics of Lithium Intercalation." *Journal of Power Sources* 97-98 (2001): 137-139.

Ravdel, B., K. M. Abraham, R. Gitzendanner, J. DiCarlo, B. Lucht and C. Campion. "Thermal Stability of Lithium-Ion Battery Electrolytes." *Journal of Power Sources* 119-121 (2003): 805-810.

Reddy, V. P., M. C. Smart, K. B. Chin, B. V. Ratnakumar, S. Surampudi, J. Hu, P. Yan and G. K. S. Prakash. "^{13}C NMR Spectroscopic, CV and Conductivity Studies of Propylene Carbonate-Based Electrolytes Containing Various Lithium Salts."

Electrochemical and Solid-State Letters 8.6 (2005): A294-A298.

Reich, H. J. *C-13 Chemical Shifts*. 2008. Department of Chemistry at the University of Wisconsin. Oct 2008 <http://www.chem.wisc.edu/areas/reich/Handouts/nmr-c13/cdata.htm>.

Root, M. J., R. Dumas, R. Yazami and A. Hamwi. "The Effect of Carbon Starting Materials on Carbon Fluoride Synthesized at Room Temperature." *Journal of the Electrochemical Society* 148.4 (2001): A339-A345.

Rozier P. and J. Galy. "$Ag_{1.2}V_3O_8$ Crystal Structure: Relationship with $Ag_2V_4O_{11-y}$ and Interpretation of Physical Properties." *Journal of Solid State Chemistry* 134.2 (1997): 294-301.

Sadoway, M. "Portable Power: Advanced Rechargeable Lithium Batteries." *MRS Bulletin* 27.8 (2002): 590-596.

Saito, T., K.Hayamizu, M.Yanagisawa and O.Yamamoto. *Spectral Database for Organic Compounds, SDBS*. 2008. National Institute of Advanced Industrial Science and Technology. Sept 2008 <http://riodb01.ibase.aist.go.jp/sdbs/cgi-bin/cre_index.cgi?lang=eng>.

Sankaram, M. B. and K. R. K. Easwaran. "CD and NMR Studies on the Interaction of Lithium Ion with Valinomycin and Gramicidin-S." *Biopolymers* 21 (1982): 1557-1567.

Sasaki, T., T. Abe, J. Iriyama, M. Inaba and Z. Ogumi. "Formation Mechanism of Alkyl Dicarbonates in Li-Ion Cells." *Journal of Power Sources* 150 (2005): 208-215.

Sato, Y., K. Itoh, R. Hagiwara, T. Fukunaga and Y. Ito. "On the So-Called "Semi-Ionic" C-F Bond Character in Fluorine-GIC." *Carbon* 42.15 (2004): 3243-3249.

Slichter, C. P. *Principles of Magnetic Resonance*, 2nd Ed. Berlin: Springer-Verlag, 1980.

Sloop, S. E., J. B. Kerr and K. Kinoshita. "The Role of Li-Ion Battery Electrolyte Reactivity in Performance Decline and Self-Discharge." *Journal of Power Sources* 119 (2003): 330-337.

Sloop, S. E., J. K. Pugh, S. Wang, J. B. Kerr and K. Kinoshita. "Chemical Reactivity of PF_5 and $LiPF_6$ in Ethylene Carbonate/Dimethyl Carbonate Solutions." *Electrochemical and Solid State Letters* 4.4 (2001): A42-A44.

Smart, M. C., B. V. Ratnakumar, S. Surampudi, Y. Wang, X. Zhang, S. G. Greenbaum, A. Hightower, C. C. Ahn and B. Fultz. "Irreversible Capacities of Graphite in Low-Temperature Electrolytes for Lithium-Ion Batteries." *Journal of the Electrochemical Society* 146.11 (1999): 3963-3969.

Smirnov, S. N. "Experiment 7. ESR Spectroscopy. Introduction." *New Mexico State University - Department of Chemisty and Biochemistry*. 2007. New Mexico State University. Dec 2008 <http://www.chemistry.nmsu.edu/studntres/chem435/Lab7/intro.html>.

Song, S. W., G. V. Zhuang and P. N. Ross, Jr. "Surface Film Formation on $LiNi_{0.8}Co_{0.15}Al_{0.05}O_2$ Cathodes Using Attenuated Total Reflection IR Spectroscopy." *Journal of the Electrochemical Society* 151.8 (2004): A1162-A1167.

Stallworth, P. E., F. S. Johnson, S. G. Greenbaum, S. Passerini, J. Flowers and W. Smyrl. "Magnetic Resonance Studies of Chemically Intercalated $Li_xV_2O_5$ Aerogels." *Journal of Applied Physics* 92.7 (2002): 3839-3852.

Stallworth, P. E., F. S. Johnson, S. G. Greenbaum, S. Passerini, J. Flowers, W. Smyrl and J. J. Fontanella. "Magnetic Resonance Studies of Chemically Intercalated $Li_xV_2O_5$ (x=1.16 and 1.48)." *Solid State Ionics* 146.1-2 (2002): 43-54.

Stallworth, P. E., S. Kostov, M. L. denBoer, S. G. Greenbaum and C. Lampe-Onnerud. "X-ray Absorption and Magnetic Resonance Spectroscopic Studies of $Li_xV_6O_{13}$." *Journal of Applied Physics* 83.3 (1998): 1247-1255.

Takeuchi, E. S. and R. A. Leising. “Melt Impregnation of Mixed Metal Oxide.” US Patent 6413669. 2 July 2002. (a); E. S. Takeuchi and R. A. Leising. “Synthetic Method for Preparation of a Low Surface Area, Single Phase Silver Vanadium Oxide.” US Patent 6566007. 20 May 2003. (b).

Takeuchi, K. J., A. C. Marschilok, S. M. Davis, R. A. Leising and E. S. Takeuchi. "Silver Vanadium Oxides and Related Battery Applications." *Coordination Chemisty Reviews* 219-221 (2001): 283-310.

Thevenin, J. G. and R. H. Muller. "Impedance of Lithium Electrodes in a Propylene Carbonate Electrolyte." *Journal of the Electrochemical Society* 134.2 (1987): 273-280.

Tucker, M. C., J. A. Reimer, E. J. Cairns, S. Choi and A. Manthiram. "^{7}Li NMR Studies of Chemically-Delithiated $Li_{1-x}CoO_2$." *Journal of Physical Chemistry B* 106.15 (2002): 3842-3847.

Vancea, L. and S. Bywater. "^{13}C NMR Studies on Anion Pairs Related to Acrylate Polymerization. 2.) Dimer Models." *Macromolecules* 14 (1981): 1776-1778.

Vijayakumar, M., S. Selvasekarapandian, K. Nakamura, T. Kanashiro and R. Kesavamoorthy. "^{7}Li MAS NMR and Vibrational Spectroscopic Investigations of $Li_xV_2O_5$ (x=1.0, 1.2 and 1.4)." *Solid State Ionics* 167.1-2 (2004): 41-47.

Vincent, C. A. "Lithium Batteries: A 50-year Perspective, 1959-2009." *Solid State Ionics* 134.1-2 (2000): 159-167.

Wang, Y. F., X. D. Guo, S. G. Greenbaum, J. Liu and K. Amine. "Solid Electrolyte Interphase Formation on Lithium-Ion Electrodes - A ^{7}Li Nuclear Magnetic Resonance Study." *Electrochemical and Solid State Lett*ers 4.6 (2001): A68-A70.

Wang, H. L., H.-M. Kao, M. Digar and T. C. Wen. "FTIR and Solid State ^{13}C NMR Studies on the Interaction of Lithium Cations with Polyether Poly(urethane Urea)." *Macromolecules* 34 (2001): 529-537.

Wang, Y. X., S. Nakamura, M. Ue and P. B. Balbuena. "Theoretical Studies to Understand Surface Chemistry on Carbon Anodes for Lithium-Ion Batteries: Reduction Mechanisms of Ethylene Carbonate." *Journal of the American Chemical Society* 123.47 (2001): 11708-11718.

Wang, Y., V. Yufit, X. Guo, E. Peled and S. Greenbaum. "^{7}Li Nuclear Magnetic Resonance Study of Lithium Insertion in Pristine and Partially Oxidized Graphite." *Journal of Power Sources* 94.2 (2001): 230-237.

Watanabe, N. "Two Types of Graphite Fluorides, $(CF)_n$ and $(C_2F)_n$, and Discharge Characteristics and Mechanisms of Electrodes of $(CF)_n$ and $(C_2F)_n$ in Lithium Batteries." *Solid State Ionics* 1.1 (1980): 87-110.

Weigert, F. J. and R. J. J. Karel. “A Fluorine NMR Database.” *Journal of Fluorine Chemistry* 37 (1987): 125-149.

West, K. and A.M. Crespi. "Lithium Insertion into Silver Vanadium Oxide, Ag2V4O11."*Journal of Power Sources* 54.2 (1995): 334-337.

Xu, K. "Nonaqueous Liquid Electrolytes for Lithium-Based Rechargeable Batteries." *Chemical Reviews* 104.10 (2004): 4303-4417.

Yang, Y.-Y., J.-P. Wan, T.-S. Chung, P. K. Pallathadka, S. Ng and J. Heller. "POE-PEG-POE Triblock Copolymeric Microspheres Containing Protein: I. Preparation and Characterization." *Journal of Controlled Release* 75.1-2 (2001): 115-128.

Yazami, R. "Surface Chemistry and Lithium Storage Capability of the Graphite-Lithium Electrode." *Electrochimica Acta* 45.1-2 (1999): 87-97.

Yoshida, H., T. Fukunaga, T. Hazama, M. Terasaki, M. Mizutani and M. Yamachi. "Degradation Mechanism of Alkyl Carbonate Solvents Used in Lithium-Ion Cells During Initial Charging." *Journal of Power Sources* 68.2 (1997): 311-315.

Zandbergen, H. W., A. M. Crespi, P. M. Skarstad and J. F. Vente. "Two Structures of

$Ag_{2-x}V_4O_{11}$, Determined by High Resolution Electron Microscopy." *Journal of Solid State Chemistry* 110.1 (1994): 167-175.

Zhao, L. W., I. Watanabe, T. Doi, S. Okada and J. Yamaki. "TG-MS Analysis of Solid Electrolyte Interphase (SEI) on Graphite Negative-Electrode in Lithium-Ion Batteries." *Journal of Power Sources* 161.2 (2006): 1275-1280.

Zhuang, G., Y. Chen and P. N. Ross, Jr. "The Reaction of Lithium with Dimethyl Carbonate and Diethyl Carbonate in Ultrahigh Vacuum Studied by X-ray Photoemission Spectroscopy." *Langmuir* 15 (1999): 1470-1479.

Zhuang, G. V., K. Xu, H. Yang, J. R. Jow and P. N. Ross, Jr. "Lithium Ethylene Dicarbonate Identified as the Primary Product of Chemical and Electrochemical Reduction of EC in 1.2 M $LiPF_6$/EC:EMC Electrolyte." *Journal of Physical Chemistry B* 109.37 (2005): 17567-17573.